Johns Hopkins Department of Medicine & Whiting School of Engineering

RESEARCH RETREAT

presents

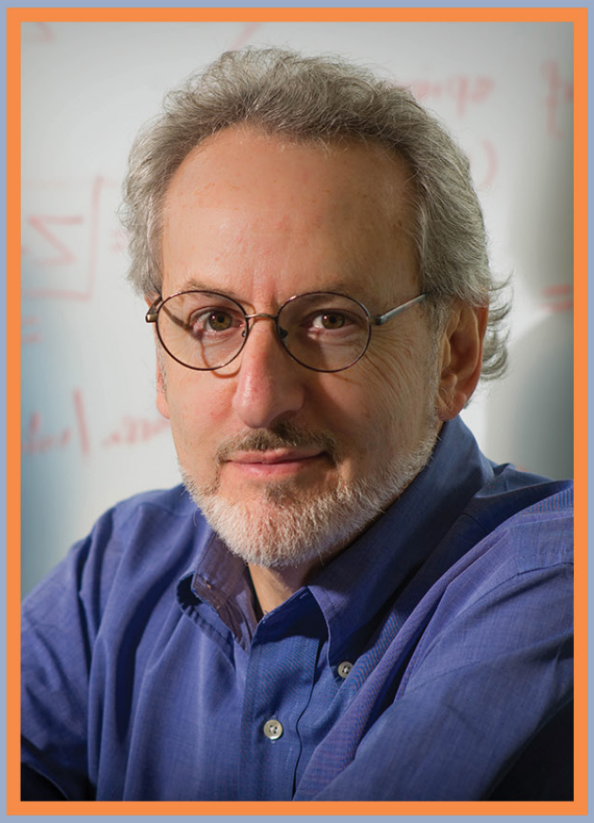

KEYNOTE SPEAKER

Donald E. Ingber, MD, PhD
Founding Director, Wyss Institute for Biologically Inspired Engineering, Harvard University
Judah Folkman Professor of Vascular Biology, Harvard Medical School and Boston Children's Hospital

SPOTLIGHT ON RESEARCH

Featuring Select Faculty and Trainees from the Johns Hopkins Department of Medicine & Whiting School of Engineering

POSTER SESSION

DATE

Friday, February 14, 2025
8:30 a.m.- 2:15 p.m.
Turner Auditorium & Concourse

JOHNS HOPKINS SCHOOL of MEDICINE

JOHNS HOPKINS WHITING SCHOOL of ENGINEERING

Welcome to the Johns Hopkins 2025 Department Of Medicine/Whiting School of Engineering Research Retreat

The Department of Medicine and Whiting School of Engineering Research Retreat and Poster Session is about connections. Connections among researchers in both schools, connections between mentors and mentees and connections between leadership and the adventurous researchers that elevate the discovery community.

Our annual retreat is the largest forum for the presentation of research by Department of Medicine and Whiting School of Engineering faculty, staff and trainees. The retreat has a long-standing history in the Department of Medicine but has seen its greatest success since joining forces with the Whiting School of Engineering in 2018.

This year, we welcome Keynote Speaker Donald Ingber, MD, PhD, founding director of the Wyss Institute for Biologically Inspired Engineering at Harvard University, Judah Folkman Professor of Vascular Biology at Harvard Medical School and Boston Children's Hospital and Hansjörg Wyss Professor of Biologically Inspired Engineering at the Harvard John A. Paulson School of Engineering and Applied Sciences.

Once again, we are thrilled that our keynote address, spotlight on research talks and award presentations will happen in conjunction with the poster session that is known to fill Turner Concourse with bold and creative research initiatives at Johns Hopkins. We hope the event will fuel new collaborations and capitalize on the investigative strengths of each enterprise.

Enjoy the connections!

Nadia N. Hansel, MD, MPH
Director, Department of Medicine
Physician-in-Chief, Johns Hopkins Hospital

T.E. (Ed) Schlesinger, PhD
Benjamin T. Rome Dean
Whiting School of Engineering

Sangwon Kim, PhD
Associate Professor of Medicine and Neuroscience
Retreat Committee Co-chair

Jamie Spangler, PhD
Associate Professor of Biomedical Engineering, Chemical & Biomolecular Engineering
Retreat Committee Co-chair

KEYNOTE SPEAKER

Donald E. Ingber, MD, PhD

Founding Director, Wyss Institute for Biologically Inspired Engineering, Harvard University
Judah Folkman Professor of Vascular Biology, Harvard Medical School and Boston Children's Hospital
Hansjörg Wyss Professor of Biologically Inspired Engineering, Harvard John A. Paulson School of Engineering and Applied Sciences

Donald Ingber is a pioneer in the field of biologically inspired engineering, and at the Wyss Institute, he currently leads scientific and engineering teams that cross a broad range of disciplines to develop breakthrough bioinspired technologies to advance healthcare and to improve sustainability. His work has led to major advances in mechanobiology, cell structure, tumor angiogenesis, tissue engineering, systems biology, nanobiotechnology and translational medicine. Through his work, Ingber also has helped to break down boundaries between science, art and design.

Ingber has authored more than 500 publications and 200 patents, founded 8 companies, and has presented more than 550 plenary presentations and invited lectures world-wide. He is a member of the National Academy of Engineering, National Academy of Medicine, National Academy of Inventors, American Institute for Medical and Biological Engineering, and the American Academy of Arts and Sciences. He was named one of the Top 20 Translational Researchers world-wide in 2012 and 2020 (Nature Biotechnology), a Leading Global Thinker of 2015 (Foreign Policy magazine), and has received numerous other honors in a broad range of disciplines, including the Robert A. Pritzker Award and the Shu Chien Award (Biomedical Engineering Society), Rous Whipple Award (American Society for Investigative Pathology), Lifetime Achievement Award (Society of In Vitro Biology), Leading Edge Award (Society of Toxicology), Founders Award (Biophysical Society), Department of Defense Breast Cancer Innovator Award, Wilbur Cross Medal from Yale University, National Institute for Materials Science Award (Japan), Marsilius Medal (Heidelberg U.), Russell and Burch Award (Humane Society of the United States), and Lush Prize (with Emulate Inc.).

Department of Medicine & Whiting School of Engineering

2025 RESEARCH RETREAT

Spotlight on Research Talks

FRIDAY, FEBRUARY 14, 10:00-10:40 a.m. (Turner Auditorium)

The Spotlight on Research is a fast-paced session that showcases some of the past year's best science from the Johns Hopkins Department of Medicine and the Whiting School of Engineering. Each presenter will share higlights of their research findings delivered in a five-minute lighning talk.

Sangmoo Jeong, PhD
Assistant Professor of Chemical and Biomolecular Engineering and Oncology Center
"Targeting cancer metabolism to stop metastasis"

Tza-Huei (Jeff) Wang, PhD
The Louis M. Sardella Professor in Mechanical Engineering and Biomedical Engineering
"Microfluidic digital DNA methylation analysis for sensitive and cost-effective cancer detection in liquid biopsies"

William Checkley, MD, PhD
Professor of Medicine
Division of Pulmonary and Critical Care Medicine
"A decade of research in household air pollution and health: from observational studies to randomized trials"

Laszlo Nagy, MD, PhD
Professor of Medicine and Biological Chemistry, Division of Endocrinology, Diabetes & Metabolism, and Co-Director of the Institute for Fundamental Biomedical Research
"Spatiotemporal control of regenerative inflammation"

Jamie Spangler, PhD
Associate Professor in Biomedical Engineering, Chemical and Biomolecular Engineering, Oncology, Ophthalmology, Molecular Microbiology & Immunology
"Engineered cytokine-antibody fusion proteins to advance immunotherapy"

Peter Kazanzides, PhD
Research Professor, Department of Computer Science & Kemar Green, DO Assistant Professor of Neurology
"The Virtual Neurology Clinic: A Human-AI Interface for Autonomous Remote Neurologic Assessments"

Andrea Fava, MD
Assistant Professor of Medicine
Division of Rheumatology
"Toward a liquid biopsy for lupus nephritis"

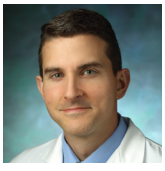

Justin Bailey, MD, PhD
Associate Professor of Medicine, Division of Infectious Diseases and Hospital Medicine
"Rational design of a hepatitis C virus vaccine"

Department of Medicine & Whiting School of Engineering

2025 RESEARCH RETREAT

Committee Members

Co-Chairs:

Sangwon Kim, PhD
Jamie Spangler, PhD

Members:

Peter Abadir, MD
Clifton Bingham, MD
Steven Clipman, PhD, MSPH
D. Brian Foster, PhD
Ankit Garg, MD, PhD
Claire Hur, MS, PhD
Waseem Khaliq, MBBS, MPH
Deok-Ho Kim, PhD
Maximilian Konig, MD
Gregory Lucas, MD, PhD
Laureano Moro Velazquez, PhD
Enid Neptune, MD
Brian O'Rourke, PhD
Jude Phillip, PhD
Faisal Rahman, BM, MBBCh, BCH
Matthew Robinson, MD
Prasanna Santhanam, MD
Florin Selaru, MD
Maunank Shah, MD
Larissa Shimoda, MS, PhD
Paul Welling, MD
William Werbel, MD, PhD

Event Coordinators:

Kelsey Bennett
Helen Harrison
Alissa Meehan
Melanie Mossman
Rebecca Spriggs

(Listed alphabetically)

Department of Medicine & Whiting School of Engineering

2025 RESEARCH RETREAT

Program

FRIDAY, FEBRUARY 14

8:30 a.m.

Welcome & Opening Remarks (Turner Auditorium)

Jamie Spangler, PhD
Associate Professor of Biomedical Engineering, Chemical & Biomolecular Engineering
Retreat Committee Co-chair

Nadia N. Hansel, MD, MPH
Director, Department of Medicine
Physician-in-Chief, Johns Hopkins Hospital

T.E. "Ed" Schlesinger, PhD
Benjamin T. Rome Dean
Whiting School of Engineering

Sangwon Kim, PhD
Associate Professor of Medicine and Neuroscience
Retreat Committee Co-chair

9:00 a.m.

Keynote Address (Turner Auditorium)

Donald E. Ingber, MD, PhD
Founding Director, Wyss Institute for Biologically Inspired Engineering, Harvard University
Judah Folkman Professor of Vascular Biology, Harvard Medical School and Boston Children's Hospital
Hansjörg Wyss Professor of Biologically Inspired Engineering, Harvard John A. Paulson School of Engineering and Applied Sciences

10:00 a.m.

Spotlight on Research Talks (Turner Auditorium)
Moderated by Peter Abadir, MD and Sangwon Kim, PhD

Sangmoo Jeong, PhD
Assistant Professor, Department of Chemical and Biomolecular Engineering and Oncology Center

William Checkley, MD, PhD
Professor of Medicine, Division of Pulmonary and Critical Care Medicine

Jamie Spangler, PhD
Associate Professor of Biomedical Engineering, Chemical and Biomolecular Engineering, Oncology, Ophthalmology, Molecular Microbiology & Immunology

Andrea Fava, MD
Assistant Professor of Medicine, Division of Rheumatology

Jeff (Tza-Huei) Wang, PhD
Professor of Mechanical Engineering and Biomedical Engineering

Laszlo Nagy, MD, PhD
Professor of Medicine and Biological Chemistry, Division of Endocrinology, Diabetes & Metabolism

Peter Kazanzides, PhD
Research Professor, Department of Computer Science

Justin Bailey, MD, PhD
Associate Professor of Medicine, Division of Infectious Diseases and Hospital Medicine

10:40 a.m.

JHTV Presentation

10:50 a.m.

Break

11:00 a.m.

Research Award Presentations (Turner Auditorium)

The W. Leigh Thompson Excellence in Research Awards
Presented by Brian O'Rourke, PhD and Clifton Bingham, MD

Basic Fellow Winner - Navid Koleini, MD, PhD
Basic Faculty Winner - Qinchuan Wang, PhD
Clinical Fellow Winner - Maryam Mojarrad Sani, MD, MPH
Clinical Faculty Winner - Wilson Tang, MSE

Whiting School of Engineering Research Awards
Presented by Jamie Spangler, PhD

Trainee Winners - Marta Martinez Yus, BS
Joseph Choy, BASc
Faculty Winner - Jochen Mueller, PhD

11:45 a.m.

Lunch Break (Turner Consourse)

12:15 p.m.

Poster Session: Odd Numbers (Turner Consourse)

1:15 p.m.

Poster Session: Even Numbers (Turner Consourse)

2:15 p.m.

Retreat Closing

THE W. LEIGH THOMPSON EXCELLENCE IN RESEARCH AWARD

Basic Research Fellow Winner

Navid Koleini, MD, PhD Abstract 109

"Reduced Hypusination of eIF5A impairs ribosomal translation resulting in Heart Failure with Preserved Ejection Fraction"

Runners-Up

Mohammad Keykhaei, MD, MPH Abstract 60

Vartika Tomar, PhD Abstract 110

Basic Research Faculty Winner

Qinchuan Wang, PhD Abstract 57

"Chronic activation of CaMKII, a key signal transducer for exercise performance and adaptation, drives sarcopenia in aging"

THE W. LEIGH THOMPSON EXCELLENCE IN RESEARCH AWARD

Clinical Research Fellow Winner

Maryam Mojarrad, MD, MPH Abstract 88

"Increased Lipoprotein(a) Levels Independently Predict a Higher Incidence of Ventricular Arrhythmias: A Comprehensive Retrospective Cohort Study"

Runner-Up

Masih Tajdini, MD Abstract 86

Clinical Research Faculty Winner

Wilson Tang, MSE Abstract 84

"Biometric Insights and Clinical Outcomes in Interstitial Lung Disease Patients on Long-Term Oxygen Therapy: A Remote Patient Monitoring Study"

Runner-Up

Nityasree Srialluri, MD, MS, MHS Abstract 59

WHITING SCHOOL OF ENGINEERING RESEARCH AWARD

Trainee Awardees

Marta Martinez Yus, BS Abstract 58

"Targeting LOXL2 against arterial stiffening in post-menopausal females"

Joseph Choy, BASc Abstract 85

"Metabolic conditioning during ex vivo stimulation of naïve tumor antigen-specific CD8 T cells"

Runners-Up

Byunggik Kim, BS Abstract 82

Dibakar Roy Sarkar, PhD Abstract 83

Pooja Hariharan, BT Abstract 87

Wenxuan Li, MEng Abstract 111

Lab Excellence Award

Jochen Mueller, PhD Abstract 145

"Recent Advances in Multimaterial Extrusion Additive Manufacturing"

ABSTRACTS

ABSTRACT 1

Cathepsin S Upregulation in Pulmonary Arterial Hypertension: Implications for Endostatin Proteolytic Cleavage and Disease Progression

Anjira S. Ambade, Mario Naranjo, Steven Hsu, Rachel L. Damico, Paul M. Hassoun

RATIONALE: Cathepsin S (CTSS) proteases are critical in cardiovascular disease progression through extracellular matrix (ECM) degradation. Our research has identified elevated endostatin (ES) derived from COL18A1 in pulmonary arterial hypertension (PAH). Increased COL18A1/ES expression is linked to PAH progression and right ventricular dysfunction. We hypothesize that increased CTSS contributes to ES cleavage from COL18A1, leading to right ventricular dysfunction during PAH development.

METHODS: Utilized Sugen/hypoxic (SuHx) rat model and Group I PAH patient serum. Assessed hemodynamics, right ventricle (RV) morphology, CTSS expression/activity in rats and CTSS activity in PAH serum with high/low ES. Pearson correlation analyzed relationships between CTSS activity and phenotypic variables in SuHx rats.

RESULTS: CTSS mRNA expression significantly increased in the RV ($p=0.007$), LV ($p=0.009$), and lungs ($p=0.0001$) of SuHx rats at 21 days. RV-associated CTSS protein levels were elevated at 7 days ($p=0.03$). CTSS enzymatic activity was increased in SuHx rat plasma at day 14 ($p=0.05$) and day 21 ($p=0.002$) versus controls. In SuHx rats, elevated CTSS activity correlated with RV remodeling and afterload measures (RV mass index: $p=0.009$; Fulton's index: $p=0.04$; RVSP: $p=0.001$). In PAH patients, high ES levels corresponded with increased CTSS activity, while low ES was associated with low CTSS activity ($p=0.005$).

CONCLUSIONS: Our findings demonstrate increased CTSS expression/activity in the SuHx rats and increased activity in PAH patient samples, suggesting a potential role of CTSS in COL18A1 cleavage and PAH pathogenesis. These findings highlight the CTSS-COL18A1-ES axis as a key player in PAH progression and RV dysfunction, presenting a potential biomarker and therapeutic target.

ABSTRACT 2

Digital Twin Virtual Reality Training for Central Line Dressing Change

Han Zhang, Yu-Chun Ku, Vinciya Pandian, Mathias Unberath

Central line-associated bloodstream infections (CLABSIs) have risen significantly since the pandemic, highlighting the need for effective and consistent training in central line care. Traditional training methods, such as video-based learning and mannequin practice, while beneficial in reducing adverse events, often fall short due to high costs, lack of realism, and limited efficacy. Furthermore, the gap between training environments and real-world practice compromises knowledge retention and application. To address these challenges, we introduce a photorealistic and interactive virtual reality simulator designed for central line dressing care. Leveraging neural rendering techniques, the system generates digital twins of medical intensive care unit (ICU) environments and associated instruments from casual video captures, offering a training context that closely replicates real-world settings. The simulator delivers standardized scenarios for central line dressing changes, providing immersive visual, auditory, and haptic feedback to guide users through clinical protocols and workflows. We evaluate the simulator's effectiveness through a user study in which healthcare professionals practice the standard central line dressing change protocol within the digital twin environment and subsequently perform the mock procedure in a real-world setting. Key metrics assessed include task load, perceived utility, eye gaze patterns, knowledge and skill acquisition, and memory retention. To measure the simulator's impact on training efficacy, these results are compared against outcomes from low-fidelity environments and traditional video-based learning methods.

ABSTRACT 3

Detrimental role of the host RNA sensor LGP2 during M. tuberculosis infection

Yazmin B. Martinez-Martinez, Somnath Shee, Benjamin Koleske, Moagi Shaku, Geetha Srikrishna, William R. Bishai

Mycobacterium tuberculosis (Mtb) is the leading infectious killer in the world and causes 10 million new tuberculosis (TB) cases per year. Mtb uses nucleic acids as PAMPs to subvert host defense pathways leading to worsened TB disease. Mtb-mediated subversion of two RNA sensors—RIG-I and MDA5—leads to exacerbated TB disease in cellular and animal models. RIG-I and MDA5 RNA sensors comprise a family known as RIG-I-like receptors (RLRs) important in antiviral defenses and mediating induction of Type I Interferon responses. The third RLR family member, LGP2, is an upstream regulator of the other RLRs, however, its role during Mtb infection remains unexplored.

In THP-1 macrophages, we found LGP2 expression upregulated in a time- and dose-dependent manner following Mtb infection, with levels significantly increased from 8 to 72h post-infection. After transfection of Mtb RNA, LGP2 and IFN-β were significantly upregulated compared to controls. LGP2-KO BMDMs contained Mtb proliferation to a greater degree than WT, releasing increased levels of proinflammatory cytokines, such as IL-1β and IL-6. Aerosol infection of LGP2-KO and WT mice with Mtb demonstrated significantly lower Mtb lung CFU counts in LGP2-KO mice at 4- and 8-weeks post-infection, with survival and mechanistic studies underway.

Loss of LGP2 host RNA sensor leads to improved Mtb containment in both BMDMs and mice. This suggests that Mtb exploits the LGP2 RNA sensing pathway to improve its survival in the host. These studies will enable to understand the role of LGP2 as a potential target for novel Mtb host-directed therapies.

ABSTRACT 4

Characterizing the molecular signatures of bronchial epithelial cells exposed to urban particulate matter

Orian Stapleton, Sean Engels, Pratik Kamat, Blanca Quiñones Díaz, Lydia Contreras, Jude Phillip

Particulate matter components, such as lead and cadmium, are commonly concentrated in populated industrial areas with significant manufacturing activity and heavy traffic. Therefore, there is a need to develop methods to investigate the effect of particulate matter on a cellular/molecular level. In previous work, human lung epithelial cells were shown to have greater susceptibility to particulate matter mixtures with high levels of cadmium. From a parental cell population, two subclones of distinct morphological features were identified, one showing greater susceptibility to cadmium rich particulate matter exposure. To further interrogate these results, we conducted bulk RNA-sequencing on the parent cell population, as well as the two subclones of higher susceptibility and lower susceptibility. In parallel, we also did single cell RNA-sequencing on the parental cell population. Our hypothesis is that there are subsets of cells in the parental cell population with molecular features that differentiate susceptibility to particulate matter. The aim is to identify signatures that inform about cells that are more prone to extensive damage prior to air pollution exposure. The bioinformatic software scissor was used to predict which cells in the parental cell populations are likely to be parents for each distinct morphological subclone based on correlated patterns of gene expression. We then conducted several downstream analyses including differential gene analysis and identified genes as well as biological processes associated with susceptibility to particulate matter. Ultimately, I want to use this framework to connect biophysical phenotypes and molecular features in the contexts of cellular states and human disease.

ABSTRACT 5

Fine Tuning of a Pretrained Gait Model for Frailty Classification/Prediction

Laura McDaniel, Ime Essien, Yuxiang Guo, Ayush Gupta, Vineet Shenoy, Peter Abadir, Rama Chellappa

This study aims to present a multimodal gait model designed to identify the frailty status of individuals based on their gait as observed in video footage. Frailty is defined as a clinically recognizable state of increased vulnerability, resulting from age-related declines in reserve and function across multiple interrelated physiological systems. These risks can manifest as an increased likelihood of falls, hospitalization, need for long-term care, disability, and mortality. While deep learning has made significant strides in various medical applications, its potential in the early detection of frailty through gait analysis is constrained by the need of copious amounts of data which is currently limited. To address this issue, we leveraged the Open gait framework, Gait base, a pretrained gait model typically used for gait surveillance and recognition applications by finetuning it with medical data to classify frailty. Data were collected using the marker-less Qualisys Motion Capture system, resulting in a dataset of 64 individuals classified by their frailty status—Non frail, frail, and prefrail—according to the Fried Frailty Phenotype. Detectron2 models were employed for panoptic image segmentation and detection, generating silhouette and box predictions held within frames from the videos. By integrating both silhouette and RGB data, our model seeks to enhance robustness and generalization across the three frailty classes. To address the challenges posed by a small dataset, we employed a combination of data augmentation techniques, hyperparameter tuning, and cross-validation to improve the model's classification accuracy. This model aims to initiate the investigation of the classification of frailty status using deep learning, which can be crucial in preventive healthcare and personalized treatment strategies for frailty. This tool can assist clinicians in assessing frailty by providing a time-efficient method that captures the complete gait profile of an individual. In this abstract, we present the model's accuracy in detecting and classifying the frailty status of individuals. Our next steps will involve incorporating metadata, such as height and weight, to further enhance the accuracy of frailty status predictions.

ABSTRACT 6

ECG-Conditioned Echocardiogram Video Synthesis

Sampath Rapuri, Sofia Sapeta Dias, Maria Salomé Carvalho, Carl Harris, Malcolm Lizzazppi, Robert Stevens

Echocardiography is a cornerstone of non-invasive cardiac health assessment, offering comprehensive insights into heart structure and function. Despite its broad diagnostic capabilities, echocardiography is a specialized, resource-intensive imaging modality. It requires significant expertise for accurate acquisition and interpretation and is challenging to deploy at scale, especially in resource-limited settings. In contrast, electrocardiography (ECG) is ubiquitous and inexpensive, and recent deep learning advances suggest it can identify certain features traditionally only seen on an echocardiogram. Using 3,849 paired apical 4-chamber echocardiograms and 12-lead ECG signals from the MIMIC-IV dataset, we trained a diffusion probabilistic model to synthesize two-second echocardiogram videos spanning one heartbeat. We evaluated two conditioning approaches: (1) ECG-only and (2) ECG with a static anatomical image taken randomly from the ground truth video. To assess the generated echocardiograms, we used the Structural Similarity Index Measure (SSIM), where higher values indicate greater similarity to the reference video, and the Learned Perceptual Image Patch Similarity (LPIPS), where lower values signify better perceptual quality. The 'ECG-only' model achieved a mean SSIM of 0.0241 and a mean LPIPS of 0.6502, demonstrating that realistic synthetic echocardiograms can be generated solely from widely accessible ECG signals. While the addition of a static anatomical image during conditioning slightly improved performance—yielding a mean SSIM of 0.0336 and a mean LPIPS of 0.6084— the 'ECG-only' approach highlights the potential of generating echocardiograms from widely available ECG data. Moreover, this approach could supplement existing echocardiographic datasets with synthetic echocardiograms, expanding echocardiographic datasets to develop machine learning models with.

ABSTRACT 7

3D electrophysiological mapping of cardiac organoids using shell microelectrode arrays

Soo Jin Choi, Zhaoyu Liu, Feiyu Yang, Hanwen Wang, Derosh George, David H. Gracias, Deok-Ho Kim

Cardiac organoids are three-dimensional (3D) multicellular constructs that recapitulate key structural and functional properties of the human heart. Their inherent 3D architecture makes them ideal for modeling tissue-scale phenomena, such as conduction blocks, reentrant circuits, and fibrosis. However, the absence of analytical tools capable of measuring electrical signals across 3D organoid surfaces with high spatiotemporal resolution remains a significant bottleneck for investigating structural arrhythmia disease models. Here, we engineered flexible microelectrode arrays (MEAs) with programmable shape-change to encapsulate cardiac organoids ranging from 0.5 to 1.5 millimeters in diameter. For the first time, we mapped signal propagation in spontaneously beating cardiac organoids by detecting the local activation times at individual electrodes and generating 3D isochrone maps. We validated the propagation patterns by producing 2D projections of the isochrone maps and comparing them with calcium imaging data. Additionally, we evaluated the shell MEA system on cardiac organoids treated with cardioactive drugs, such as isoproterenol, E-4031, and serotonin, and observed region-specific electrophysiological responses. This shell MEA system demonstrates significant potential for long-term monitoring of tissue-scale arrhythmic events and advancing the development of 3D compartmentalized cardiac organoids while preserving their natural self-organized structure.

ABSTRACT 8

Provable Probabilistic Imaging using Score-based Generative Priors

Yu Sun, Zihui Wu, Yifan Chen, Berthy Feng, and Katherine L. Bouman

Estimating high-quality images while also quantifying their uncertainty are two desired features in an image reconstruction algorithm for solving ill-posed inverse problems. In this paper, we propose plug-and-play Monte Carlo (PMC) as a principled framework for characterizing the space of possible solutions to a general inverse problem. PMC is able to incorporate expressive score-based generative priors for high-quality image reconstruction while also performing uncertainty quantification via posterior sampling. In particular, we develop two PMC algorithms that can be viewed as the sampling analogues of the traditional plug-and-play priors (PnP) and regularization by denoising (RED) algorithms. To improve the sampling efficiency, we introduce weighted annealing into these PMC algorithms, further developing two additional annealed PMC algorithms (APMC). We establish a theoretical analysis for characterizing the convergence behavior of PMC algorithms. Our analysis provides non-asymptotic stationarity guarantees in terms of the Fisher information, fully compatible with the joint presence of weighted annealing, potentially non-log-concave likelihoods, and imperfect score networks. We demonstrate the performance of the PMC algorithms on multiple representative inverse problems with both linear and nonlinear forward models. Experimental results show that PMC significantly improves reconstruction quality and enables high-fidelity uncertainty quantification.

ABSTRACT 9

High-dimensional droplet digital PCR of multiple hepatitis B splice variants

Tanner Grudda, Chenkai Jiang, Ashwin Balagopal, Chloe Thio

Splice variants of HBV (spHBV) in elevated proportions are associated with increased incidence of hepatic fibrosis, hepatocellular carcinoma, and decreased response to pegylated interferon α therapy. The roles of spHBV in human infection are poorly understood partly due to limitations in quantitative methods. We designed a long amplicon (0.3-2kbp) single reaction multiplex droplet digital PCR (ddPCR) assay that simultaneously quantifies the four most frequently observed spHBV isoforms (sp1, sp2, sp3, and sp9, accounting for 93% of circulating spHBV) alongside unspliced pgRNA. Our innovations include use of ddPCR, long amplicons, and high-dimensional multiplexing to create a "plug-and-play" platform for spHBV quantitation. We tested primers and probes using synthetic DNA targets to identify high-fidelity combinations for use with HBV genotype A viruses. We optimized denaturation and annealing temperatures to enrich for spHBV.

To achieve higher-order multiplexing, we tested >360 oligo probe concentration combinations to maximize sensitivity and specificity, which was further improved by increasing the number of cycles to 80 and adding a post-reverse transcription cleanup step. Because each spHBV and pgRNA measured has different-sized amplicons, we also calibrated PCR efficiencies for each target. The post-PCR fluorescence amplitude was unique for each target, allowing us to distinguish multiple mRNA isoforms in a single 2-color reaction. The optimized assay successfully quantified spHBV and pgRNA in serum, liver, and HBV infected HepG2 cells. Our assay enables direct, sensitive quantification of spHBV and full-length pgRNA from liver tissue and blood, which will facilitate studies to determine the impact of spHBV on HBV infection outcomes in people.

ABSTRACT 10

Long-acting Injectable Nanoparticle Formulation for Sustained Release of Anti-TNF-α Antibody Therapeutic in Ulcerative Colitis Treatment

Yicheng Zhang , Ling Li, Jarvis Kong, Anna Long, Sachin Kammula, Julia Lu, Florin M. Selaru, and Hai-Quan Mao

Introduction: Chronic colitis, characterized by persistent inflammation of the colonic mucosa, presents a significant burden to patients due to its recurrent nature and impact on quality of life. The therapeutic landscape has evolved with the introduction of biologics like infliximab, a monoclonal antibody against tumor necrosis factor-alpha (TNF-α), which has demonstrated efficacy in reducing inflammation and maintaining remission. However, conventional treatment regimens require frequent dosing, leading to decreased patient compliance. A delivery system that can sustain therapeutic levels of biologics over an extended period can offer significant advantages. This study seeks to develop a nanoparticle-based delivery system for infliximab to achieve a controlled release profile and sustained serum concentrations for two months in a mouse model. This delivery system can potentially reduce dosing frequency, improve patient compliance, and provide consistent disease management outcomes.

Results, Discussions and Conclusion: Through the refinement of the FNC/FNP processes, we obtained a nanoparticle formulation with an average size of ~300 nm (Fig, 1A), which exhibited a sustained release profile over a 100-day period at physiological temperature (37°C) in phosphate-buffered saline (PBS, Fig. 1B). We then loaded the NPs into hydrogel MPs to form the antibody LAI for further experiments. This LAI system can achieve tunable release rate and duration ranging from a few days to 80 days in mice (Fig. 1C). The steady state of antibody concentration in serum can be tuned between 20 and 100 ng/mL. By adjusting the antibody dose in different combinations of nanoparticles with different release profiles, the LAI formulation administered intramuscularly at two different levels (12.5 mg/kg or 30 mg/kg TNF-α antibody) in C57BL/6 mice showed an extended duration of serum concentration of antibody remained above the therapeutic threshold for around 3 months. The therapeutic efficacy of this optimized LAI treatment protocol is currently under evaluation using a chronic colitis model.

In conclusion, an injectable sustained release system for TNF-α antibody is engineered to maintain serum concentrations in mice. This system can significantly reduce the frequency of injections and potentially lower treatment cost and enhance patient compliance.

ABSTRACT 11

CR1 deficiency defines catastrophic antiphospholipid syndrome (CAPS) and response to complement inhibition

Nikhil Ranjan, Michael Cole, Gloria F. Gerber, Mark A. Crowther, Evan M. Braunstein, Daniel Flores-Guerrero, Kathy Haddaway, Alexis Reed, Michael B. Streiff, Keith R. McCrae, Michelle Petri, Shruti Chaturvedi, and Robert A. Brodsky

Background: Catastrophic antiphospholipid syndrome is characterized by widespread thrombosis leading to multi-organ failure and is associated with over 30% mortality despite best available treatment. We previously established that complement dysregulation is a pathogenic driver of CAPS and identified a germline predisposition for complement activation in nearly 50% of CAPS. Building on the finding of Complement Receptor 1 (CR1) gene variants in patients with CAPS, we investigated the functional significance of these variants, and molecular mechanisms regulating CR1 expression in CAPS.

Methods: CRISPR/Cas9 genome editing of TF-1 (erythroleukemia) cells was performed to generate CR1 "knock-out (KO)" (positive control) and "knock-in (KI)" lines with patient-specific CR1 variants. Complement-mediated cell killing was measured using the modified Ham (mHam) assay. To investigate the role of methylation in CR1 expression in patients with reduced CR1 expression without CR1 variants, we performed reduced-representation bisulfite sequencing (RRBS) of the CR1 promoter region of healthy controls and CAPS cohort.

Results: A novel germline variant (CR1-V2125L; rs202148801) led to almost complete loss of CR1 expression at transcriptional and translational levels and increased complement-mediated cell death. Erythrocyte CR1 expression by flow cytometry was reduced in 6 additional CAPS patients with a history of thrombotic storm or anticoagulant-refractory thrombosis. We further demonstrated that immune complexes influenced the degree of pathogenicity and C5 inhibition (C5i) significantly lowered the thrombotic events from 54.3 to 10.2 events per 100 patient years following the initiation of C5i therapy.

Conclusion: CR1 deficiency, due to genetic or epigenetic down-regulation identifies a subset of CAPS that is particularly responsive to C5i.

ABSTRACT 12

The Advanced Robotics and Computationally AugmenteD Environments (ARCADE) Lab

Mathias Unberath

Artificial intelligence and robotics are slated to positively transform diagnostic and interventional medicine over the next decades. With my research group, I create the discoveries that will make this future a reality. We engage in fundamental research at the intersection of medical robotics, image analysis, machine learning, and human-computer interaction to not only create the intelligent systems that will improve healthcare but also understand how key stakeholders may best leverage them for transformational benefit.

ABSTRACT 13

Neuropulse: A wearable in-ear EEG/ECG microdevice for monitoring and modulating arousal for neurological care

Alessandro Ascani Orsini, Mingfeng Cao, Pierce L. Perkins, Johnnie A. Johnson, Kevin Toralez, Prachi Agarwal, and Nitish V. Thakor

A decrease in arousal is a critical issue in various neurological injuries involving Acute Brain Injury (ABI). Current arousal monitoring devices are too bulky, slow to apply, and prone to artifact to be used in critical cases, creating an urgent need for compact, efficient tools that can monitor arousal and provide timely intervention. Neuropulse meets this need as a fully wearable in-ear device that wirelessly monitors and modulates arousal. It integrates EEG/ECG sensing with non-invasive auricular vagus nerve (AVN) stimulation, allowing real-time assessment and improvement of arousal. This study evaluates Neuropulse's ability in determining the arousal state in a rodent model. The device was tested across three levels of anesthesia (2.2%, 1.8%, 1.2% isoflurane) to demonstrate its sensitivity to different arousal states. The device records EEG/ECG signals at a 12.5 KHz sampling rate across four bipolar channels in the ear, with reference in the contralateral mastoid. EEG data estimates cortical activity changes, while ECG-derived Heart Rate Variability reflects subcortical dynamics. For high-fidelity recording, dry PDMS/PEDOT:PSS electrodes were used for better adhesion to the ear canal. Neuropulse includes a fifth custom current-controlled channel to stimulate AVN, expected to elevate arousal. Preliminary data shows that Neuropulse is able to pick up both EEG/ECG and reliably determine arousal state. Future work will focus on validating the effects of AVN stimulation on arousal. Neuropulse's ability to track arousal changes in real time through in-ear EEG and ECG, paired with AVN stimulation's therapeutic potential, highlights its clinical translatability for severe ABI cases like stroke or coma.

ABSTRACT 14

Ultrawide Property Range Thiol-Ene Photopolymers for 3D Printing

Zefang Li, Ziying Xu, Sarah Propst, Zachariah A. Page, Yun Chen, Carmel Majidi, Jochen Mueller

Multimaterial 3D printing enables the integration of materials with vastly different mechanical properties. Yet, in practice, existing multimaterial 3D printing methods are often constrained in the range of achievable properties within a single print, necessitating continued reliance on manual assembly for several applications such as soft robotics. Various material systems have been developed to address this limitation by incorporating novel chemistries and/or modifying process parameters. Complementing these advancements, we introduce a thiol-ene-based photopolymer resin for multimaterial 3D printing that broadens the achievable range of elastic modulus and hardness, spanning five orders of magnitude and two full Shore hardness scales, respectively. It is defined by two extreme materials with disparate crosslinking densities, but compatible photopolymerization mechanisms, providing access to intermediate properties upon blending. Moreover, we demonstrate continuous gradients via in situ material mixing and controlled
diffusion, even at subvoxel scales. The versatile resin is compatible with direct ink writing, vat photopolymerization, and potentially other processes like material jetting, opening opportunities in soft electronics, personal protective equipment, and biomedical implants.

ABSTRACT 15

Elevated Fucosylation and the Role of Fut1 in Asthma: A Key Contributor to Abnormal Glycosylation in Airway Epithelial Cells

Wenjing Gu, Zhifeng Chen, Rongrong Yan, Shuang Yang, Chuangli Hao, Peisong Gao

Rationale: Glycosylation, a critical post-translational modification of proteins, plays a vital role in numerous cellular functions. One of the pathological features of asthma is the excessive secretion of mucus, which is rich in glycoproteins. This study aimed to identify abnormal glycosylation in asthmatic patients and explore the underlying mechanisms contributing to these changes.

Methods: Saliva samples were collected from asthmatic and healthy children. Glycans were isolated from the saliva and analyzed using MALDI-ToF mass spectrometry. An asthma mouse model was generated using cockroach allergen (CRE), and the expression of fucosyltransferases was assessed via PCR. Further in vitro analysis of glycosylation and its related enzymes in CRE-treated epithelial cells was conducted.

Results: Glycan analysis revealed increased fucosylation of the sugars N5H3 and N5H3G2 in the saliva of children with asthma. The presence of multiple fucose residues in these glycans correlated with asthma severity, classified into mild, moderate, and severe groups. In the asthma mouse model, increased fucosylation, particularly α1,2-fucosylation, was observed in lung tissues, as demonstrated by WGA and UEA-1 staining. Additionally, Fut1 (Fucosyltransferase 1), a key enzyme in the fucosylation pathway, was found to be highly expressed in the lung tissues of the asthma mouse model and in CRE-treated airway epithelial cells.

Conclusion: This study identifies increased fucosylation, particularly α1,2-fucosylation, as a potential contributor to asthma pathogenesis. The elevated expression of Fut1 in both lung tissues and airway epithelial cells suggests a pivotal role for this enzyme in the abnormal glycosylation observed in asthma, warranting further investigation.

ABSTRACT 16

Automated Quality Assurance in Label Propagation for Large-scale Surgical Data Synthesis

Blanca Inigo, Benjamin D. Killeen, Michelle Song, Ali Uneri, Christopher Bailey, Axel Krieger, Mathias Unberath

Simulated data is essential for developing AI in surgical applications by allowing simultaneous data and label synthesis for supervised training. However, automatic label generation can introduce errors that remain undetected in large datasets, affecting quality and downstream tasks. To address this, we propose a multi-stage framework to ensure label accuracy in large-scale surgical data synthesis.

We focus on annotating the transpedicular corridor of vertebrae in 3D CT scans, crucial for simulating X-ray-guided procedures like vertebral augmentation. Our labeling pipeline includes three steps: 1) vertebral segmentation, 2) registration of a statistical shape model (SSM), and 3) transpedicular route propagation. Safeguard mechanisms are implemented at each stage, including 1) explainable AI for detecting segmentation failures, 2) learning-based identification of registration errors, and 3) detection of cortical breaches. These safeguards help detect where label propagation may fail.
In our evaluation of 1,403 thoracolumbar vertebrae from a 3D CT dataset, safeguards identified 148 segmentation errors, 276 registration errors, and 89 propagation errors. After filtering, 479 vertebrae (70%) were deemed suitable for further processing. The safeguarding techniques demonstrated high sensitivity thresholds, validated by manual inspections and quantitative assessments on test splits.

The proposed framework for automated label propagation with safeguards reliably annotates CT data for large-scale X-ray image synthesis. Future work will focus on improving annotation safeguards for pathologic anatomy and developing performance estimates for large datasets where manual review is not feasible.

ABSTRACT 17

Baseline Sex Hormone Binding Globulin Level Modifies Intensive Lifestyle Intervention Effect on Blood Pressure in Post-Menopausal Females

Jiahuan Helen He, Jianqiao Ma, Mark Woodward, Erin Michos, Chigolum P. Oyeka, Rita R. Kalyani, Jeanne M. Clark, Dhananjay Vaidya, Wendy L. Bennett

Background: The Look AHEAD (Action for Health in Diabetes) randomized controlled trial showed that Intensive Lifestyle Intervention (ILI) targeting weight loss caused greater reductions in systolic and diastolic blood pressure (SBP and DBP) than Diabetes Support and Education (DSE) in patients with body mass index (BMI) ≥25 kg/m2 and type 2 diabetes (T2D). Nonetheless, treatment assignment alone did not explain the individual variations in BP improvement. We hypothesize that baseline sex hormone binding globulin (SHBG), which is inversely associated with hypertension in both males and females, might modify the effect of ILI on BP.

Methods: We selected a random sample of 1167 post-menopausal females and 1167 males from the Look AHEAD trial in our analysis. We retained the randomized design and created sex-stratified linear mixed models to examine whether log-transformed baseline SHBG levels modify the treatment effects (i.e., absolute difference between ILI and DSE) on SBP and DBP reduction after 1 year, adjusting for age, race, study site, baseline BMI and use of anti-hypertensive medications.

Results: In our study sample (age: 60.0 [SD, 6.2] years; 14.8% black; 50% female), median [IQI] baseline SHBG levels were 32.9 [22.2-54.0] nmol/L in females and 29.0 [19.9-44.8] nmol/L in males. Mean (SD) baseline SBP and DBP were 130 (17.3) and 67.6 (9.2) mmHg for females, 128.6 (16.3) and 73.1 (8.9) mmHg for males. Females with 2-fold higher baseline SHBG had 3.0 (95%CI: 1.0, 5.0) mmHg and 1.3 (95%CI: 0.3, 2.2) mmHg greater reduction in SBP (Figure, panel A) and DBP (panel B), respectively, due to ILI compared to DSE. However, treatment effects in males did not vary significantly with baseline SHBG (heterogeneity p-values: 0.81 SBP, 0.98 DBP).

Conclusion: Females with higher baseline SHBG had more BP lowering due to ILI, compared to DSE, but this effect was not seen in males. Future research is needed to confirm if baseline SHBG can identify female patients with T2D who benefit most from ILI, and to determine whether those with low SHBG levels need more aggressive BP management in combination with ILI.

ABSTRACT 18

Machine-Learning Based Model Accurately Identifies the Probability of Choledocholithiasis and Provides a Personalized Management Plan

Arpita N. Jajoo, Babak Moghadas, Jianing Li, Mohammed Rifat Shaik, Nirav Agrawal, Meher Gujral, Melody Tu, Navdeep Singh, Viswanadh Polana, Aditya Chandrashekar, Abhinav Jha, Pranay Marlecha, Sweta Sahu, Sukhmanpreet Sandhu, Grace Rozycki, Alistair J Kent, Ivy Mannoh, Paul Martin, Mouen Khashab, Brian S. Caffo, Venkata S. Akshintala

Background: Current guidelines for predicting choledocholithiasis (CDL) have suboptimal accuracy, leading to diagnostic uncertainty and overutilization of endoscopic retrograde cholangiopancreatography (ERCP). Improved predictive models could help triage patients to lower-risk, cost-effective interventions.

Methods: A gradient boosting machine model was developed to predict CDL using presenting clinical features. The model was trained on cases from Johns Hopkins hospitals and community centers and evaluated for accuracy using 10-fold cross-validation and area under the receiver operating characteristic curve (AUC). Missing values were addressed via nearest-neighbor imputation. A decision-making tool was created to guide management based on CDL probability, triaging low-risk patients to cholecystectomy with intra-operative cholangiogram (CCY + IOC), intermediate-risk patients to magnetic resonance cholangiopancreatography (MRCP), intermediate-high-risk patients to endoscopic ultrasound (EUS), and high-risk patients to ERCP.

Results: The model included 2342 patients (mean age 56.7 years, 61% female, 46% with CDL). Key predictors of CDL included bilirubin and liver enzyme elevations, imaging findings, and patient demographics. The model achieved 86% accuracy, 85% precision and an AUC of 95% in identifying CDL. It missed only 0.5% of common bile duct (CBD) stones by suggesting CCY + IOC. It assigned only 3% of non-CDL patients to ERCP, compared to 13.8% using ASGE 2019 guidelines.

Conclusions: This machine learning model offers individualized risk assessment for CDL and guides clinical management, improving upon existing guidelines. Risk-stratification enhances triage, reducing procedural morbidity from unnecessary ERCPs and promoting cost-effective, high-value care for patients with biliary disease.

ABSTRACT 19

Demystifying Large Language Models for Abstract Screening for Systematic Reviews

Shanshan Lin, Ravi Gupta, Renee Wilson, Michael DiStefano, Halima Amjad, Jacqualine Woo, Emily Mao, Emmanuel Drabo, Jodi B. Segal

Background: Large language models (LLMs) offer potential for streamlining systematic reviews by automating abstract screening at low cost. To demonstrate this, we used ChatGPT in an ongoing systematic review on patient preferences for dementia interventions (PROSPERO #CRD42024601055), focusing on evaluating different prompting strategies.

Methods: We created a dataset of 979 abstracts screened by two independent reviewers, selecting 150 excluded and 50 included abstracts. We employed a zero-shot learning technique with GPT-4o-mini and developed three prompts with increasing complexity, including the screening goal, inclusion and exclusion criteria, and additional instructions. We iteratively refined the final prompt (Prompt 4) to maximize the sensitivity. We tested each prompt five times for cross-validation, and applied the most sensitive prompt to the full dataset, evaluating sensitivity, specificity, positive and negative predictive values (PPV and NPV), and Matthew's correlation coefficient (MCC).

Results: Prompt 1 (goal, inclusion and exclusion criteria) had the highest specificity (0.94) and PPV (0.68) at threshold 1.0 across all prompts. Prompt 2 (goal, inclusion and instructions) had a sensitivity of 0.56 and specificity of 0.82 at threshold 1.0. Prompt 3, which included all components, had the highest MCC (0.81 sensitivity, 0.71 specificity). Prompt 4, refined from Prompt 3, achieved the highest sensitivity (0.92) and included 116 abstracts at a 1:5 threshold. Sensitivity ranged from 0.74 to 0.86 and specificity from 0.55 to 0.74 when applied to the full dataset, resulting in 491 abstracts (50%) included.

Conclusions: LLM, with a well-designed prompt strategy, is a useful tool for abstract screening, reducing our abstract screening workload by 50% for $10.

ABSTRACT 20

Dietary quality among pregnant people with overweight/obesity: comparison between randomized controlled trial participants in early pregnancy with non-pregnant NHANES matched participants

Tianxu Chen, Christine McKinney, Emmanuel Fulgence E, Nae-Yuh Wang, Lindsay Martin, Divya Nair, Nowella Durkin, Janelle Wilder Coughlin, Mostafa Borahay, Wendy Bennett

Poor dietary quality is associated with perinatal obesity, including excess gestational weight gain, a risk factor for future cardiometabolic disease. Despite the need to assess and intervene on dietary quality in pregnancy, few studies have identified convenient dietary screeners with comparable performance in the general population. This study sought to describe the dietary patterns of participants in early pregnancy using the Dietary Screener Questionnaire (DSQ) and compare the results with a matched respondent sample from the 2009-2010 wave of the National Health and Nutrition Examination Survey (NHANES) to demonstrate the external validity of the DSQ results. Baseline DSQ responses were collected at ≤ 15 weeks of gestation from an ongoing randomized controlled trial (RCT) to assess the effectiveness of a remote lifestyle intervention targeting dietary quality on gestational weight gain. Matched non-pregnant controls were selected from NHANES by age (20-44), sex (female), BMI (≥ 25), and complete DSQ data. We estimated daily intake of added sugar (total and from sweetened beverages), fiber, fruits and vegetables, and dairy using the standard scoring procedures and compared the samples using the Mann-Whitney U test. This study identifies similar dietary patterns of RCT participants in early pregnancy and matched non-pregnant NHANES 2009-2010 participants, except for sugar intake, indicating that the DSQ screener and its results may be useful for and generalizable to a broader population. The lower intake of added sugar, particularly from sweetened beverages, may reflect changes in early pregnancy or secular trends in the last 15 years.

ABSTRACT 21

Expansion of neoantigen-specific patient T cells using neoepitope-based artificial antigen-presenting cells

Emily Ariail, Sojung Kim, Mathias Oelke, Jonathan Schneck

Immunotherapies utilizing patient-derived tumor neoepitopes have begun to gain attention in the field of oncology and represent the future of personalized cancer treatments. However, there are many barriers to therapeutic development of neoepitopes, including challenges with their selection and immunogenicity and a lack of modular treatment platforms for incorporation of these peptides. We have previously developed artificial antigen-presenting (aAPC) nanoparticles that present peptide-MHC complexes and anti-CD28 antibodies for the expansion of antigen-specific cytotoxic T cells. Herein, we have demonstrated a workflow for selecting patient-specific neoepitopes and applying them to aAPC's for expansion of tumor-specific patient CD8+ T cells. We first validated the ability of our aAPCs to expand healthy donor T cells to MART1 and EBV peptides. Then, tumor sequencing and HLA-profiling data for a stage IV lung cancer patient was performed and we identified candidate HLA-A24-restricted neoepitopes. Twenty-six candidate peptides were screened using three independent healthy donor T cells. We utilized this information on immunogenicity, as well as IC50 values from NetMHC predictions, to choose a cocktail of 5 neoepitopes that were loaded on to aAPCs. This aAPC cocktail was used to successfully expanded patient-derived T cells to 4/5 of the chosen neoepitopes including a P53-neoptiope specific mutation. These cells are currently being analyzed using single cell sequencing for phenotype and TCR verification. This work demonstrates that healthy donor responses may be used to predict neoantigen immunogenicity in patients and validates that our aAPC platform can be translated for the expansion of CD8+ T cells for patient-specific cancer immunotherapy.

ABSTRACT 22

Transcription Regulatory Networks Driving Proliferative Cell State Transitions in The Kidney Distal Convoluted Tubule

Hyun Jun Jung, Boyoung Kim, Mohammed Ferdaus, Lama Al-Qusairi, Eric Delpire, Paul A. Welling

Cell-cell interactions and cell-extracellular matrix (ECM) interactions regulate cellular homeostasis in tissue and organ development, and dysregulation can result in disease. A variety of cell and tissue culture systems are commonly used to study these physiological and pathological processes; however, two-dimensional (2D) culture systems enable only partial capture of cell-cell interactions. The cellular heterogenicity, in situ architecture, and mechanical functions of the tissue microenvironment can only be accurately recapitulated in vitro using 3D systems, such as organoids. However, many organoid models are also limited to one cell type in one ECM or artificial cocultures of multiple cell types in the same ECM, which do not match the tissue anatomy. Many organoid models also experience significant size variation between organoids and introduce non-physiological crosstalk between organoids that form within the same well. Here, we present a protocol for generating multi-compartment assembloids, which are organoid models that incorporate multiple cell types and ECMs to match the tissue structure. The resulting assembloids are size-consistent, spatially controlled by the compartmentalized seeding of cells and ECM, and individually isolated to avoid organoid-organoid crosstalk. Realistic substrate stiffness, cell-ECM adhesion, and 3D cell interactions allow this assembloid model to accurately capture the architectural, molecular, and functional expression patterns of healthy tissues. Our protocol offers a robust alternative for modeling healthy and diseased tissues as a bridge between 2D cell culture and animal models.

ABSTRACT 23

Sleep Apnea in Persons Receiving Medication for Opioid Use Disorder (MOUD)

H. Elizabeth Bird, Patrick Finan, Ariel Hoadley, Eric C. Strain, Charlene Gamaldo, Andrew S. Huhn

Background: Chronic opioid use is associated with sleep disordered breathing and is a risk factor for central sleep apnea. This post hoc analysis compared sleep apnea in methadone and buprenorphine-maintained OUD patients.

Methods: Opioid treatment program patients were recruited to a clinical trial and underwent an ambulatory Type 3 sleep study (via Nox T3) during enrollment. Data included total apnea-hypopnea index (AHI) including central and obstructive apneas and hypopneas.

Results: Participants were maintained on buprenorphine (any dosage form, n=52) or oral methadone (n=87); 59% were female, mean (standard deviation) age was 45.2 (10.8) years, and BMI was 30.6 kg/m2 (6.5). Self-reported race was 57.6% white, 35.3% black/African American, 5.8% >1 race, and 1.4% American Indian, with 2.9% Hispanic background of any race. The unadjusted odds of at least mild sleep apnea (AHI≥5) were nearly 4 times higher in methadone versus buprenorphine patients (OR=3.97, 95% CI=1.92-8.20). The relative risk of severe apnea (AHI≥30) compared to non-clinical apnea (AHI<5) was over 4 times higher for methadone versus buprenorphine patients (RRR=4.16, 95% CI=1.21-14.33). Five individuals had central sleep apnea (≥5 central apneas/hour with central apnea accounting for >50% of the total AHI score); all were on methadone. Clinically-significant obstructive sleep apnea (AHI≥15 without a central apnea diagnosis) was evident in 25% of the sample, and did not significantly differ by MOUD (OR=1.42, 95% CI=0.63-3.21).

Conclusions: Methadone patients were more likely to present with severe and central sleep apnea versus buprenorphine patients. Obstructive sleep apnea was prevalent among both methadone and buprenorphine-maintained individuals.

ABSTRACT 24

Integrating Clinical Decision Support Tools in Chronic Kidney Disease Management

C. Elena Cervantes, Heather Thiessen Philbrook, Dipal Patel, Jack Bitzel, Steven Menez, Bernard Jaar, Morgan Grams, Chirag Parikh

Integrating clinical decision support (CDS) tools into nephrology outpatient clinics offers an opportunity to enhance patient care by utilizing electronic medical records (EMR) data. This study evaluated the implementation and impact of three CDS tools at Johns Hopkins nephrology clinics: (A) "Patient Insight," a longitudinal EMR viewer, (B) KFRE (Kidney Failure Risk Equation) on the EMR dashboard, and (C) KFRE dotphrase for clinic notes. These tools provide information on evidence-based therapies and risk scores to guide treatment decisions.

The study analyzed clinical practices before (2020–2021) and after (2022–2023) implementing these tools in patients with advanced kidney disease (eGFR < 30 mL/min/1.73m² or 2-year KFRE > 10%), including a subgroup with diabetes. Medication records were categorized using the Unified Medical Language System (UMLS) to identify therapy classes.

Results showed significant engagement, with over 70% of nephrology providers accessing Patient Insight for more than 500 patients. Clinical practices improved, evidenced by increased prescription rates of therapies to reduce proteinuria and slow disease progression: ACEi/ARB (66% to 70%), SGLT2i (15% to 30%), MRA (11% to 14%), and GLP-1 (10% to 15%). Additionally, the KFRE dotphrase was incorporated into 25% of clinic notes, and albuminuria measurement rates improved.

While CDS tools demonstrated their potential to align practices with guideline-based care, limitations included reliance on EMR data and the inability to assess medication adherence. Further research is needed to elucidate the mechanisms by which CDS tools influence clinical behavior and outcomes.

ABSTRACT 25

Symmetric Bistability in 3D-Printed Metastructures via Programmed Thermal Buckling

Kaveh Barri and Jochen Mueller

Bistable mechanisms, known for their ability to maintain two stable positions without energy consumption, are highly suitable for applications demanding long-term stability. However, traditional 3D-printed bistable structures often suffer from asymmetric minimum potential energy levels at their stable states due to geometric biases introduced during fabrication. This asymmetry typically favors the printed state, creating a natural tendency for the structure to revert to it. This study presents a novel fabrication approach for monolithically 3D-printed bistable structures featuring symmetric geometry and balanced potential energy. The key innovation lies in harnessing residual stress through a combination of UV post-curing and a tailored thermal cycle, leveraging the viscoelastic behavior of the material. This process induces precisely controlled residual stress throughout the structure, enabling the design of bistable mechanisms that utilize elastic buckling. This approach allows for tunable deformation and adjustable switching load amplitude between stable states through precise geometric configurations. Experimental studies, complemented by comprehensive finite element analysis, confirm the mechanical reliability and robustness of the proposed method. This innovative fabrication process unlocks the potential for creating bistable and multistable meta-structures with complex geometries, offering diverse applications in robotics, automotive engineering, prosthetics, orthotics, energy absorption, morphing matter, and other fields that demand symmetric bistable mechanisms with equal switching load amplitudes.

ABSTRACT 26

Lipid nanoparticle-mediated nucleic acid delivery for microvascular endothelial cell metabolic modulation

Autumn Greco, Jinghan Lin, Leonardo Cheng, Nicolas Philip, Hai-Quan Mao, Karthik Suresh

IMPORTANCE: Fever of unknown origin (FUO) and inflammation of unknown origin (IUO) continue to be commonly utilized medical diagnoses. Given the existing literature does not address the optimal contemporary diagnostic structures and evaluation processes for these conditions, developing a consensus set of recommendations would be useful for clinicians, researchers, and patients around the world.
OBJECTIVE: To develop expert-driven consensus recommendations on needed FUO and IUO research, clinical practice, education, and advocacy based on a modified Delphi technique.

EVIDENCE REVIEW: A 5-round modified Delphi process with data analysis was performed from October 2022 to July 2023. The process used an iterative Delphi technique and involved 4 rounds of online surveys and 2 live video conferences to achieve consensus among an expert member panel. RedCap, an online survey approach to conducting modified Delphi panels, was used. This panel consisted of international experts in adult fever and inflammation of unknown origin, or both, recruited by email from lists of prior peer-reviewed published studies and focused professional groups.

FINDINGS: Of 50 invited experts, 26 (52.0%) agreed to participate in the panel. Twenty-three panelists completed the first round of the survey, 21 completed round 2 and 3 of the survey, 20 completed round 4, and 7 participated in the round 5 live video discussions. Female panelist (n=6) completed all survey rounds. Consensus was reached on high-priority statements within 5 themes: (1) epidemiology (e.g., geographical location and travel history), (2) minimal diagnostic defining criteria, (3) evaluation, (4) classification of associated diseases, and (5) empirical therapy (e.g., antimicrobials, corticosteroids, and anti-inflammatory agents). Experts strongly disagreed with use of 18FDG-PET/CT as an important component of the diagnostic criteria for FUO. Moderate agreement was reached on the topics of importance to the site of temperature measurement, 3-week time-based criterion, need for a standard definition of relapsing fevers, and use of similar diagnostic approaches for both conditions.

CONCLUSIONS AND RELEVANCE: The findings of this qualitative study provide consensus-based recommendations for clinicians and highlight research gaps important to clinical care in FUO and IUO that are highly pragmatic as a guide for practice and research.

ABSTRACT 27

Reducing Payload Heterogeneity in Lipid Nanoparticles for RNA-Based Therapeutics

Turash Haque Pial, Sixuan Li, Jinghan Lin, Tza-Huei Wang, Hai-Quan Mao, Tine Curk

Lipid nanoparticles (LNPs) are a leading platform for RNA-based therapeutics. However, their self-assembly process often results in heterogeneous compositions and a bimodal RNA loading distribution, with a significant proportion of empty LNPs. This payload variability can impact therapeutic efficacy, reducing transfection efficiency and potentially triggering immune responses. To improve the potency and safety of LNP-RNA therapeutics, precise control over LNP composition is crucial. In this study, we employ molecular dynamics, kinetic Monte Carlo simulations, and ensemble machine learning to investigate LNP formation and RNA payload distribution, with experimental validation through single-particle fluorescence microscopy. Our results show that heterogeneous RNA loading is caused by slow diffusive mixing compared to lipid assembly kinetics. We demonstrate that optimized turbulent mixing reduces empty LNPs and narrows RNA payload distribution without altering LNP size. Additionally, changes in salt concentration and PEGylated lipids affect RNA loading in a volume-dependent manner. These findings provide essential design principles for optimizing LNP-based RNA therapeutics, highlighting the importance of mixing kinetics and the energy barrier for LNP fusion. The methods developed also offer valuable tools for optimizing biomolecular assembly processes.

ABSTRACT 28

Delineo disease modeling: small-town interactive disease simulation

Mahmoud Said, Allen Gong, Emmett Springer, Hajin Jang, Iason Mihalopoulos, Jeff Cui, Jin Hong Moon, Keeyan Mukherjee, Lixing Wu, Michelle Wang, Navya Mehrotra, Neil Patel, Ryan Lu, Sanghyup Lee, Scott Klosen, Siva Indukuri

The Delineo project is a disease simulator that focuses on realistic disease infection modeling on a smaller scale than traditional disease models or simulations. Rather than focusing on world-wide pandemic or nationwide modeling, Delineo instead focuses on modeling small, precomputed geographic areas marked as "convenience zones," where the focus is to maximize the population movement within each zone and minimize the movement coming in and out of the zone. This allows for much more efficient and resource-efficient modeling on specific communities, as the maximized isolation allows for each zone to be simulated separately without having to consider foreign sources of disease infection entering from outside the community. From the Delineo website, users are able to customize disease and population parameters to their own specification and run realistic small-scale simulations, all within their browser.

ABSTRACT 29

GLP-1 Receptor Agonists Rarely Cause De-Novo Acute Pancreatitis But May Cause Serum Lipase Elevations Of Unclear Clinical Significance

Li, Jianing; Chandrashekar, Aditya; Ravikumar, Richu; Denishya Prabhakaran, Saju; Krishnan, Gokul; Chowdhury, Reezwana; Afghani, Elham; Singh, Vikesh; Akshintala, Venkata Sandeep

Background: Pancreatic acinar cells express GLP-1 (Glucagon like peptide-1) receptors in addition to beta cells, yet the impact of GLP-1 receptor agonists (RAs) on the exocrine pancreas remains controversial, particularly regarding acute pancreatitis (AP). Conflicting reports have restricted GLP-1 RA prescriptions, potentially preventing certain patients from benefiting. This study investigates the causal relationship between GLP-1 RAs and AP, adjusting for known risk factors and exploring underlying mechanisms.

Methods: Using the Prospective Pancreatitis database, we identified patients with lipase ≥3 times the upper limit of normal (ULN) from December 2020 to October 2024 who were on GLP-1 RAs. Clinical data, imaging, and laboratory results were reviewed. AP diagnosis required clinical features and imaging confirmation within 48 hours of lipase elevation. For patients with AP and GLP-1 RA use, underlying etiologies were determined. Pancreatic volume changes were compared among patients with and without lipase elevation using abdominal CT scans.

Results: Of 2,600 patients with lipase ≥3 times ULN, 53 were on GLP-1 RAs (49.05% female, mean age 55.23±14.04 years). Imaging confirmed AP in 21 (40.4%) patients, with most cases attributed to gallstones, hypertriglyceridemia, alcohol, trauma, genetics, or post-ERCP. Only 6 cases (28.6%) lacked a clear etiology, possibly linked to GLP-1 RAs. Pancreas volume increased in 80% of hyperlipasemia patients with imaging before and after GLP-1 RA initiation, suggesting acinar cell hypertrophy/hyperplasia.

Conclusion: Most patients on GLP-1 RAs with lipase elevation do not have AP, and the safety profile of GLP-1 RAs regarding the exocrine pancreas is favorable. Hyperlipasemia-associated acinar cell changes merit further investigation.

ABSTRACT 30

Baseline Androgenic State Modifies the Effect of Intensive Lifestyle Intervention on Triglyceride Levels in Males with Diabetes: The Look AHEAD Trial Sex Hormone Study

Jianqiao Ma, Jiahuan Helen He, Mark Woodward, Erin D. Michos, Chigolum Pamela Oyeka, Rita R. Kalyani, Jeanne M. Clark, Wendy L. Bennett, Dhananjay Vaidya

Background: In people with type 2 diabetes (T2D), weight loss due to an intensive lifestyle intervention (ILI) reduces triglyceride (TG) levels, a risk factor for cardiovascular disease. However, efficacy of treatment varies between people. Both testosterone and estradiol are associated with TG level. We examined whether baseline androgenic state, i.e., the ratio of testosterone to estradiol (T/E), modifies the treatment effect and partially explains the TG variability.

Methods: The Look AHEAD Study was a randomized control trial of 5145 individuals with T2D and overweight/obesity to evaluate the effect of ILI compared to the control group on cardiovascular outcomes. We selected a random sample of 1166 postmenopausal females and 1166 males (mean age 60 years [SD 6.2]) to examine heterogeneity of treatment effect by baseline T/E ratio on changes in TG at years 1 (weight loss nadir) and 4. We created longitudinal mixed models stratified by sex, and modeled the interaction between log-transformed baseline T/E ratio, ILI (vs control), and year, with log-transformed TG as the outcome. We plotted the estimated treatment effects over time for 25th and 75th percentile of baseline T/E ratio.

Results: Figure, panel A, shows that males with T/E ratio at the 75th percentile (vs 25th percentile) had a larger reduction in TG due to ILI (vs control) at year 1 ($p = 0.002$), which is no longer statistically significant at year 4 ($p = 0.14$, overall heterogeneity for both years, $p = 0.009$). We did not detect any statistically significant heterogeneity in TG levels by T/E ratio for females (panel B, $p = 0.87$).

Conclusion: Greater baseline androgenic state (T/E ratio) in males, but not females, was associated with a larger reduction in TG due to ILI, compared to the control at year 1 but not year 4. Males with lower T/E ratio might need more aggressive lipid treatment to achieve TG-reducing benefits of ILI.

ABSTRACT 31

GenEx: Generating an Explorable World

Taiming Lu, Tianmin Shu, Junfei Xiao, Luoxin Ye, Jiahao Wang, Cheng Peng, Chen Wei, Daniel Khashabi, Rama Chellappa, Alan L. Yuille, and Jieneng Chen

Understanding, navigating, and exploring the 3D physical real world has long been a central challenge in the development of artificial intelligence. In this work, we take a step toward this goal by introducing GenEx, a system capable of planning complex embodied world exploration, guided by its generative imagination that forms priors (expectations) about the surrounding environments. GenEx generates an entire 3D-consistent imaginative environment from as little as a single RGB image, bringing it to life through panoramic video streams. Leveraging scalable 3D world data curated from Unreal Engine, our generative model is grounded in the physical world. It captures a continuous 360◦ environment with little effort , offering a boundless landscape for AI agents to explore and interact with. GenEx achieves high-quality world generation and robust loop consistency over long trajectories, and demonstrates strong 3D capabilities such as consistency and active 3D mapping. Powered by the generative imagination of the world, GPT-assisted agents are equipped to perform complex embodied tasks, including both goal-agnostic exploration and goal-driven navigation. These agents utilize predictive expectations regarding unseen parts of the physical world to refine their beliefs, simulate different outcomes based on potential decisions, and make more informed choices. In summary, we demonstrate that GenEx provides a transformative platform for advancing embodied AI in imaginative spaces and brings potential for extending these capabilities to real-world exploration.

ABSTRACT 32

Myoblast therapy ameliorates chronic skeletal muscle denervation atrophy

Shaquielle Dias, William Padovano, Chenhu Qiu, Emma Rowley, Thomas Harris, Erica Lee, Eszter Mihaly, Xiaoya Julia Lu, Dallas Altamirano, Hai-Quan Mao, Warren Grayson, Sami Tuffaha

Approximately 2% of all traumatic extremity injuries are associated with a nerve injury, with up to two-thirds of these injuries being untreated or undiagnosed at initial discharge from the hospital. Many of these patients fail conservative delayed surgical repair and have a persistent functional deficit for which there is no available treatment. This limited functional recovery is thought to be due to significant skeletal muscle atrophy during nerve regeneration, resulting in poor muscle targets for reinnervation. Despite the robust expansion of muscle stem cells during this period, chronically denervated muscle fails to recover. We hypothesized that targeted delivery of syngeneic myoblasts will reverse chronic denervation atrophy in a translational rodent forelimb model by supporting myoblast engraftment and myogenesis. Myoblasts were delivered in either saline or a nanofiber hydrogel composite (NHC) loaded with agrin and insulin-like growth factor 1 (IGF-1) nanoparticles. Irrespective of the delivery vehicle, satellite cell-rich myoblast therapy caused sustained improvement in stimulated grip strength beyond the reduced functional plateau caused by chronic denervation. Histological evaluation demonstrated the reversal of whole muscle atrophy, increased mean myofiber cross-sectional area, the fraction of regenerating fibers (centrally nucleated fibers), and reduced fibrotic deposition. Correlation analysis demonstrated functional improvements were driven by increased myofiber cross-sectional area. Taken together, this data indicates that targeted administration of syngeneic myoblasts can reverse skeletal muscle atrophy chronically after nerve injury.

ABSTRACT 33

The DCT2/CNT is the Major Site of Regulated ROMK-Mediated K+ Secretion

Lama Al-Qusairi, Celio Damacena de Angelis, Richard Coleman, Kyriakos Papanicolaou, Brian O'Rourke, Paul A. Welling

The Renal Outer Medullary potassium channels (ROMK) are major potassium exit channels in the distal nephron. The Textbook view presents the Collecting Duct (CD) as the chief site of regulated potassium (K+) secretion mediated by ROMK. This view is challenged by recent studies showing the Late Distal Convoluted Tubules (DCT2) and the Connecting Tubules (CNT) are the main sites of ROMK action. To settle the debate, we developed the first nephron segment-specific DCT2/CNT ROMK knockout (KO) mouse using the novel DCT/CNT Cre-driver, Emx1.

ROMK flox/flox, Emx1 Cre-positive (ROMKDCT2/CNT KO, n=6) and Wild-type ROMK wt/wt, Emx1 Cre-positive (ROMK Control, n=6) were randomized to standard (1%K+) or high K+ (HKD: 5%K+) diets for 2 days. Urinary K+ excretion was examined using metabolic cages. Blood electrolytes and protein levels of key components of the K+ secretion machinery were analyzed under both standard and HKD.

Using immunofluorescence imaging of ROMK and segment-specific markers, we confirmed specific ROMK deletion in the DCT2/CNT while ROMK in the Thick Ascending Limb (TAL) and the CD remained unaffected. In contrast to total ROMK KO mice, ROMKDCT2/CNT KO mice did not exhibit a Bartter syndrome phenotype and hydronephrosis. Instead, ROMKDCT2/CNT KO mice fed the standard K+ diet, exhibited higher plasma K+ than control mice (4.5 versus 3.8 mmol/L in KOs and controls, respectively; p-value: 0.02) and diminished urinary K+ handling despite a compensatory reduction in NCC. On HKD, ROMKDCT2/CNT KO mice became hyperkalemic (6.3 versus 4.6 mmol/L in KOs and controls, respectively; p-value: 0.009). Despite the hyperkalemia, K+ excretion in the KO was significantly reduced compared to the control mice. Western blot analysis revealed that total NCC was severely reduced in the hyperkalemic KO compared to the normokalemic control mice. Additionally, ENaC full-length and cleaved forms were higher in the KO compared to control mice, likely reflecting a secondary response to the hyperkalemia and the expected increase of Aldosterone.

In conclusion, ROMK in the DCT2/CNT plays a key role in regulated K+ secretion. On standard K+ intake, mice lacking ROMK in this segment can partially compensate for ROMK deletion by reaching a new balance with higher plasma K+ and lower NCC levels. On high K+ intake, ROMKDCT2/CNT KO became hyperkalemic due to blunted K+ secretion despite the presence of ROMK in the CD, indicating DCT2/CNT is the chief site of ROMK-mediated K+ secretion.

ABSTRACT 34

HIV decreases both hepatitis B antibody titer and neutralization after spontaneous HBV control

Che-Min Lo, Maraake Taddese, Ernesto T. Marques, Mallory D. Witt, Steven M. Wolinsky, Eric C. Seaberg, Justin R. Bailey, Chloe L. Thio

HIV increases the risk of hepatitis B virus (HBV) reactivation after spontaneous HBV control (SC), which we hypothesized was due to differences in HBV-specific antibody responses between people with HIV (PWH) and people without HIV (PWoH).

We studied stored sera from 136 males (98 PWH, 38 PWoH) in the MACS/WIHS Combined Cohort Study with documented incident HBV and SC at their first HBsAg negative visit (v1), six months after v1 (v2), and 24 months after v2 (v3). Sera were assessed for (i) anti-HBs titer (EIA) and (ii) neutralization capacity using HepG2-NTCP HBV infection system. Neutralizing antibody (NAb) responses were quantified by area under the neutralization curve (AUC). Correlations were assessed using Spearman's rank correlation. Comparisons were made using Generalized Estimating Equations model in R (geepack). Statistical significance $p< 0.05$.

Age was similar in PWH and PWoH (median (yr); IQR) 31 (26-39) and 35 (30-43), respectively). Baseline CD4 count (cells/mm^3) (median; IQR) was 506 (400-679) for PWH and 958 (766-1,210) for PWoH (P=2.2e-08). HIV viral load (VL) (copies/ml) (median; IQR) at v1 was 11,235 (1,386 -25,278) with 4 receiving ART. At v1, anti-HBs titers were similar between PWoH and PWH. However, at v2 and v3, titers were significantly higher in PWoH compared to PWH ($p \leq 0.001$). In PWoH, titers increased from v1 to v2 and v3 ($p = 1.6e-06$) (mean increase of 0.31 units/yr) whereas titers in PWH declined (0.11 units/yr) (P comparing trends in PWH and PWoH = 5.1e-07). A cutoff of 10,000 HIV copies/ml was used to stratify PWH into high (H) and low (L) VL groups. Anti-HBs titers were significantly higher at v1 in the L vs H VL group ($p < 0.001$). Over time, a significant mean decrease in anti-HBs titers was only seen in the H VL (0.1 units/year ($p = 0.04$)) (Figure). In general, NAb AUC correlated with anti-HBs titers in PWH and PWoH with strongest correlation at v1 in both groups (PWoH rs = 0.79, PWH rs = 0.81, $p < 0.001$). The NAb AUC was significantly higher in PWoH than PWH at v1 ($p < 0.01$), v2 ($p < 0.001$), and v3 ($p < 0.001$). Amongst PWH, CD4 count and ART use did not affect titer or NAbs.

Over the first 30 months after HBV SC, PWoH have a stronger anti-HBs and HBV NAb response than PWH, which may explain the increased risk of HBV reactivation in PWH. Notably, rising anti-HBs titers in PWoH suggest ongoing sAg stimulation. The mechanism underlying the association of high HIV VL with declining anti-HBs requires further study.

ABSTRACT 35

Optimizing Orthopedic Implants: Processing Mg-Ca Alloys for the Advancement of Biodegradable Bone Fixation Devices

Andrew Kim, Sreenivas Raguraman, Adam Griebel, Timothy Weihs

Biodegradable magnesium alloys have gained significant recognition as promising materials for orthopedic implants due to their exceptional mechanical properties that closely mimic those of human bone, combined with their biocompatibility and ability to naturally degrade into the body. These properties place magnesium alloys as superior alternatives to conventional permanent implant materials including titanium and stainless steel. Despite these advantages, their clinical application is hindered by rapid corrosion, which compromises their mechanical integrity and limits their practical use. Addressing this challenge requires the development of material processing strategies and alloying approaches that simultaneously reduce degradation rates and maintain mechanical performance, paving the way for the successful development and implementation of biodegradable bone implants. Recent FDA approval of lean magnesium alloy screws for bone fixation, such as RemeOs developed by Bioretec, highlights the growing interest and clinical potential of these materials for medical applications. Building on this progress, binary magnesium-calcium (Mg-Ca) alloys present a compelling alternative, as calcium not only supports bone regeneration but offers the potential for controlled corrosion behavior. This study explores the effects of various processing techniques on lean Mg-Ca alloys, evaluating their corrosion resistance and mechanical properties to advance the development of next-generation biodegradable orthopedic materials.

ABSTRACT 36

Voxel interface control in multimaterial extrusion 3d printing

Daniel C. Ames, Sarah Propst, Aadarsh Shah, Jochen Mueller

Interfaces are crucial in natural and engineered systems, dictating essential biological, ecological, and technological properties that augment performance, functionality, and user experience. Yet, achieving precise interfacial control poses significant challenges in both conventional and additive manufacturing, where scalability constraints impede the controlled deposition of quasi-2D layers within 3D objects. We introduce Voxel-Interface 3D Printing (VI3DP), which enables comprehensive control over extruded voxel interfaces irrespective of the printhead diameter that conventionally dictates feature size. VI3DP can seamlessly fabricate multimaterial filaments and interfaces in a single process. Notable applications include creating tight fits and movable mechanisms through non-adhesive interfaces, fabricating bio-inspired composites with tailored failure modes, and a single filament capacitive touch sensor. VI3DP opens new avenues for enhanced functionality and efficiency across multiple fields, including biomedical technology, electronics, optics, and nanotechnology.

ABSTRACT 37

Regulation of LOXL2 by nitric oxide in the vasculature

Helen Wang, Marta Martinez Yus, and Lakshmi Santhanam

Introduction: Vascular stiffening is a critical factor in cardiovascular system degradation, advancing the progression of cardiovascular diseases (CVD), the predominant cause of mortality worldwide. This condition stems from the aging of vascular tissues, characterized by endothelial dysfunction and diminished nitric oxide (NO) availability, causing detrimental changes in cellular dynamics and vascular architecture. This study targets lysyl oxidase-like 2 (LOXL2), a matrix-remodeling enzyme that crosslinks collagens, where increased LOXL2 expression promotes matrix stiffening. Understanding LOXL2 regulation in aging vasculature could lead to innovative treatments that prevent or even reverse vascular stiffening.

Methods and results: This research employed human aortic smooth muscle cells (HASMCs) and human aortic endothelial cells (HAECs) to elucidate LOXL2 regulation by NO. In HAMSCs, RT-qPCR indicated LOXL2 mRNA expression decreased when NO incubation time (0-48h) and NO concentration (0-100uM) increased. Co-culturing HASMCs and HAECs with NO inhibition via L-NAME (250 μM) simulated aged vessels, demonstrated LOXL2 upregulation. Western blotting showed that in the extracellular matrix (ECM) and culture media, LOXL2 protein decreased with increased NO availability in a time and concentration-dependent manner. Co-culturing HASMCs with HAECs yielded consistent findings, with decreased LOXL2 protein levels in the presence of NO, and an increase when NO was inhibited via L-NAME.

Conclusion: Reduced NO availability, a hallmark of vascular aging, influences LOXL2 expression at mRNA and protein levels. Decreasing NO simulates aged conditions, increasing LOXL2 activity and abundance, whereas higher NO levels decrease LOXL2. Future research will further explore regulatory processes affecting LOXL2 in vasculature, including protein turnover, synthesis, and degradation.

ABSTRACT 38

Sex-Specific Variations in Vascular Properties Across Pulmonary and Systemic Circulations

Mahin Gadkari, Travis Brady, Marta Martinez Yus, Phillip Azarcon, Diego Almodiel, Karthik Suresh, Lakshmi Santhanam

Many cardiovascular diseases exhibit sex-specific differences in severity and incidence. For example, reproductive-age females have a lower incidence of systemic hypertension and more favorable outcomes compared to males. However, for pulmonary hypertension (PH), younger females have a higher incidence, though males still experience worse outcomes. The physiological mechanisms underlying these disparities are poorly understood, partly due to incomplete understanding of baseline differences in vessel properties between the pulmonary and systemic vascular beds. This study examines sex differences in vascular properties across these vascular beds.

Using male and female wild-type Wistar Kyoto rats, we assessed the mechanical properties of the pulmonary artery (PA) and aorta via uniaxial mechanical testing. We also evaluated endothelial-dependent and independent vasorelaxation by testing the response to acetylcholine (Ach) and sodium nitroprusside (SNP), respectively, this was done with and without indomethacin to explore the role of COX in vascular function.

Female PAs showed higher stiffness than males, with a steeper stress-strain curve and increased incremental modulus in the collagen-mediated range. No significant differences were observed in the aorta. Both female PAs and aortas exhibited greater endothelial-dependent and -independent maximal relaxation compared to males, and COX inhibition eliminated these sex-based differences. These findings highlight distinct sex differences in vascular mechanics and function between the pulmonary and systemic circulations. The differences in the mechanical properties and vascular responses of female and male vessels could contribute to sex-specific outcomes in cardiovascular diseases.

ABSTRACT 39

TAVR outcomes for severe aortic stenosis according to baseline resting gradient

Matthew Czarny, Maeve Jones-O'Connor, Rani Hasan, Faisal Rahman, Hamza Aziz, Michael Robich, Daniel Haugan, Jon Resar

Transcatheter aortic valve replacement (TAVR) outcomes for patients with severe aortic stenosis (AS) but a low resting aortic valve mean gradient (MG) are largely unknown. Patients who underwent TAVR using a self-expanding bioprosthesis from 2015 to 2022 and eligible for 1-year follow-up from the Society of Thoracic Surgeons/American College of Cardiology Transcatheter Valve Therapy Registry (STS/ACC TVT Registry) in the U.S.A. were included. The cohort comprised 80,429 patients with a mean age of 80.7±7.9 years. Patients were divided into 6 subgroups according to resting MG (0-<20, 20-<25, 25-<30, 30-<35, 35-<40, 40+ mmHg). The Kaplan-Meier 1-year all-cause mortality rate was 10.8% for the entire cohort, 20.9% in the 0-<20 mmHg subgroup and 9.3% in the 40+ mmHg subgroup with a significant trend (P <0.001) of decreasing mortality across the 6 MG subgroups. Patients in the 0-<20 mmHg subgroup had the lowest mean Kansas City Cardiomyopathy Questionnaire (KCCQ) summary scores at all time points (42.6 at baseline, 70.0 at 1 month, and 75.5 at 1 year), also with a significant trend (P <0.001) of increasing scores across the 6 MG subgroups (P <0.001 at all-time points). The Valve Academic Research Consortium 3 KCCQ ordinal outcome of substantial or moderate improvement occurred in ≥65% of patients in each of the MG subgroups at 1 month and ≥50% at 1 year. In conclusion, baseline aortic valve MG is a strong predictor of 1-year all-cause mortality in patients undergoing TAVR. However, most had meaningful improvements in QoL measures at 1-year post-TAVR regardless of baseline MG.

ABSTRACT 40

Small Proline-Rich Protein 2A Drives Epithelial Remodeling in Eosinophilic Chronic Rhinosinusitis with Nasal Polyps via SAA2 Upregulation

Shaobing Xie

Background: Eosinophilic chronic rhinosinusitis with nasal polyps (eCRSwNP) is a severe subtype of chronic rhinosinusitis characterized by eosinophilic inflammation, type 2 (T2) immune responses, and tissue remodeling in the sinonasal mucosa.

Objective: We sought to identify genes contributing to eCRSwNP pathogenesis and elucidate their roles in epithelial dysfunction and tissue remodeling.

Methods: Transcriptome sequencing was conducted on nasal tissues from patients with eCRSwNP, non-eosinophilic CRSwNP (neCREwNP), and healthy controls and from CRSwNP mouse model with Sprr2a knockout (Sprr2a-/-) mice. Epithelial-mesenchymal transition (EMT) was examined in CRSwNP mouse model and air-liquid interface (ALI) culture system with nasal epithelial cells.

Results: Transcriptomic analysis revealed that SPRR2A expression was significantly elevated in eCRSwNP nasal tissues compared to non-eosinophilic CRSwNP (neCRSwNP) and healthy controls. High SPRR2A expression correlated with increased eosinophil infiltration, epithelial thickness, and IL-13 levels. In a CRSwNP mouse model, Sprr2a-/- mice displayed reduced epithelial thickness, fewer nasal polyps, lower IL-4 and IL-13 levels, and attenuated EMT. In vitro, nasal epithelial cells from Sprr2a-/- mice demonstrated reduced EMT markers and preserved barrier integrity. Further transcriptomic analysis identified serum amyloid A3 (Saa3) as a downstream mediator of SPRR2A. Saa3 expression was reduced in Sprr2a-/- mice, while SAA2 (human) was upregulated in eCRSwNP compared to neCRSwNP and healthy controls and positively correlated with SPRR2A levels. In ALI cultures, Saa3 induced EMT, barrier dysfunction, and increased IL-6, IL-33 and TGF-β1 production.

Conclusions: These findings suggest that SPRR2A promotes eosinophilic inflammation and tissue remodeling via SAA2, highlighting the SPRR2A-SAA2 axis as a potential therapeutic target in eCRSwNP.

ABSTRACT 41

Metagenomic whole genome sequencing of stool samples demonstrates distinct profiles in AKI and CKD participants from the NIH Kidney Precision Medicine Project

Sanjeev Noel, James White, Shishir Patel, Steve Menez, Dominic Raj, Chirag Parikh, Hamid Rabb, Kidney Precision Medicine Project

Background: Prior studies used 16S RNA sequencing and demonstrated alterations in gut bacteria following acute kidney injury (AKI) in mice and dysbiosis in chronic kidney disease (CKD) patients. However, detailed profiling of gut microbiota in AKI patients is lacking.
Methods: Untargeted metagenomic whole genome sequencing (mWGS; >25 million reads/sample) of stool from well characterized, biopsy proven, AKI (n=7) and CKD (n=70) patient from KPMP was performed. Stool metagenomic data of healthy controls (n=94) from 4 published studies was used. Kraken2 and Metaphlan3 were used for species level taxonomic assignments and HUMAnN3 for functional annotation. Unsupervised clustering was performed using pheatmap, and comparisons between groups computed with non-parametric Mann-Whitney U test.

Results: Kraken2 analysis showed a decline in the percent mean abundance of genus Chryseobacterium in AKI (0.05) compared to CKD (0.07; p=0.05) and healthy individuals (0.20). Ruminococcus bicirculans declined in AKI (1.82) compared to CKD (6.47; p=0.07) and healthy individuals (2.42; p=0.01). Conversely, Gordonibacter pamelaeae increased in AKI (0.07) compared to healthy individuals (0.03) but was less abundant compared to CKD (0.30; p=0.05). MetaPhlAn3 identified significant increase in Clostridium asparagiforme in AKI (11.68) compared to CKD (0.03; p=0.06) and healthy (0.01; p=0.001) individuals. Roseburia hominis, Roseburia intestinalis, Dorea longicatena and Gemmiger formicilis were significantly reduced in AKI compared to CKD and healthy individuals. HUMAnN3 analysis showed significant correlation between amino acid metabolism and several bacterial species identified in AKI participants.

Conclusions: These results demonstrate distinct stool microbiota profiles in AKI and CKD patients compared to healthy individuals. Future studies are needed to confirm and examine the pathophysiologic significance of these findings.

ABSTRACT 42

Cardiac MRI measures of T1Rho, a novel imaging marker of diffuse fibrosis, are elevated in postpartum women with preeclampsia

Kevin Sun, Laila Sheikh, Allison G. Hays, Anum Minhas

Background: Preeclampsia, a hypertensive pregnancy disorder, increases long-term cardiovascular disease (CVD) risk. While subclinical cardiac dysfunction postpartum has been reported, the role of myocardial fibrosis, scar tissue from injury, remains unclear. T1Rho (T1ρ), a new CMR mapping parameter, quantifies myocardial fibrosis without contrast and was validated in heart failure. However, its value in postpartum women with preeclampsia, who have chronic inflammation, is unknown. We tested the feasibility of measuring T1rho using 3T CMR and hypothesized that T1ρ (myocardial fibrosis), is elevated in postpartum women with preeclampsia compared to controls.

Methods: We enrolled 21 women with and 23 without preeclampsia at a median of 4.5 months postpartum, matched for age, BMI and race/ethnicity who underwent research CMR (cardiovascular magnetic resonance). Mean cardiac T1ρ was measured in blinded manner (QMass/Medis software) and values compared between groups using t-tests for significance ($p<0.05$).

Results: Women with and without preeclampsia were similar in age (mean 32.6 ± 5.7 years), BMI (mean: 28.3 ± 10.8 kg/m^2), and race/ethnicity (50% White, 32% Black, and 7% Hispanic). T1ρ measures were significantly higher among women with (45.0 ± 2.3) vs, without preeclampsia (42.7 ± 2.9), p=0.007 (Figure 1).

Conclusions: Women with preeclampsia have higher levels of diffuse myocardial fibrosis compared to controls. These findings provide novel evidence that increased myocardial fibrosis may contribute to increased long-term CVD risk in preeclamptic women.

ABSTRACT 43

Euclidean mirrors and first-order changepoints in network time series

Tianyi Chen, Zachary Lubberts, Avanti Athreya, Youngser Park, and Carey E. Priebe

We describe a model for a network time series whose evolution is governed by an underlying stochastic process, known as the latent position process, in which network evolution can be represented in Euclidean space by a curve, called the Euclidean mirror. We define the notion of a first-order changepoint for a time series of networks, and construct a family of latent position process networks with first-order changepoints. We prove that a spectral estimate of the associated Euclidean mirror localizes these changepoints, even when the graph distribution evolves continuously, but at a rate that changes. Simulated and real data examples on brain organoid networks show that this localization captures empirically significant shifts in network evolution.

ABSTRACT 44

Machine Learning-Driven Analysis and Predictive Modeling for Molten Salt Reactor Electrochemical Behavior

Omobolade A. Odedoyin

Molten Salt Reactors (MSRs) offer transformative advancements in nuclear energy, including enhanced thermal efficiency, improved safety, and the potential for medical isotope production. With the ability to generate short-lived isotopes like Technetium-99m (Tc-99m) and Fluorine-18 (F-18), MSRs offer safer, more efficient production methods than traditional reactors, supporting diagnostic imaging and therapies such as PET scans and cancer treatments. However, the extreme chemical environment of MSRs presents challenges, including sensor degradation and corrosion under high temperatures and irradiation, complicating accurate monitoring and analysis.

This research addresses these challenges by developing predictive machine learning (ML) models to analyze electrochemical behaviors critical to MSR stability. Cyclic Voltammetry (CV) and Open-Circuit Potentiometry (OCP) data were collected, focusing on features like cycle direction, scan rate, applied voltage, resulting current, and solute concentration. Qualitative features were transformed into numeric representations through a weighted integration of normalized molar mass and ionization energy, with Bayesian optimization identifying the optimal weights.

The datasets underwent preprocessing and feature selection via Recursive Feature Elimination with Cross-Validation (RFECV), and training with nested cross-validation to optimize regressors and hyperparameters. The Random Forest Regressor with optimized weights achieved a test mean absolute error (MAE) of 0.0044, significantly outperforming baseline methods. The best-performing configuration used a Random Forest Regressor with optimized hyperparameters and optimal weight combinations for transforming qualitative features. The optimal feature selection included all features available with the optimal weight for qualitative feature transformation and achieved a test MAE of 0.00441, significantly outperforming baseline methods.

These models demonstrate improved predictive accuracy, enabling reliable monitoring of MSRs. By addressing key challenges in sensor data analysis, this framework enhances reactor safety, efficiency, and potential applications in medical isotope production, contributing to sustainable nuclear energy solutions.

ABSTRACT 45

Impact of Obesity Status on Management and Outcomes of Cardiogenic Shock

Anushka Desai, Anum Minhas, Faisal Rahman

The obesity paradox in cardiovascular disease has been previously used to explain favorable prognoses seen in obese patients. However, its relevance to patients with cardiogenic shock has been understudied.

We analyzed cardiogenic shock related hospitalizations in adults using the National Inpatient Sample database (years 2016-2021). Multivariable logistic regression, with adjustment for demographics, cardiovascular comorbidities, and prior cardiac interventions was performed to assess differences in procedural utilization and clinical outcomes in obese versus non-obese patients.

Of 1,052,485 cardiogenic shock admissions, 18.1% were for patients with obesity. Obese patients with cardiogenic shock were, on average, 6 years younger and more likely to be female, be seen at an urban teaching hospital, have greater cardiovascular comorbidity burden, experience longer lengths of stay, and incur higher costs of hospitalization than those not obese. These patients were also more likely to receive CABG (aOR 1.35 [95% CI 1.30-1.41]) and ECMO (aOR 1.09 [95% CI 1.01-1.18]), but less likely to receive PCI (aOR 0.87 [95% CI 0.84-0.89]), IABP (aOR 0.94 [95% CI 0.90-0.97]), pLVAD (aOR 0.95 [0.91-0.99]) than their non-obese counterparts. Comparing clinical outcomes, obese patients were less likely to die in-patient (aOR 0.86 [95% CI 0.84-0.88]) and receive less invasive mechanical ventilation (aOR 0.92 [95% CI 0.89-0.94]).

Obese patients with cardiogenic shock exhibit distinct clinical profiles and procedural utilization compared to those non-obese. Despite higher resource utilization, obese patients experience lower in-hospital mortality, underscoring the need for further research into the mechanism behind the obesity paradox in shock states.

ABSTRACT 46

The Role of Olfactory Receptor 78 in Experimental Acute Kidney Injury

Shishir K Patel, Qisen Guo, Radhika Kapoor, Mahta F Gooya, Mackenzie Kui, Tara Fallah Rastegar, Ryo Matsuura, Lois J. Arend, Sanjeev Noel, Jennifer Pluznick & Hamid Rabb

Background: Olfactory receptor 78 (Olfr78) is a short-chain fatty acids receptor activated by acetate and propionate derived from the gut microbiome. Olfr78 is expressed in afferent arteriole, vascular smooth muscle cells, and immune cells. We investigated the role of Olfr78 in AKI induced by ischemia and cisplatin in mice.

Methods: Male and female wild-type (wt) and Olfr78 knockout (Olfr78-/-) C57BL6 mice were subjected to bilateral ischemic or cisplatin AKI. Long-term effects were studied after severe unilateral ischemic AKI (UIRI). Endpoints included survival, kidney function (SCr, GFR), histology, and flow cytometry.

Results: In moderate bilateral ischemic AKI, Olfr78-/-mice had worse survival at 72 hrs than wt mice (P<0.01). However, no changes were found in kidney function/structure. Cisplatin-induced AKI was comparable in Olfr78-/-and wt mice. In UIRI model, Olfr78-/- had lower GFR than wt at baseline (1369.9±106.4vs1170.7±196.5, P≤0.05), 24h after UIRI (959.4±8vs837.0±7, P< 0.05) and after 21d (1166.1±54.5vs807.6±11, P< 0.0001). After severe UIRI, Olfr78-/- mice showed a decrease in TCR+CD4-CD8-cells (9.6±1.6vs.4.0±1.6%, P<0.001) and an increase in TCR+CD4+CD8+cells (0.2±0.1vs.0.5±0.3%, P<0.001). In CD4+ cells, CD69 (32.6±4vs74.8±7.6%, P< 0.0001), effector-memory (CD44+CD62L-) (93.11±.2vs94.6 ±0.93%, P<0.05), and TIGIT+ cells (12.8±4.5vs21.9±3.9%, P<0.01) increased in Olfr78-/- vs. wt. In CD8+ cells, increase in CD69 (40.8±8vs55.8±8.6%, P<0.01), TIGIT (7.9±2.4vs17.4±11.3 %, P<0.01) and CTLA4 (0.1±0.14vs0.7 ±0.5%, P<0.01).

Conclusion: Olfr78 affects survival and renal immunologic changes during AKI but with only modest effects on kidney structure and function. Male mice were more susceptible to ischemic acute kidney injury, while female mice were more susceptible to nephrotoxic acute kidney injury.

ABSTRACT 47

Concordance of pre-biopsy and post-biopsy diagnosis in patients with acute kidney injury

Max McGredy, David Hu, Heather Thiessen Philbrook, Pamela Corona, Avi Z. Rosenberg, Dennis G. Moledina, Steven G. Coca, Chirag R. Parikh, Steven Menez

Background: Kidney biopsy remains the gold standard for the diagnosis of acute kidney injury (AKI) when clinicians are unable to establish a diagnosis based on pre-biopsy history, exam, and non-invasive diagnostic testing. Among patients with AKI, two key diagnoses that often drive the decision to pursue kidney biopsy are suspected acute interstitial nephritis (AIN) and acute tubular injury (ATI).

Methods: We leveraged data collected prospectively through the ongoing Novel Approaches in the Investigation of Kidney Disease (NAIKiD) Study, in which adult patients scheduled for kidney biopsy at the Johns Hopkins Hospital consent to provide biosamples paired with data collection. Up to 3 pre-biopsy clinical diagnoses were recorded for each patient, along with up to 3 post-biopsy diagnoses. We investigated the concordance of pre- and post-biopsy diagnoses among participants with suspected AIN or ATI.

Results: Among 164 total participants, 29 had suspected AIN and 47 had suspected ATI pre-biopsy. Among the participants with suspected AIN, only seven (24%) had AIN confirmed on biopsy. Of the 22 other participants, alternative histological findings included focal segmental glomerulosclerosis (FSGS), ATI, and various glomerular diseases. Out of 47 participants with suspected ATI, only 27 (57%) had ATI confirmed on biopsy. Among the 20 other participants, alternative histological findings also included glomerular diseases, diabetic nephropathy, and FSGS predominantly.

Conclusion: Patients with suspected ATI or AIN are often found on biopsy to have alternative, significant findings present on histology. Among patients without relative or absolute contraindications, kidney biopsy remains an essential part of evaluation.

ABSTRACT 48

scLCM and ddPCR reveals HDV heterogeneity in liver biopsy from a person with HBV/HDV

Chi-Fen Lee, Tanner Grudda, Ahmet Gurakar, Ashwin Balagopal, Chloe L. Thio

Hepatitis D virus (HDV) relies on hepatitis B virus (HBV) envelope proteins for entry into hepatocytes. There are limited data on the distribution of HDV in liver or whether every HDV-infected cell requires HBV co-infection. To investigate this, we performed HBV and HDV ddPCR on 252 single hepatocytes isolated by laser capture microdissection (LCM) from end-stage explanted liver from a person with HBV/HDV co-infection taking nucleoside analogue (NUC) therapy with serum HBV DNA <29 IU/mL. We used primer pairs targeting the conserved ribozyme region of HDV and three HBV amplicons that distinguish transcripts derived from cccDNA and integrated HBV DNA (iDNA). HDV RNA was detected in 9.5% of hepatocytes with a median (range) of 72.01 (8-6619) copies/cell; a minority 4/24 cells had markedly abundant viral RNA levels >1000 copies/cell. HBV surface transcripts were found in 14.3% of cells and their abundance was comparatively low (median [range] 8 [8-16] copies/cell). The majority of HBV transcripts were from iDNA, consistent with our previous findings. Surprisingly, only 1.2% of hepatocytes with HDV also had HBV transcripts. These data are the first look at the single-cell intrahepatic landscape in HBV/HDV. We conclude that 1) the HDV distribution in the liver is heterogeneous and differs from HBV; 2) HDV propagation may be sustained by iDNA-derived envelope proteins during NUC; and 3) intracellular HDV does not appear to require HBV genes to achieve high-level transcription. Applying our technique to more individuals before and after treatment with existing and investigational therapeutics will yield insights into HBV/HDV dynamics and cure strategies.

ABSTRACT 49

Revealing neural mechanisms underlying species-specific vocalization in marmosets

Yang Zhang, Sherry Xinyi Shen, Chenggang Chen, Michael S Osmanski, Xiaoqin Wang

Species-specific vocalizations are behaviorally critical sounds that are essential for the survival and social interactions of both humans and vocal animals. However, it is largely unknown how the brain processes communication sounds such as speech and species-specific vocalizations. Previous studies in humans suggest a role of a cortical dorsal-ventral dual pathways in supporting speech and language processing, while the evolutionary root of the dual pathways is unclear. In addition, previous studies identified a voice patch system on the lateral superior temporal gurus (STG) in the human brain that is selective to human voices over other sounds. Similar vocalization-selective regions were also found on the rostral portion of the temporal lobe outside of the auditory cortex in both macaques and marmosets, it is yet clear whether vocalization-selective regions are present in the auditory cortex. To fill the gap in our knowledge, my research has focus on two aspects: 1) studying the evolution of speech and language networks using comparative analysis with ultra-high field diffusion MRI data to elucidate what is unique in humans and what is conserved across species; and 2) investigating whether voice patches exist in marmoset auditory cortex and characterizing neural response properties of the voice patches using multi-modal wide-field optical imaging. Our results demonstrate homologous auditory dorsal and ventral fiber tracks in marmosets and macaques as in humans and illustrate the human-specific specializations for speech and language processing. We also demonstrate the existence of two voice patches, which are functionally connected and hierarchically organized, in marmoset auditory cortex that preferentially responded to marmoset vocalizations over other sounds and carry call types and identity information. These findings provide important insights into the evolution of auditory pathways in primates and reveal cortical architectures for recognizing species-specific vocalizations.

ABSTRACT 50

Neuronal regulation of brain organoids via 3D electrical stimulation for induced learning

Chris Acha, Derosh George, Lauren Diaz, Dowlette-Mary Alam El Din, Eva Loftus, Gandhali Mangalvedhekar, Sai Rayasam, Lena Smirnova, Brian S. Caffo, Erik C. Johnson, David H. Gracias

Brain organoids, three-dimensional self-aggregates of neural cells, can recapitulate some of the functions and developmental characteristics of the human brain in vitro. However, the advancement of replicating cognition or learning on these organoid models remains challenging due to a lack of 3D microelectrode array (MEA) interfaces, establishing appropriate learning protocols, and supportive glial cells showcasing spontaneous electrophysiological activity. We previously reported 3D shell MEAs designed to match the unique architecture of brain organoids.[1] Unlike 2D MEAs, mapping the three-dimensional functionality of a human brain or brain organoid has yet to be realized. Here, we present a self-folded MEA capable of interfacing with submillimeter-sized brain organoids capable of both stimulation and recording for open-loop and closed-loop learning experiments over weeks. In open-loop learning, unidirectional instructional stimuli without feedback can be used to monitor brain organoid activity, while closed-loop learning incorporates an adaptive framework based on continuous feedback. We have identified electrical sensory inputs that elicit a change in firing patterns, indicating their ability for stimulation-triggered learning. A parametric study showed an increase in firing rate in the instance following the stimulation. The capability of this physical embodiment of a recurrent neural network to respond to an electrical sensory input is being explored for reservoir-based open-loop learning by using modulated inputs at various time series. This study is an important step in advancing the previously described concept of "Organoid Intelligence" (OI),[2] which seeks to develop neuromorphic computational devices using brain cells.

References: [1] Huang et al., Sci Adv (2022). [2] Smirnova et al., Frontiers in Science (2023).

ABSTRACT 51

High proportion of HBV-human chimeric transcripts is associated with minimal declines in HBsAg levels

Monika Mani, Che-Min Lo, Richard K Sterling, Mark S Sulkowski, Ashwin Balagopal, Chloe L Thio

HBV DNA integrated into the host chromosome produces HBsAg so may be a barrier to functional cure. Data on transcriptionally active HBV integrations (iDNA) in liver tissue from HBeAg-positive (EPI) and HBeAg-negative infection (ENI) during nucleos(t)ide analogues (NUC) treatment are limited. We performed 10X Visium Spatial Gene Expression Analysis (VSGEA) on liver biopsies from 16 participants with chronic HBV-HIV: eight EPI and eight ENI.

NUC duration in EPI and ENI was median (IQR) 3.1 (1.6-13.3) years and 7.0 (5.0-8.3) years, respectively. Among all 16 tissues, there were 4837 total chimeric reads (median[IQR] 14[3-259]). Of these, 86.3% had HBV-human junctions located between DR2 and DR1. Median(IQR) chimeric reads were higher in EPI (334.5 [19.8-1072.0]) than ENI (4.0 [1.0-11.8]; p=0.03). However, percentages of chimeric/total HBV reads were similar in EPI (median [IQR]) (3.1 [1.6-13.3] and ENI (7.3 [5.0-13.0]) p=0.3). Combining EPI and ENI, the percentage HBV chimeric reads positively correlated with increasing NUC duration (R=0.73, p=0.0019). Interestingly, in 5 of 6 participants on NUCs ≥ 9 years, ≥ 12.5% of total HBV reads were chimeric. In contrast, the inverse correlation between qHBeAg levels and percentage of HBV chimeric reads was weak (R=-0.54, p=0.04). Percentage of HBV chimeric reads inversely correlated with maximum qHBsAg declines during NUCs (R=-0.72, p=0.0025).
The percentage of transcriptionally-active iDNA is similar between EPI and ENI but enriches with prolonged NUCs in both groups. A lower proportion of iDNA pre- NUCs was associated with a greater decline in qHBsAg during NUCs. These data indicate that, regardless of HBeAg status, transcriptionally active iDNA maintains HBsAg levels during NUCs.

ABSTRACT 52

The application of AI guided laser processed iPSC-derived cardiomyocytes

Peyton Krajcarski, Prakaimuk Saraithong, Joseph Criscione, Deok-Ho Kim, Todd J. Herron

At this time, purification of induced pluripotent stem cell derived cardiomyocytes (iPSC-CMs) requires either lengthy protocols resulting in low cell counts or metabolic manipulation causing poor cell function. A novel purification method is presented to address these challenges using an artificial intelligence (AI) guided laser processing device to purify iPSC-CMs. This approach for iPSC-CM purification, referred to as CM-AI, decreases protocol length, increasing cell counts, and revealing the devices utility in the bio-manufacturing of iPSC-CMs. Validated on atrial specific cardiomyocytes (A-CMs), the functional behavior of the purified CMs when replated as monolayers is conserved. As an application of the A-CMs purified by the processing device, the CMs can be cast as 3D engineered heart tissues (3D-EHTs) to assess function via contractile parameters. Spontaneous force measurements confirm the function of these A-CMs as 3D-EHTs. The application of these CM-AI purified A-CMs as 3D-EHTs provide an opportunity to complete drug testing and disease modeling in a higher throughput manner, immediately impacting cardiac regeneration and biomedical engineering research.

ABSTRACT 53

An engineered heart tissue model of dystrophic cardiomyopathy for screening microdystrophin gene therapies

Joseph Criscione, Gwangjun Go, Julian Chow, Jason Kim, Zhanping Ren, David Hammers, David Kass, Deok-Ho Kim

Duchenne muscular dystrophy (DMD) is an X-linked genetic disorder characterized by the loss of dystrophin in striated muscle, leading to progressive muscle wasting. As management of orthopedic symptoms has improved, heart failure has become the leading cause of death for DMD patients. Microdystrophin gene therapies aim to treat DMD via expression of a truncated version of dystrophin containing only essential subdomains. While murine models show variable efficacy among different microdystrophin constructs, their relative performance in human contexts remains unknown. Furthermore, in vivo efficacy studies take over one year to complete, slowing the development of new therapies.

To address these challenges, we validated a human engineered heart tissue (EHT) model of dystrophic cardiomyopathy for more rapid and higher throughput screening of microdystrophin therapies. EHTs were fabricated using either patient-derived or CRISPR-edited human induced pluripotent stem cell-derived cardiomyocytes to directly compare isogenic disease and control EHTs. Dystrophic EHTs exhibited reduced twitch forces, slower contraction kinetics, diminished calcium transient amplitudes, and slower calcium kinetics. Additionally, we developed novel methods for in situ, longitudinal, aseptic assessment of EHT passive mechanical properties, which were used to reveal that dystrophic EHTs were stiffer than controls, consistent with DMD pathology.

Treatment of dystrophic EHTs with microdystrophins via AAV9 transduction demonstrated significant, dose-dependent improvements in twitch force for a murine-efficacious construct, while a murine-deleterious construct showed no effect. These findings suggest microdystrophins can improve cardiac function in DMD and highlight the utility of this EHT model as platform for more rapid screening of microdystrophin therapies.

ABSTRACT 54

From Occurrence to Consequence: A Comprehensive Data-driven Building Fire Risk Analysis

Chenzhi Ma, Hongru Du, Shengzhi Luan, Ensheng Dong, Lauren M. Gardner, and Thomas Gernay

Building fires remain a critical threat to lives, property, and infrastructure, highlighting the urgent need for innovative strategies to better understand and mitigate fire risks. This innovative study introduces a data-driven framework for fire risk analysis across the United States, marking the first effort to integrate over one million fire incident reports with diverse datasets, encompassing social determinants, building inventories, weather patterns, and event-specific factors. By leveraging advanced statistical models, including generalized additive models (GAMs) and machine learning algorithms, the research identifies key drivers of fire occurrence and severity. Notably, vulnerable communities, characterized by socioeconomic disparities and the prevalence of aging or vacant buildings, experience significantly higher fire risks. Event-specific factors, such as fire origins and the presence of safety measures like fire detectors and Automatic Extinguishing Systems (AES), emerge as critical in reducing fire spread and injuries. Buildings equipped with these systems show a marked reduction in fire-related consequences, underscoring their lifesaving impact. This study emphasizes the value of integrating localized, multidimensional data to inform targeted interventions, such as mandating fire safety systems in high-risk areas and providing financial support to disadvantaged communities. By identifying at-risk populations and actionable solutions, this research offers a transformative pathway to reducing fire risks, protecting vulnerable populations, and fostering safer, more equitable communities nationwide. The findings provide a compelling call to action for policymakers, urban planners, and stakeholders to prioritize fire prevention and resilience.

ABSTRACT 55

Associations Between Social Determinants of Health, Cardiovascular Health, and Mortality Outcomes Among Sexual Minority Individuals in the United States

Danish Iltaf Satti, Jeffrey Shi Kai Chan, Reed Mszar, Adhya Mehta, Yaa Adoma Kwapong, Raymond Ngai Chiu Chan, Olayinka Agboola, Erica S. Spatz, Jared A. Spitz, Khurram Nasir, Zulqarnain Javed, Jason A. Bonomo, Garima Sharma

Background: The relationship between social determinants of health (SDOH) and cardiovascular health (CVH) outcomes in sexual minority (SM) individuals remains understudied.

Objectives: To examine the associations between SDOH profiles and CVH and mortality outcomes among SM individuals in the U.S.

Methods: Participants aged ≥18 years from the 2013–2017 National Health Interview Survey were included, excluding those with missing data on SM status, CVH, SDOH, or covariates. SM status was self-reported as lesbian/gay, bisexual, or uncertain. SDOH profile was quantified using a six-domain, 38-item score (higher scores indicated worse deprivation). CVH was assessed using a seven-item score from the American Heart Association's Life's Essential Eight framework (higher scores indicated worse CVH). Additionally, cardiovascular mortality was ascertained through the national death index.

Results: The study included 57,182 participants (representing 82.8 million individuals). A worse composite SDOH score was associated with a worse CVH score in both heterosexual (adjusted rate ratio 1.14 [95% confidence interval 1.13-1.15], $p<0.001$) and SM individuals (adjusted rate ratio 1.16 [1.12-1.20], $p<0.001$), with associations appearing to be potentially stronger in the latter (pinteraction=0.042). Subgroup analysis demonstrated consistent associations among gay/lesbian and bisexual individuals, but not in those with uncertain sexual orientations. Further exploratory analysis showed that a worse composite SDOH score was significantly associated with higher risk of cardiovascular mortality in both heterosexual and SM individuals, with associations being significantly stronger in the latter (pinteraction=0.006).

Conclusions: An unfavorable SDOH profile was disproportionately associated with worse CVH scores and higher cardiovascular mortality risk among SM individuals in the U.S. compared to their heterosexual counterparts.

ABSTRACT 56

Time Code for Multifunctional 3D Printhead Controls

Sarah Propst and Jochen Mueller

Direct ink writing is an extrusion-based 3D printing technique with broad potential in both engineering and medicine due to its compatibility with a diverse range of materials, including polymers, ceramics, metals, and biomaterials. Further, it is possible to integrate multifunctional printheads with features such as coaxial printing, nozzle shape-changing, in-situ curing, material switching, and material mixing. Despite advancements in material and nozzle design, incorporating auxiliary controls into Geometry Code (G-Code), the standard programming language for extrusion-based printers, remains challenging. G-Code must be executed line-by-line, requiring auxiliary control commands to interrupt the print path motion leading to defects, increased print times, and mechanical burden on the printer. These limitations become increasingly apparent as researchers strive for higher printing resolution and complexities, such as functionally graded structures where frequent tailoring along the print path is required. In this study, we propose a generalizable time-based synchronization approach called Time Code (T-Code), which decouples auxiliary control from G-Code, enabling uninterrupted print path enrichment. We demonstrate the method's effectiveness by fabricating functional gradients for energy absorption and optical properties as well as by parallelizing printhead auxiliary devices for mass customization. T-Code reduces defects, enhances print speed, and minimizes the mechanical burden on 3D printers, enabling the rapid creation of complex multimaterial structures.

ABSTRACT 57

Chronic activation of CaMKII, a key signal transducer for exercise performance and adaptation, drives sarcopenia in aging

M. Bene, W. A. Fountain, S. J. Jeong, G. Rosales-Soto, E. Hernandez-Ochoa, C. Antonescu, L. Florea, T. H. Chung, J. Walston, Q. Wang

Sarcopenia, the loss of muscle mass and strength, is a major risk factor for physical frailty in older adults. Ca2+/calmodulin-dependent protein kinase II (CaMKII) is activated by Ca2+ and reactive oxygen species in contracting muscles to enhance muscle performance and adaptation to exercise training. We assessed CaMKII activity in the skeletal muscles of young (4-month-old) and old (20-month-old) mice and found significantly increased CaMKII activity in old mice at rest, suggesting that CaMKII activity is chronically elevated and disconnected from muscle contractile activity in aged muscles. To determine the role of increased CaMKII activity, we used an adeno-associated viral vector (AAV9) to express a CaMKII inhibitor, CN19o, in the tibialis anterior (TA) muscles of 20-month-old mice and found a significant improvement of muscle contractile force at 24 to 26 months of age. Conversely, expressing a constitutively active CaMKII (CaMKIICA) in the TA muscles of young mice (3-month-old), led to a striking reduction of muscle contractility. Electromyography studies showed that the muscles expressing CaMKIICA had a subtle but significant reduction of compound muscle action potential (CMAP) that could not explain the reduction of contractile force. Histological assessments showed that long-term CaMKIICA expression led to the formation of ragged red fibers, indicative of mitochondrial dysfunction. Expressing CaMKIICA in young muscles led to global transcriptomic changes resembling effects of aging, while CaMKII inhibition partially rejuvenated muscle transcriptome in older muscles. Our findings suggest that CaMKII hyperactivation is a driver and potential therapeutic target of sarcopenia.

ABSTRACT 58

Targeting LOXL2 against arterial stiffening in post-menopausal females

Marta Martinez Yus, Travis Brady, Diego Almodiel, Mahin Gadkari, Philip Azarcon, Helen Wang, Kavitha Nandakumar and Lakshmi Santhanam

Introduction: Cardiovascular disease (CVD) is the leading cause of death, with post-menopausal women experiencing a disproportionate risk acceleration. Aortic stiffening, as occurs in aging, is predictive of adverse cardiovascular outcomes. While estrogen loss is linked to increased CVD risk, it is not the sole factor. This study aims to explore LOXL2, a matrix remodeling enzyme, as a potential therapeutic target for vascular stiffening in post-menopausal women.

Methods and Results: Female C57Bl/6J and Loxl2+/- mice underwent ovariectomy (OVX) or sham surgery. We measured pulse wave velocity (PWV) and blood pressure from 3 to 18 months. Loxl2+/- OVX and sham mice showed improved arterial stiffness compared to wild-type (WT) OVX mice. Body weight gain was also lower in Loxl2+/- OVX mice. At 18 months, Loxl2 deletion reduced stiffness in intact aortic rings, with similar results in decellularized rings. Wire myography showed improved contractility and endothelial relaxation in Loxl2+/- OVX mice. Western blotting indicated increased LOXL2 processing in OVX WT females. In vitro studies in human aortic smooth muscle cells showed that using dihydrotestosterone and estradiol to mimic post-menopausal hormonal levels resulted in increased LOXL2 expression.

Conclusion: LOXL2 depletion improves vascular stiffness and body weight gain in OVX mice, supported by reduced stiffening in aortic rings and improved contractility. LOXL2 is modulated by sex hormones, with higher activation under post-menopausal hormonal conditions. Targeting LOXL2 offers a promising strategy for combating arterial aging in post-menopausal women. Future research will investigate the molecular mechanisms of LOXL2's role in vascular aging and hormonal modulation of LOXL2.

ABSTRACT 59

Impact of Intensive Lifestyle Intervention on Kidney Disease Progression In People With Type 2 Diabetes: The Look AHEAD Study

Nityasree Srialluri, Jiahuan Helen He, Jianqiao Ma, Chigolum Pamela Oyeka, Teresa Gisinger, Rita Kalyani, Erin D. Michos, Mark Woodward, Jay Vaidya, Wendy Bennett

Introduction: T2DM increases CKD risk by 2-3 fold. While lifestyle intervention (ILI) is shown to reduce very high-risk CKD in individuals with T2DM, its impact on earlier CKD progression and kidney function vs diabetes support and education (DSE) is less clear.

Methods: This Look AHEAD ancillary study included males and postmenopausal females with T2DM and BMI ≥25 kg/m2 over 8 years. High-risk CKD is defined as eGFR ≤60 mL/min/1.73 m² or urine albumin to creatinine ratio (ACR) >300 mg/g. Cox regression assessed CKD progression, while mixed-effects models analyzed longitudinal eGFR trajectories, adjusting for age and baseline diabetes duration.

Results: At baseline, participants had a mean age of 60.2 ± 6.2 years, eGFR of 90.5 ± 15.0 mL/min/1.73 m², median ACR 8.9 mg/g (5.4-19.0), and diabetes duration of 5 years (2-10). Over 8 years, 20% (N=468) progressed to high-risk CKD. ILI reduced CKD risk vs DSE (HR: 0.80; 95% CI: 0.67-0.96). ILI slowed eGFR decline vs DSE (-1.45 vs. -1.59 mL/min/1.73 m² annually, p=0.07). The eGFR difference between groups widened over time, suggesting cumulative ILI benefit on kidney function (Fig. 1). After adjustment, annual eGFR decline was -0.66 vs. -0.52 mL/min/1.73 m² for DSE and ILI, respectively (p=0.07).

Conclusion: ILI preserves kidney function in T2DM by maintaining higher eGFR and slowing CKD progression, emphasizing its importance in mitigating early renal decline and preventing CKD.

ABSTRACT 60

Post-infarction Cardiac Function is Improved in Mice with TSC2-/- Macrophages

Mohammad Keykhaei, Navid Koleini, Mariam Meddeb, Masih Tajdini, Farnaz Farshidfar, Kejun Liu, Mark J. Ranek, David A. Kass

Introduction: Macrophages (MΦ) play critical roles in myocardial ischemia/reperfusion (I/R) injury. The mechanistic target of rapamycin (mTOR), regulated by tuberous sclerosis complex 2 (TSC2), is pivotal in MΦ functionality. This study investigates how TSC2-mediated regulation of mTORC1 affects MΦ in I/R-injured hearts.

Methods/Results: MΦ-specific TSC2 knockout mice (MΦTSC2-/-) were generated by crossing floxed Tsc2 mice with those expressing LysM-Cre, leading to constitutive activation of mTORC1, as evidenced by increased S6K1 and 4E-BP1 phosphorylation. When exposed to lipopolysaccharide, MΦTSC2-/- mice showed greater proinflammatory responses and reduced M2-like features. To assess the impact of MΦTSC2-/- on infiltrating myocardial macrophage subtypes post-ischemia/reperfusion (I/R), we performed flow cytometry on myocardial infiltrates. This analysis revealed an increase in anti-inflammatory CCR2- MHC-II- phenotypes in MΦTSC2-/-, which correlated with improved cardiac function, evidenced by higher ejection fractions (74.2±10.3% vs. 47.2±14.3%, P=0.002) and smaller left ventricular end-systolic diameters. This cardioprotective effect was confirmed even with neutrophil depletion using anti-Ly6G antibodies. Immunohistochemical analysis showed reduced fibrosis in MΦTSC2-/- hearts, and RNA expression profiling indicated lower levels of fibrotic markers. A reversal experiment involving intraperitoneal rapamycin post-I/R restored the phenotypic changes to wild-type levels, validating the TSC2-mTORC1 axis's critical role. Further investigation into the protective mechanisms via spatial transcriptomics identified GPNMB as a significant mediator, with its expression markedly increased in MΦTSC2-/- post-I/R.

Conclusion: TSC2 deletion in MΦ, resulting in continuous mTORC1 activation, confers significant cardio-protection in I/R injury. This study elucidates a novel signaling mechanism coupling mTORC1/TSC2 with myocardial recovery, offering promising avenues for enhancing post-ischemic cardiac repair.

ABSTRACT 61

Taxonomy-Based Prompt Engineering to Generate Synthetic Drug- Related Patient Portal Messages

Natalie Wang, Sukrit Treewaree, Ayah Zirikly, Yuzhi L. Lu, Michelle H. Nguyen, Bhavik Agarwal, Jash Shah, James Michael Stevenson, Casey Overby Taylor

The objectives of this study were to: (1) create a corpus of synthetic drug-related patient portal messages to address the current lack of publicly available datasets for model development, (2) assess differences in language used and linguistics among the synthetic patient portal messages, and (3) assess the accuracy of patient-reported drug side effects for different racial groups.

We leveraged a taxonomy for patient- and clinician-generated content to guide prompt engineering for synthetic drug-related patient portal
messages. We generated two groups of messages: the first group (200 messages) used a subset of the taxonomy relevant to a broad range of drug-related messages and the second group (250 messages) used a subset of the taxonomy relevant to a narrow range of messages focused on side effects. Prompts also include one of five racial groups. Next, we assessed linguistic characteristics among message parts (subject, beginning, body, ending) across different prompt specifications (urgency, patient portal taxa, race). We also assessed the accuracy and frequency of patient-reported side effects across different racial groups and compared to real world data.

The study generated 450 synthetic patient portal messages, and we assessed linguistic patterns, accuracy of drug-side effect pairs, frequency of pairs compared to real world data. Linguistic analysis with LIWC revealed variations in language usage and politeness and analysis of positive predictive values identified differences in symptoms reported based on urgency levels and racial groups in the prompt. We also found similar levels of drug-side effect pair occurrence to the SIDER database.

This study demonstrates the potential of synthetic patient portal messages as a valuable resource for healthcare research. After creating a corpus of synthetic drug-related patient portal messages, we identified significant language differences and evaluated the accuracy and frequency of drug-side effect pairs across various prompts.

ABSTRACT 62

Immune checkpoint molecule TIGIT modulates kidney T cell mitochondrial respiration and glucose uptake: implications for acute kidney injury and cancer

Radhika Kapoor, Shishir K Patel, Tara Fallah Rastegar, Ryo Matsuura, Hamid Rabb & Sanjeev Noel

Background: Acute kidney injury (AKI) is a serious clinical problem with no specific therapy. We previously demonstrated that immune checkpoint molecule TIGIT mediates AKI. Additionally, TIGIT-knockout (KO) kidney T cells have enrichment of metabolism related genes and increased glucose transporter 1 (GLUT1) during AKI. We hypothesized that TIGIT modifies kidney T cell energetics and glucose uptake.

Methods: CD3+ T cells were isolated from spleen and kidney of WT and TIGIT-KO mice, activated and cultured in the presence of CD3/CD28 and interleukin-2 for 5 days. Cells were treated with CoCl2 (200μM) for 5hrs to study TIGIT's role in hypoxia. Seahorse assay was used to measure oxygen consumption rate (OCR), extracellular acidification rate (ECAR), maximal respiration and spare respiratory capacity (SRC). Additionally, glucose uptake was assessed in cultured kidney T cells.

Results: TIGIT-KO splenic T cells showed higher OCR (29.13±1.68 vs 27.83±2.36 pmol/min/cell), maximal respiration (89.29±0.44 vs 60.92±6.10 pmol/min/cell) and SRC (66.65±1.82 vs 40.75±5.58 pmol/min/cell) compared to WT cells. Hypoxia decreased OCR in WT and TIGIT-KO spleen T cells. TIGIT-KO kidney T cells exhibited higher OCR (26.24±0.03 vs 19.33±1.09 pmol/min/cell) and basal respiration (20.02±0.72 vs 15.36 ±0.68 pmol/min/cell), with decreased maximal respiration (46.82±5.41 vs 59.12±6.46 pmol/min/cell) and SRC (26.80±5.55 vs 43.76±6.22 pmol/min/cell) compared to WT cells. Under hypoxic conditions, TIGIT-KO and WT kidney T cells had reduced mitochondrial respiration and increased ECAR. TIGIT-KO kidney T cells had increased glucose uptake (4831±684.0 vs 2361±336.0 RLU; $P<0.05$) compared to WT cells.

Conclusion: These results demonstrate that TIGIT modulates kidney T cell cellular energetics. TIGIT targeting for metabolism reprogramming is a potential mechanistic and therapeutic opportunity for AKI and cancers.

ABSTRACT 63

The Burden of Preserved Ratio Impaired Spirometry (PRISm) in a High HIV Prevalence Cohort: Prevalence and Predictors

Nicole Robertson, Jacquie Astemborski, Meredith McCormack, Sarath Raju

Introduction: People living with HIV (PLWH) are at increased risk of lung function abnormalities; PRISm represents early lung injury that may lead to COPD and is associated with increased respiratory symptoms and mortality. The burden of PRISm among PLWH is unknown. We aimed to determine the prevalence and predictors associated with PRISm among PLWH.

Methods: PRISm was defined as normal FEV1/FVC (≥0.70) with decreased FEV1 (<80%predicted). We analyzed longitudinal sociodemographic, clinical, and lung function data within the SHIELD cohort 2009-2019 in Baltimore, MD. SHIELD includes PLWH and HIV-uninfected participants with shared risk factors. Post-bronchodilator spirometry was performed at 6-month study visits. Multivariable logistic regression models analyzed the association between HIV and PRISm adjusting for age, sex, race, BMI, education, tobacco, and prior chest infections and surgeries.

Results: Among 2040 participants (1111 PLWH) the prevalence of PRISm was 25.3% (n=517). Participants with PRISm were more likely to be Black, male, less educated, and had fewer pack-years of tobacco use. HIV was a significant predictor of PRISm (OR 1.53, 95%CI: 1.22,1.91, p=0.0002). CD4 count≤200 carried increased odds of PRISm (OR 2.21, 95%CI: 1.50,3.26, p<0.0001). Significant risk factors of PRISm included female sex, black race, obesity, low educational attainment, and pneumonia history (p<0.01).

Conclusions: Within an urban, high-HIV prevalence cohort there was high prevalence of PRISm affecting one-fourth of participants. Identifying high-risk patients (i.e.,PLWH) for PRISm can facilitate early detection of lung function impairments. Further research is needed to evaluate the relationship between PRISm and risk for progressive lung function decline among PLWH.

ABSTRACT 64

Assessment of Interstitial Fibrosis and Tubular Atrophy on Kidney Biopsy Using Urine Uromodulin Levels

Manav Parikh, Heather Thiessen Philbrook, David Hu, Jack Bitzel, Dennis G. Moledina, Steven G. Coca, Chirag Parikh, Steven Menez

Urine uromodulin (UMOD) is the most abundant protein produced by the thick ascending limb and is a biomarker of kidney health. Interstitial fibrosis and tubular atrophy (IF/TA) is a histological feature indicating kidney tissue scarring associated with poor kidney health. Assessment of IF/TA on kidney biopsy helps determine the intensity of treatment for acute and chronic conditions. As most patients cannot get a kidney biopsy, assessment of IF/TA by non-invasive methods is helpful in disease management. The purpose of the study was to examine the relationship between urine UMOD levels and the degree of IF/TA.

Urine UMOD concentrations were measured using the Meso Scale Discovery platform in 200 participants that underwent native kidney biopsy at the Johns Hopkins Hospital between 2020-2023. The primary exposure was urine UMOD indexed to urine creatinine (UMOD:Cr). The degree of IF/TA (<10%, 10-50%, >50%) was determined based on clinical pathology reports. Other participant characteristics were obtained from electronic health records.

Urine UMOD:Cr concentrations were lower with higher severity of IF/TA (p<0.001). Using ordinal regression, doubling of UMOD:Cr was significantly associated with a decreased odds of IF/TA, with an unadjusted odds ratio (95% confidence interval) of 0.61 (0.51, 0.73) and adjusted of 0.81 (0.65, 1.0). Results were similar for urine UMOD concentration, not indexed to urine creatinine.

UMOD:Cr was lower with higher levels of IF/TA on kidney biopsy. Future research is needed to develop non-invasive assessments of underlying IF/TA without kidney biopsy.

ABSTRACT 65

Characterizing the role of PDGFRa as the primary cause of pulmonary disease

Sydney Delman, Angela Zhu, Alla Malinina, Sarah Gidner, Xiao Peng, Christy Sadreameli, Enid Neptune

Platelet derived growth factors receptors (PDGFR) are highly expressed by several cell types and play critical roles in the lung. Platelet derived growth factors (PDGF) bind to PDGFR, inducing autophosphorylation and downstream signaling cascades that affect cell differentiation, proliferation, and migration. In mouse-models, knocking out either the receptor (PDGFRa) or the ligand (PDGF-A) leads to a lack of alveolar septation due to defects in myofibroblast differentiation and localization.

We have identified two individuals with neonatal respiratory insufficiency, early-onset pulmonary emphysema and hemorrhage, and tissue pathology showing poor alveolarization, dilated distal airways, and elastic fragmentation. They share a heterozygous autosomal dominant nonsynonymous missense variant of unknown significance (VUS) in PDGFRA, the gene that encodes PDGFRa. We hypothesize that this VUS mechanistically contributes to early-onset, severe, progressive lung disease via a haploinsufficiency, dominant negative (DN) or atypical gain-of-function (GOF) effect in pulmonary myofibroblasts. Our research group has created a primary dermal fibroblast line from the index cases.

Using immunoblotting techniques, we aimed to define the disturbances in receptor expression, phosphorylation, and downstream phosphoprotein levels associated with the variant. We found that the index cases had a baseline activation of the receptor with no ligand treatment while the age/gender matched control cells did not. This finding supports our hypothesis that the early-onset severe lung disease in the index patients is due to an atypical GOF effect in pulmonary myofibroblasts. Moving forward, we will be creating a genetic knock-in mouse model to test various treatments that could potentially help future patients with this mutation.

ABSTRACT 66

Hybrid Formative-Additive Manufacturing (HyFAM)

Nathan Brown, Jochen Mueller

Material extrusion additive manufacturing (AM) provides extensive design flexibility and exceptional material versatility, enabling the fabrication of complex, multifunctional objects ranging from embedded electronics to soft robotics and vascularized tissues. The bottom-up creation of these objects requires discretization into layers and voxels. However, the voxel size, determined by the nozzle diameter, limits extrusion rate, creating a conflict between resolution and speed. To address these inherent scalability challenges, we propose a hybrid formative additive manufacturing technology that combines the respective strengths of each method—speed and quality with complexity and flexibility. Our approach involves 3D-printing complex geometries, multimaterial features, and bounding walls of bulky, lower-resolution volumes, which are rapidly filled via casting or molding. By precisely controlling the materials' rheological properties—while maintaining similar solidified properties and high interfacial strength—we eliminated several typical AM flaws, such as bulging and internal voids, achieving exponentially faster production speeds for objects with varying feature sizes.

ABSTRACT 67

Hypusination of Eukaryotic Initiation Factor 5A controls ubiquitination in fibroblasts

Thea Angela Calahatian, Navid Koleini, Mark J. Ranek, David A. Kass

Protein ubiquitination, driven by sequential actions of E1-E2-E3 enzymes, mediates proteasomal degradation to ensure protein quality control. Free ubiquitin availability depends on its precursors (UBB, UBC, RPS27a, Uba52) and deubiquitinases (DUBs). Translation blockage with cycloheximide eliminates free ubiquitin generation, suggesting a broad regulatory role. Our preliminary results in cardiomyocytes showed inhibiting hypusination, a post-translational modification of the ribosomal subunit eIF5A, diminishes ubiquitin levels by impairing translation of UBC and DUBs. Hypusination of eIF5A is required for translation of proline-rich and some other motifs. Ribosome sequencing revealed inefficient translation of these targets, indicating that hypusination of eIF5A is crucial for maintaining free ubiquitin bioavailability across mammalian cells. We hypothesized that eIF5A hypusination regulates free ubiquitin bioavailability and therefore protein ubiquitination in fibroblasts.

First, we have screened the entire human genome and found UBC possess multiple motifs that requires hypusination for translation. Second, we showed that inhibiting DOHH (the last enzyme in eIF5A hypusination) using a specific inhibitor (Ciclopirox) significantly reduces eIF5A-Hypusine in 3T3-NIH fibroblasts and decreases the cell viability. This inhibition was associated with depressed de novo protein synthesis as assessed by puromycin chase assay. We have found that inhibition of hypusination via CPX leads to a decreased accumulation of ubiquitinated proteins following 4-hour MG-132 addition when compared to controls. Our findings of the lack of ubiquitinated protein accumulation in MG-132 and CPX-treated cells suggest the responsibility of eIF5a hypusination in the translation of UPS-involved proteins highlighting a new mechanism in regulation of free-ubiquitin bioavailability that has not been studied before.

ABSTRACT 68

Microfluidic shell for embryo-inspired 3D chemical patterning

Derosh George, Jingxun Chen, Itzy E. Morales Pantoja, Chris Acha, Soo Jin Choi, Jonathan Lau, Lena Smirnova, David H. Gracias

3D chemical patterns, like gradients, are essential for controlling information flow in biology and have extensive applications in tissue engineering, microphysiological systems, and developmental biology. Although researchers have developed various microfluidic systems for tissue engineering, they are mainly limited to 2D form factors. Here, we report the development of a 3D self-folding biocompatible microfluidic shell that can precisely inject liquid around 3D millimeter and submillimeter objects, enabling spatiotemporally controlled chemical patterning similar to embryos. Guided by computational fluid dynamics simulations, we show how complex gradients can be formed in gels and tissue constructs using this 3D self-folding microfluidic system. We also show its ability to perform multi-chemical patterning and facilitate complex chemical reactions inside 3D entities. Finally, we demonstrate the biocompatibility of these 3D microfluidic shells and their unique ability to selectively patterning brain organoids within an assembly of organoids. The presented work has potential broad applicability in chemistry, self-organization, tissue engineering, and developmental biology. Combined with our work on a shell microelectrode array, the presented microfluidic shell can be a multimodal interrogation and stimulation platform relevant to various research studies on organoids, including the developing field of organoid intelligence.

ABSTRACT 69

Engineering Soluble Neuropilins for the Treatment of Corneal Neovascularization

Xinran An, Jamie Spangler, Akrit Sodhi

Corneal neovascularization (CoNV) is a sight-threatening condition that affects over 1.4 million people annually. It results from an imbalance between angiogenic and anti-angiogenic signals, leading to the abnormal growth of vascular and lymphatic vessels into the normally avascular cornea. Despite ongoing research, no curative treatment exists, though anti-angiogenic therapies have shown promise due to their efficacy and relatively low incidence of adverse effects. Combination therapies that target multiple proangiogenic pathways, could provide a significant therapeutic advantage for treating CoNV through synergetic effects. Two angiogenic factors, Angiopoietin-like 4 (ANGPTL4) and vascular endothelial growth factor (VEGF), are key drivers of pathological vascular and lymphatic vessel growth in CoNV. These factors synergize as vasoactive molecules, binding with high affinity to the vascular endothelial cell receptor Neuropilin-1 (NRP1). This project focuses on engineering a high-affinity soluble NRP1 (sNRP1) to serve as a decoy receptor, sequestering VEGF and ANGPTL4 away from NRP1 receptors. Using error-prone PCR and yeast surface display, we generated a mutant library and successfully identified clones with up to a 7.5-fold improvement in sNRP1's binding affinity to VEGF. By inhibiting the interaction of these key angiogenic factors with NRP1, sNRP1 is designed to synergistically suppress angiogenesis, effectively preventing or reversing vision loss in patients with CoNV. In conclusion, this innovative therapeutic approach holds great promise in addressing a critical unmet need, offering a potential breakthrough in the treatment of CoNV.

ABSTRACT 70

A Robustness Analysis of High Dimensional Consensus (HDC) Mass Spectra in Forensic Drug Identification

Wencheng Zhong, Amudhan Krishnaswamy Usha, Briana A. Capistran, Anthony J. Kearsley

Mass spectrometry is a powerful tool for identifying compounds, but fragmentation complexity and measurement variability can make it difficult to distinguish compounds with similar mass spectra using a single query spectrum. Most forensic labs use gas chromatography-electron ionization mass spectrometry (GC-EI-MS) in their workflows to identify controlled substances. While a single spectrum is typically used for identification, we propose a novel method called High Dimensional Consensus (HDC) mass spectra, leveraging multiple measurements for improved accuracy.

We tested HDC on 160 mass spectra, comprising 10 replicates of 16 distinct compounds generated by GC-EI-MS, including common controlled substances and adulterants. Our results show HDC achieves 100% identification accuracy, excelling at differentiating structurally similar compounds. For example, despite a cosine similarity of 0.997 between methamphetamine and phentermine, HDC produced a score of 3.6092e-34, effectively distinguishing the two.

In comparative studies, HDC outperformed traditional machine learning models, such as logistic regression, random forest, and XGBoost, as well as a deep learning classifier, achieving up to 12.5% higher accuracy on real-world data without synthetic noise. In robustness tests, HDC maintained high performance even with moderate synthetic noise, simulating measurement inconsistencies.

Overall, HDC offers reliable and explainable results, demonstrating strong potential for forensic applications. It enhances seized drug identification by accurately distinguishing complex mass spectra, aiding forensic scientists in combating drug-related crimes and supporting public health efforts.

ABSTRACT 71

Manipulating stress granules to protect cardiac myocytes from cell death

Yashas Mallikarjun, Hannah Swimm, Bryan Ho, Deepthi Ashok, Brian O'Rourke, D. Brian Foster, Natasha E. Zachara, & Kyriakos N. Papanicolaou

Stress granules (SGs) are cytoplasmic assemblies that form during acute cellular stress. They lack a membrane, and they enclose mRNA, translation initiation factors, ribosomal subunits, and other proteins that participate in protein-protein interactions and phase-separation. SG formation protects cells during stress by rewiring translation, sequestering signaling proteins, maintaining the integrity of macromolecules, and preserving ATP levels. Their role in neuronal cell death have been extensively researched, but their importance in cardiomyocyte viability remains unknown. We therefore wanted to investigate if increasing or decreasing SG formation improves the survival of cardiac myocytes against stress. O-GlcNAc is a post-translational modification of a protein and may be involved in the pathway of stress granule formation. We also sought to consider if it played a role in SG formation. We found that promoting SG formation utilizing a SA treatment enhanced cell survival against staurosporine. Additionally, G3BP1/2 knockdown strongly reduces cell viability both at baseline and in the presence of a death agent. Salubrinal strongly improves cell viability against staurosporine although it did not promote SG formation. Finally, we found that O-GlcNAcylation and stress granules colocalize in the cytoplasm. Collectively, our data suggests that reducing baseline expression of SGs reduces cell viability and increasing it has a protective effect. Additionally, we found that O-GlcNAc is strongly associated with stress granule formation. Possible areas of investigation could be utilizing simulated ischemia via coverslip in order to improve biological coherence. Alternatively, OGT knockdown experiments may show if a modulating effect exists with regulators of SG formation.

ABSTRACT 72

Elevated Complement Component 3 (C3) in Allergic Rhinitis: Implications for Macrophage Polarization and Disease Severity

Xuan Yuan, Shaobin Xie, Liyuan Liu, Peisong Gao

Background: Complement component 3 (C3) is a crucial protein in the complement system, playing a vital role in the innate immune response. Initial RNA-seq analysis has revealed elevated levels of C3 in the nasal mucosa of patients with allergic rhinitis (AR). This study aimed to confirm the expression of C3 in AR and investigate its impact on macrophage polarization.

Methods: RNA-seq analysis was conducted on nasal mucosa samples from AR patients and healthy controls (HC) (n=8 per group). The expression of C3 was further validated by RT-PCR in an independent cohort (n=30 per group). To explore the role of C3 in macrophage polarization, bone marrow-derived macrophages (BMDMs) were treated with recombinant C3 and C3aR antagonist (SB290157) or were derived from C3-deficient mice.

Results: The RNA-seq analysis identified C3 as one of the most up-regulated genes in the nasal mucosa of AR patients compared to healthy controls. This increased expression was confirmed by RT-PCR in a larger cohort, with C3 levels correlating with AR severity. Immunostaining analysis demonstrated that C3 is predominantly expressed in nasal epithelial cells. Functional studies in BMDMs revealed that treatment with C3 promoted polarization into M2 macrophages, as indicated by increased expression of M2 markers (Arg-1, Ym2, and Chi3l3) and decreased expression of M1 markers (iNOS, TNF-α, and IL-1β). Conversely, treatment with the C3aR antagonist SB290157 induced M1 polarization. The same pattern was observed utilizing C3-deficient BMDMs.

Conclusion: Our findings indicate that C3 is significantly up-regulated in the nasal mucosa of AR patients and influences macrophage polarization.

ABSTRACT 73

Single iso-center location optimization for effective radiotherapy treatment of multi-lesion brain metastasis

Jing Liu, LiCheng Kuo, Gourav Jhanwar, Masoud Zarepisheh, and Kimia Ghobadi

Single iso-center stereotactic radiosurgery (SRS) for multiple brain metastases (BMs) reduces treatment time while maintaining dose precision; however, determining the optimal iso-center is crucial for plan quality. We developed an AI approach that integrates the Eclipse volumetric modulated arc therapy (VMAT) optimization engine with Bayesian Optimization to simultaneously optimize the iso-center location and machine parameters (e.g., beam intensities and shapes). Unlike traditional methods that rely primarily on tumor geometry or manual selection based on clinicians' experience, our technique prioritizes key clinical metrics, including how well the radiation dose conforms to the tumor (conformity index) and how rapidly the dose falls off outside the tumor (gradient index). It also accounts for uncertainty scenarios, such as patient movement or setup errors, to ensure robust treatment outcomes. We validated the framework on eight clinical cases at Memorial Sloan Kettering Cancer Center, observing significant improvements in treatment quality. The plans generated by our method improved dose conformity by up to 14% and dose fall-off by up to 15% compared to conventional approaches, even under uncertainty conditions. By automating a process traditionally performed manually or geometrically, our approach enhances treatment precision, reduces healthy tissue exposure, and ensures efficient workflows in clinical practice.

ABSTRACT 74

Enhancing Fall Risk Prediction: Integrating EHR Variables into the Johns Hopkins Fall Risk Assessment Tool

Fardin Ganjkhanloo, Erik H Hoyer, Daniel L Young, Kimia Ghobadi

Falls remain a critical concern in inpatient settings, with significant implications for patient safety and healthcare resource utilization. The Johns Hopkins Fall Risk Assessment Tool (JHFRAT) is widely employed to identify high-risk patients; however, its reliance on static, predefined risk factors limits its predictive accuracy. This study demonstrates the value of augmenting the JHFRAT with electronic health record (EHR) variables, including standardized mobility measures such as AMPAC and JHHLM scores, comorbidity profiles, and demographic data.

Using a dataset of over 54,000 inpatient admissions across three hospitals, we developed two enhanced models: an XGBoost framework to benchmark predictive performance and a constrained logistic regression (CLR) model to maintain clinical interpretability. Results showed that the XGBoost model achieved an AUC-ROC of 0.98 and an AUC-PR of 0.84, significantly outperforming the baseline JHFRAT (AUC-ROC: 0.89, AUC-PR: 0.44). The CLR model also demonstrated improved predictive capabilities (AUC-ROC: 0.93, AUC-PR: 0.65) while preserving the hierarchical structure of JHFRAT components. Feature importance analysis revealed that mobility-related EHR variables provided critical insights into fall risk, complementing traditional factors. The proposed models align with clinical workflows, enabling more accurate risk stratification without disrupting decision-making processes.

This work highlights the potential of integrating EHR data into established clinical tools to improve fall prevention strategies. Future directions include dynamic risk modeling and prospective validation to assess the impact on clinical outcomes and healthcare costs.

ABSTRACT 75

Association of Aortic Valve Calcification with Chronic Kidney Disease: The Multi-Ethnic Study of Atherosclerosis

Ashkan Abdollahi; Maryam Mojarrad Sani; Mahsima Shabani; Bruna S. Matuck; Michael J. Blaha; Colin O. Wu; Bharath Ambale-Venkatesh; Matthew J. Budoff; Jordan B. Strom; Jerome I. Rotter; Wendy S. Post; Roger S. Blumenthal; David A. Bluemke; João A. C. Lima; Seamus P. Whelton

Background: Aortic valve calcium (AVC) is associated with an increased risk of cardiovascular disease, non-cardiovascular disease such as dementia, and all-cause mortality. Traditional atherosclerotic cardiovascular disease risk factors are associated with both AVC and chronic kidney disease (CKD), but whether there is an association between AVC and CKD is unknown.

Objectives: To ascertain whether AVC quantified by cardiac CT scanning is independently associated with the long-term risk of incident CKD among individuals without a previous history of cardiovascular disease.

Methods: We examined 6,346 Multi-Ethnic Study of Atherosclerosis (MESA) participants who underwent cardiac CT scanning at Visit 1 (2000-02) and had an eGFR of ≥ 60 mL/min/1.73 m2. AVC was quantified using the Agatston method and categorized as 0, 1-99, and ≥100. Incident CKD was defined as an eGFR < 60 mL/min/1.73 m2 accompanied with an at least 40% decline in eGFR from baseline, and/or a diagnosis of CKD and indicators of end stage renal disease extracted from hospital records using the International Classification of Disease (ICD) codes. We performed Kaplan-Meier survival curve analyses along with multivariable Cox proportional hazard regression models, adjusted for age, gender, race/ethnicity, highest level of education and traditional cardiovascular risk factors along with coronary artery calcium (CAC), lipoprotein (a) (Lp[a]), and the APOE-ε4 genotype to examine the association between AVC (categorical and log-transformed) and incident CKD.

Results: Participants had a mean age 62.2±10.1 years, 53% were women, and AVC >0 was present in 795 (12%) participants. During a median follow-up time of 16.9 years, 982 (15%) participants developed incident CKD. AVC examined as a continuous variable was associated with a significantly increased risk of developing CKD (per log-unit [AVC+1] HR 1.06 [95% CI: 1.02-1.10]; p = 0.005). There was a stepwise increased risk for CKD with higher AVC levels (Figure). Similarly, in the multivariable adjusted Cox models, participants with AVC ≥100 had a higher risk of incident CKD, compared with the AVC=0 group (HR 1.48 [95% CI: 1.15-1.89]; p = 0.002). The observed associations remained after further adjusting for CAC score (p = 0.024), Lp (a) (p = 0.004), and the APOE-ε4 genotype (p = 0.004).

Conclusions: In a multi-ethnic cohort of participants free of CKD at baseline, AVC was independently associated with a higher risk of incident CKD.

ABSTRACT 76

The Role of SETDB2 in Regulating Acetaminophen Induced Acute Liver Injury

Yang Yang

Acetaminophen (APAP)-induced acute liver injury (AILI) is a leading cause of drug-induced liver injury and subsequent liver failure in both adults and children in the US. The immune response contributes to the underlying AILI acute hepatotoxicity and the hepatocyte regeneration afterward to repair the damage. SETDB2 belongs to the KMT1 sub-family of lysine methyltransferase enzymes, and it regulates both innate and adaptive immune responses in different animal models. Our lab has previously found that SETDB2 deficiency differentially regulates proinflammatory gene expression in a two-step endotoxemia model in bone marrow derived macrophages. Based on these preliminary studies, we hypothesized that SETDB2 may play a role in AILI by regulating the associated pro-inflammatory immune response which could point to SETDB2 as a novel potential therapeutic target for AILI.

No significant difference in the extent of liver injury were observed in mice with SETDB2 deficiency in hepatocytes and kupffer cell compared to the wild-type mice; however, significantly less liver injury was found in mice with SETDB2 myeloid cell deficiency (SETDB2-MKO). Further, the metabolomic analysis revealed key differences in purine metabolites. IMP levels significantly increased in wild-type mice but decreased in SETDB2-MKO mice after AILI. Meanwhile, inosine and AMP levels remained higher in SETDB2-MKO mice compared to wild-type mice. These results suggest that purine metabolism is reprogrammed differently in SETDB2-MKO mice during AILI. Further investigations are needed to clarify the precise mechanisms by which SETDB2 regulates purine metabolism during AILI and whether the altered purine profile contributes to the protection from liver damage.

ABSTRACT 77

Deciphering the protective effects of sustained BRAF signaling in OGT cardiomyopathy

Clara Cho

O-GlcNAcylation, a dynamic post-translational modification regulated by O-GlcNAc Transferase (OGT) and O-GlcNAcase (OGA), is critical for cardiac homeostasis and mitochondrial function. In cardiomyocyte-specific OGT knockout (OGT-icko) mice, loss of O-GlcNAcylation leads to heart failure, characterized by transcriptional disruptions in metabolic and mitochondrial pathways. Previous studies identified that O-GlcNAcylation is necessary for optimal activation of ERK1/2, a key component of the mitogen-activated protein kinase (MAPK) pathway critical in cardiac stress responses. Given this relationship, it was hypothesized that sustained ERK1/2 signaling could counteract the detrimental effects of OGT loss. To test this, the BRAFV600E model was used, which induces constitutive activation of the ERK1/2 pathway. Double-transgenic (DTG) mice that are both OGT-deficient and express BRAFV600E were also used to evaluate the protective potential of sustained ERK1/2 activation.

Transcriptomic analyses revealed profound transcriptional dysregulation in OGT-icko cardiomyocytes, including downregulation of genes central to energy metabolism and ATP production. BRAFV600E activation in DTG hearts partially restored these pathways, as evidenced by quantitative real-time PCR gene expression analyses of key cardiac markers (Myh6, Myh7) and fibrosis-related genes (Postn, Col1). This molecular recovery was accompanied by the mitigation of pathological gene expression profiles, underscoring the protective role of ERK1/2 signaling in OGT-deficient hearts.

ABSTRACT 78

Electrostatic dose modulation improves lifespan of beam-sensitive specimens for advanced electron crystallography technqiues

Daniel L. Foley, Partha P. Das, Barnaby D. A. Levin, Bryan W. Reed, Daniel J. Maisel, Runlai Wang, John D. Tovar, Alejandro Gomez-Perez, Monika Budayova-Spano, Wai Li Ling, Anna Mian, Sergi Plana-Ruiz, Stavros Nicolopolous, Mitra L. Taheri

Electron-based crystallographic techniques such as 3-dimensional electron diffraction (3DED) have grown rapidly in popularity relative to traditional x-ray methods due to their high spatial resolution as well as their ability to probe low densities of small crystals. For beam-sensitive crystals such as those of proteins and other macromolecules, the use of cryogenic electron microscopy (CryoEM) is necessary to maintain the specimen's crystallinity throughout the electron dosing of the experiment. We demonstrate a technique where useful electron diffraction data can be acquired at room temperature through the combined application of electrostatic dose modulation (EDM) and a direct electron detector. During the diffraction experiment, the beam is rapidly blanked by the EDM system at cycles as low as 2 microseconds. This allows not only extremely precise control of the electron dose, but also distributes the dose over a wider time period. We find that the application of this techniques improves the lifespan of beam-sensitive crystals, both as a function of total time (enabling acquisition of 3DED datasets) and also as a function of electron dose. This means that not only is damage being spread out over time, but electron beam-induced damage accumulation is being avoided altogether, opening the door to high-resolution, room-temperature electron crystallography.

ABSTRACT 79

"Affinity cocktails" of antibody-radioconjugates for solid tumor-penetrating alpha-particle radionuclide therapy and their digital twin

Aira Sarkar, Rajiv Nair, Pooja Hariharan, Mihail Kavousanakis, Rohit Chaudhari, Kathleen Gabrielson, Yannis Kevrekidis, Stavroula Antibody-

Antibody-radioconjugates are among the leading approaches in targeted alpha-particle therapies for the treatment of established/vascularized solid tumors that are not responsive to approved therapies. The complex double-strand DNA breaks caused by alpha-particles, when traversing cells, render them impervious to resistance, if delivered optimally. However, the diffusion-limited tumor penetration of strongly binding antibody-radioconjugates combined with alpha-particles' short-range in tissue (40-80μm), result in heterogenous patterns of tumor irradiation. The latter is the root cause of treatment failure in the clinic, because cancer cells not being hit by alpha-particles will not be killed.

To enable more uniform/deeper tumor irradiation, we engineered "affinity cocktails" of separate actinium-225 antibody-radioconjugates, each exhibiting different affinities for the same receptor on cancer cells. "Affinity cocktails" comprise (a) "high affinity" antibody-radioconjugates, which deliver their cargo in tumor cells closer to the vasculature, from which the "lower affinity" antibody-radioconjugates clear too fast, and (b) "low affinity" antibody-radioconjugates that penetrate the deep parts of tumors farther from the vasculature, where the "high affinity" antibodies fail to reach. The efficacy of "affinity cocktails" was assessed on mice with subcutaneous xenografts of different: cancers (BT474/breast, HEPG2/hepatic, BxPC3/pancreatic), expression levels of the targeted receptor, and/or receptor type (HER2, HER1).

On all mouse models, "affinity cocktails" of antibody-radioconjugates resulted in the best tumor growth inhibition and/or longer survival, even at lower tumor absorbed doses, compared to any antibody-radioconjugate alone. Optimum activity split ratios among antibody-types, predicted by a digital twin were validated in vivo.

This generalizable approach may enhance strongly-binding antibody-radioconjugates already in the clinic.

ABSTRACT 80

Uncertainty Bounds on Classification (including Diagnostic) Uncertainty under

Andrew Henrichsen, Paul Patrone, Anthony Kearsley

Developing tools in classification theory has applications in both Machine Learning and diagnostics. Specifically, the concept of prevalence, i.e. the proportion of individuals with a particular condition is fundamental to the probabilistic uncertainty of a particular outcome. This principle, of uncertainty measured on a point-by-point basis, is called local accuracy, and is meaningful for establishing rigorous uncertainty quantification for the classification space. Developed on the binary classification space, prior work has established rigorous values for the local accuracy given sufficient data. However, the question of what is sufficient data had hitherto been unanswered. This work establishes probabilistic bounds on this uncertainty as a function of data quantity, which enables desired bounds of uncertainty to be obtained, under certain assumptions about the classification boundaries.

ABSTRACT 81

Personalized Nutrition Recommendation with Food Item Replacement: A Generalized Observation Noise Inverse Optimization Approach

Emmett Springer, Kimia Ghobadi

Quality nutrition is a well-known factor in the prevention and mitigation of many common chronic illnesses such as diabetes, hypertension, and cardiovascular disease, but adherence to a one-size-fits-all diet plan remains a challenge. Data-driven inverse optimization (IO) has been proposed to infer patient preferences and eating patterns from self-reported dietary behavior data. This preference inference is then used to recommend personalized diet plans which maximize patient taste and adhere to clinical nutritional guidelines. Existing data-driven IO methods adjust the amounts of foods in a patient's diet to improve nutrition but cannot effectively recommend new food to try. In this research, we build a model to recommend healthier alternatives to existing foods in the patient's diet via a generalized observation noise inverse optimization model. Recommendation optimality is achieved through minimal perturbation of both the food amounts (the decision observations) and nutritional content of foods (the left-hand side constraint parameters) necessary to create a diet feasibly to the given nutrition constraints. We apply our model to a retrospective cohort of MyFitnessPal users and show that our model recommendations are more reasonable compared to previous models.

ABSTRACT 82

Engineering High-Throughput Human Neuromuscular Microphysiological System for Phenotypic Drug Testing

Byunggik Kim, Zhanping Ren, Minjae Do, Wonjin Yun, Joseph Criscione, Andres Parra, Roma Desai, Gabsang Lee, and Deok-Ho Kim

Current in vitro neuromuscular junction (NMJ) models lack scalability and long-term functionality, limiting their utility in high-throughput drug screening and disease modeling. We addressed these challenges by creating a novel NMJ microphysiological system that combines engineered human muscle and optogenetically driven motor neurons in 96-well plate formats. A customized magnetic sensing platform, synchronized with optical pacing, enables non-invasive, real-time assessment of muscle contractility.

This system offers enhanced sensitivity over conventional technologies, employing a 3D NMJ model within microfluidic chips. Maintaining separate neuronal and muscle compartments with efficient nutrient exchange confers greater functional longevity and scalability. NMJ tissues generated under these conditions display stable ultrastructure, including a 50% upregulation of the acetylcholine receptor epsilon subunit, indicative of essential synaptic maturation. Over four weeks, human skeletal muscle tissues respond to electrical stimuli with forces stabilizing from day 7 to 28, ranging from 1 Hz twitches at 18.04 ± 10.47 μN (n=5) to 30 Hz tetanic forces at 93.27 ± 51.87 μN (n=5). Stable expression of myosin heavy chain and ion-regulating proteins underscores progressive muscle maturation at the transcriptional level.

Upon optogenetic stimulation, tissues exhibit robust contractile responses and post-synaptic phenotypic changes, outperforming existing models in both stability and physiological relevance. Overall, its scalability, functional readouts, and physiological fidelity make this platform a powerful tool for drug screening, disease modeling, and in vitro NMJ research, accelerating the development of therapies for neuromuscular disorders.

ABSTRACT 83

Accelerating Traumatic Brain Injury Modeling with Neural Operators: Toward Personalized Protective Gear Design

Dibakar Roy Sarkar and Somdatta Goswami

Traumatic brain injury (TBI), including mild TBI and concussion, remains a significant public health challenge with severe consequences. Computational models that account for the anisotropic and heterogeneous biomechanics of the brain provide valuable insights into the relationships between skull acceleration, brain deformation, and injury mechanisms, helping to guide the design of protective headgear and safety standards. However, existing 3D models are typically validated using experimental data from animal studies and cadavers, which differ significantly from the responses of a living human brain. Moreover, these models are computationally expensive, limiting their feasibility for designing personalized protective equipment. Our research focuses on developing an efficient surrogate model that maps demographic-specific brain anatomy to displacement and deformation patterns. This model provides a comprehensive predictive framework by integrating magnetic resonance elastography (MRE) data, anatomical imaging, frequency-dependent responses, and demographic variables. Once trained, it can reliably generalize to unseen cases, offering predictions in a fraction of a second. This capability enables inverse analysis for designing personalized protective equipment while accounting for individual variations in brain structure and material properties. By addressing the limitations of traditional models, this work offers scalable and cost-effective solutions for TBI prevention, paving the way for customized interventions that advance both engineering and medicine.

ABSTRACT 84

Biometric Insights and Clinical Outcomes in Interstitial Lung Disease Patients on Long-Term Oxygen Therapy: A Remote Patient Monitoring Study

Wilson Tang, Sonye Danoff

This study explores the relationships between biometric data obtained through remote patient monitoring (RPM) and disease progression in patients with Interstitial Lung Disease (ILD) on long-term oxygen therapy (LTOT). Among the 87 participants who consented for the study, 44 initiated the RPM; the remaining 43 patients either withdrew consent, moved, died or received a lung transplant prior to initiating RPM. Of the 44 participants who completed some portion of the RPM, 19 (43%) experienced 29 events (24 hospitalizations, 2 urgent care visits and 3 deaths).

Among the 34 participants with evaluable lung function studies, 53% experienced a change greater than 5% in percent predicted forced vital capacity (FVC), with 10 declining, 16 remaining stable, and 8 improving. Baseline characteristics showed similarity between participants with stable or improved FVC, while those who declined were generally older, with higher baseline FVC and lower prescribed oxygen flow.

Patient-reported outcomes (PROs) were similar across groups, though the SGRQ-I Impact score significantly differed between participants whose FVC declined compared with those whose were stable/improved. Hospitalized patients had higher SGRQ-I scores indicating greater impairment.

Twenty-nine predefined events were recorded, exceeding our estimate and indicating the disease severity of this patient population. Biometric data revealed elevated heart rates and increased desaturation time prior to exacerbations. These findings underscore the potential of RPM in monitoring ILD patients and warrant further investigation into the physiology predicting clinical events.

ABSTRACT 85

Metabolic conditioning during ex vivo stimulation of naïve tumor antigen-specific CD8 T cells

Joseph Choy, Sydney Shannon, Si-Sim Kang, Shuyi Li, Kenneth Adusei, Shaelyn R. Marx, Hai-Quan Mao, Jonathan Schneck

This study explores the use of the glutamine antagonist 6-diazo-5-oxo-L-norleucine (DON) to optimize the ex vivo expansion of antigen-specific CD8 T cells for adoptive cell therapy (ACT). The goal is to generate allogeneic, tumor-antigen-specific cytotoxic T cells with a memory-like, less exhausted phenotype, using a process that avoids genetic manipulation and utilizes naïve T cell precursors. Artificial antigen-presenting cells (aAPCs) were employed to expand CD8 T cells targeting melanoma antigens (H-2Kb:SIY and H-2Kb:Trp2) in a dendritic cell-free system.

Despite glutaminolysis being crucial for T cell activation, DON did not reduce the proportion of antigen-specific T cells but instead promoted a central-memory phenotype (CD44+CD62L+), while lowering PD-1 and TIM3 expression. Non-cognate T cells also shifted towards a naïve phenotype (CD25-CD44-CD62L+). Dose-response experiments revealed that early DON application during T cell activation was critical for its effects, while sustained exposure provided additional benefits. Mechanistic studies with high-affinity antigen stimulation showed that DON modulated early activation kinetics, preserving TCR expression and promoting a less differentiated phenotype in high-affinity primed cells.

These findings suggest that metabolic conditioning with DON enhances the quality of ACT products by fostering a memory-like phenotype and reducing exhaustion markers, particularly during early priming of high-affinity T cells. This approach offers a promising strategy for improving ACT efficacy in cancer treatment by leveraging broad glutamine antagonism to optimize T cell function and differentiation.

ABSTRACT 86

Cystatin C to Albumin Ratio as a Prognostic Indicator in Heart Failure with Preserved Ejection Fraction

Masih Tajdini, Mohammad Keykhaei, Vivek Jani, Radu Tanacli, Virginia Hahn, David Kass, Kavita Sharma

Introduction: The urgent need to establish an individualized therapeutic approach in heart failure underscores the importance of biomarkers. NT-proBNP, faces challenges in Heart Failure with Preserved Ejection Fraction (HFpEF), such as higher levels in atrial fibrillation, commonly found in HFpEF patients, or lower levels in obese patients. The Cystatin C to Albumin Ratio (CysC/Alb) has not been assessed previously in HFpEF. This study examines the association between the CysC/Alb ratio and echocardiographic parameters, right heart catheterization findings, mortality, and hospitalization among patients with HFpEF.

Methods: Patients enrolled in the Johns Hopkins HFpEF registry from July 2014 to January 2024 were included. The study involved a comprehensive examination, including clinical assessments, laboratory evaluations, and echocardiography. To predict outcomes, ROC curve analysis identified the most effective marker, characterized by the highest odds ratio and optimal area under the curve (AUC). Trends in variables associated with the CysC/Alb ratio were analyzed using multivariate linear regression and an independent sample T-test for clinical, echocardiographic, and exercise right heart catheterization between high and low levels of this ratio. Kaplan-Meier survival analysis was performed to assess the CysC/Alb ratio with the combined outcome of heart failure hospitalization and all-cause mortality.

Results: The study involved 281 subjects, with an average age of 65 years; 65% of the patients were female. The median follow-up duration was 41 months. Among various biomarkers, the CysC/Alb ratio demonstrated the highest odds ratio and the best AUC for predicting mortality and hospitalization (OR=13.09 [3.41-56.61], AUC 0.656, $p < 0.001$), and these associations remained significant after adjusting for age, gender, body mass index, total bilirubin, and GFR ($\beta = 2.68$ [2.2 - 98.03], p=0.043). Two groups of patients were identified based on Youden's J statistic and the Cys/Alb ratio (High level > 0.6 and Low level ≤ 0.6). Significant associations were found between higher levels of the Cys/Alb ratio and LA Diameter, Left Ventricular Mass Index, A wave, and E/E' for diastolic function, as well as right ventricular systolic pressure. Consistent correlations were observed between the ratio and PCWP, even in various exercise stages during right heart catheterization (Table 2). Boxplot revealed higher Cys/Alb ratios in patients experiencing mortality or hospitalization. The Kaplan-Meier graph indicated a less favorable outcome in patients with higher levels of the ratio (figure).

Conclusions: The study demonstrates the potential of the CysC/Alb ratio as a strong predictive marker in HFpEF patients. The findings reveal significant associations with key clinical indicators and emphasize its role in predicting mortality and heart failure hospitalization.

ABSTRACT 87

Low-dose chemotherapy Empowers alpha-Particle Radionuclide Therapy Against Metastatic Triple Negative Breast Cancer

Pooja Hariharan, Rajiv Nair, Aira Sarkar, Prof. Daniele. M. Gilkes, Prof. Kannan Rangaramanujam, Prof. Stavroula Sofou

Breast cancer brain metastases (BCBM) remain incurable. Despite multi-modal therapies, the location of the tumor makes it difficult to treat aggressively, due to adverse consequences to neighboring brain, rendering prognosis extremely poor. Additionally, patients ultimately develop resistance to approved therapies.

We unexpectedly found that when we combine alpha-particle RadioPharmaceutical Therapy (αRPT) with low-dose DNA-damaging chemotherapy, we observe significantly prolonged survival of animals bearing triple-negative BCBM, compared to the survival of animals treated with each modality alone. This is surprising, because αRPT is orders-of-magnitude more powerful than any chemotherapy and/or other radiotherapies. This study aims to understand the reasons explaining this outcome and optimize treatment scheduling.

High-energy, short-range (40-80μm) alpha-particles unequivocally kill cancer cells by causing double-strand DNA-breaks. αRPT is impervious to resistance and ideal for treating BCBM, because irradiation of the peripheral brain is minimal. However, cancer cells not being hit by α-particles will not be killed. Therefore, to spread the radioactivity within brain tumors, αRPT was attached on systemically injected dendrimers (dendrimer-radioconjugates) that selectively accumulated in brain tumors and associated with "tumor-infiltrating" tumor-associated macrophages.

Our findings demonstrate that administration of low-dose chemotherapy, 24 hours before injecting αRPT, enabled greater tumor uptake of αRPT and/or better intratumoral spreading of αRPT; this partially explains the prolonged survival of mice treated with the combined modalities. Additionally, the two modalities were found to form an exceptionally lethal DNA-attacking cocktail when acting on the same cells. Importantly, however, the two modalities physically co-localize only at the tumors, keeping off-target toxicities to a minimum.

ABSTRACT 88

Increased Lipoprotein(a) Levels Independently Predict a Higher Incidence of Ventricular Arrhythmias: A Comprehensive Retrospective Cohort Study

Maryam Mojarrad Sani, Tarek Harb, Thorsten Leucker, Jonathan Chrispin

Background: Lipoprotein(a) [Lp(a)] is a causal risk factor for atherosclerotic cardiovascular disease (ASCVD), which is associated with an increased risk of ventricular arrhythmias (VA). Beyond its role in cholesterol metabolism, Lp(a) possesses pro-inflammatory properties, including promoting endothelial dysfunction and inflammation, which may independently contribute to arrhythmogenesis. However, whether Lp(a) is linked with VAs independent of ASCVD remains unknown.

Objective: To examine the association of Lp(a) with VAs in a population-based, retrospective cohort study utilizing data from the TriNetX Research Network.

Methods: We conducted a retrospective analysis of the data from 87 healthcare organizations within the TriNetX Research Network. Patients over 18 years old with available serum Lp(a) measurement were included. Participants were divided into two cohorts based on their Lp(a) levels: cohort 1 (Lp(a) ≤75 nmol/L), and cohort 2 (Lp(a) ≥76 nmol/L). Follow-up time to VA occurrence was calculated from the time of Lp(a) level measurement within each cohort. The composite endpoint was the incidence of VAs, which included ventricular tachycardia, ventricular fibrillation, ventricular flutter, or cardiac arrest due to underlying cardiac conditions. We compared the two cohorts using Kaplan-Meier survival analysis along with Cox proportional hazard regression analysis after propensity score matching.

Results: 70,345 patients were included in cohort 1 and 37,223 in cohort 2. After propensity score matching, both cohorts had 36,018 patients. In cohort 1, 735 patients experienced VAs, compared to 583 in cohort 2. The mean age was 53.3 ± 15.7 years, with 53.35% of participants being female, 12.1% being Black, and 68.89% being White. The Kaplan-Meier survival analysis showed a higher survival probability at the end of the study period for the Lp(a) ≤75 compared to the Lp(a) ≥76 cohort (94.65% vs 85.08% p=0.003). The hazard ratio (HR) for VA was 0.789 (95% CI: 0.675–0.922, p = 0.045), indicating that lower Lp(a) levels are associated with reduced VA risk.

Conclusion: This study demonstrates that elevated Lp(a) levels are independently associated with a higher incidence of VA, even after adjusting for traditional ASCVD risk factors, including previous myocardial infarction and atherosclerotic heart disease of the native coronary artery. Future research should focus on the mechanisms underlying the relationship between Lp(a) levels and VA and whether Lp(a) reduction can reduce the risk of VA and other cardiovascular outcomes.

ABSTRACT 89

Genomic Signatures of Aging for Frailty in the NHLBI TOPMed Program

Lisa R. Yanek, Megan T. Lynch, Aaron Aragaki, Traci Bartz, Kathryn Lunetta, B. Gwen Windham, Ramon Casanova, Douglas Kiel, Fangyu Liu, Simin Liu, Anne Newman, Michelle Odden, Alexander P. Reiner, Shivani Sahni, Jean Wactawski Wende, Dan Arking, Chunyu Liu, Karen Bandeen-Roche, Jeremy Walston, Chloé Sarnowski, Alexander Bick, Joshua Weinstock, Paul Auer, Jennifer A. Brody, Nona Sotoodehnia, Mengyao Wang, Josef Coresh, Charles Kooperberg, Joanne Murabito, Bruce M. Psaty, Rasika A. Mathias, Margaret A. Taub, TOPMed Longevity and Healthy Aging Working Group

Background: To assess association of dynamic genome metrics (telomere length [TL], clonal hematopoiesis of indeterminate potential [CHIP], mitochondrial DNA copy number [mtDNAcn]) with frailty, we used WGS generated through the NHLBI TOPMed Program.

Methods: Four TOPMed cohorts (ARIC, CHS, FHS, WHI) were included. Frailty was assessed with the Fried criteria (scored 0-5: 0=robust, 1-2=pre-frail, 3-5=frail). Dynamic genome measures were centrally called at the TOPMed IRC. Cross-sectional multivariable three-level ordinal regression models were run in each cohort with frailty as the dependent variable and TL, mtDNAcn, or CHIP as the independent variable of interest, adjusting for the difference between age at blood draw and age at frailty assessment, age at frailty assessment, sex, race, education, BMI, smoking, and cohort-specific covariates. Results were meta-analyzed.

Results: Participants (n=8788: n=727 frail, n=4350 prefrail, n=3711 robust) were 65.2 ± 10 yrs at blood draw, 73.6 ± 7.6 yrs at frailty assessment; 61.7% female; 85% European ancestry, 14.3% African ancestry, 0.7% Hispanic. Adjusting for all covariates, lower mtDNAcn was significantly associated with risk of worse frailty status in FHS ($\delta\wr$; 95% CI = -0.466; -0.7927, -0.1393) and meta-analysis (Z = -2.5, p = 0.01). Shorter TL showed significant association with risk of worse frailty for CHS (-0.15; -0.25, -0.01) and FHS (-0.22; -0.38, -0.07) in unadjusted models only. Neither TL nor CHIP showed significant association with frailty in meta-analysis.

Conclusions: Only mtDNAcn revealed association with frailty after covariate adjustment. Future work will extend investigation to mosaic chromosomal alterations, epigenetic aging, and accelerated aging across multiple measures.

ABSTRACT 90

Dynamic Biomarkers of T cell Senescence

Ladaisha Thompson, Annaka Saffron, Gabrielle Reynolds, Chanhong Min, Jeremy Walston, Jude Phillip

Cellular senescence, a hallmark of T-cell aging, involves permanent cell cycle arrest, reduced activation capacity, and hypersecretion of pro-inflammatory molecules. Chronic antigen exposure and unrepaired DNA damage drive an increase in senescent T cells, which contribute to immune system decline and premature aging in solid organs. This research aims to develop an ex vivo platform to study CD4+ T-cell senescence, identify novel biophysical biomarkers, and explore the functional impacts of senescence. We induced senescence-like phenotypes in human CD4+ T cells by subjecting them to repeated antigen stimulation with anti-CD3/CD28 Dynabeads over three-week intervals, with or without doxorubicin. Cells were analyzed for protein biomarkers of senescence, including p16, CD57, and KLRG1, using mass cytometry. Perturbed cells were embedded in type-I collagen hydrogels and imaged live for three hours using brightfield microscopy. Using our computational pipeline, CaMI, we identified distinct motility behaviors distinguishing senescent from non-senescent cells. Senescent-like cells showed reduced proliferation, increased senescence marker expression, and altered motility. Perturbed cells traveled faster, farther, and more directionally compared to non-senescent cells. These findings demonstrate a robust framework for inducing and characterizing T-cell senescence while uncovering behavioral impacts. This platform provides new insights into age-dependent immune phenotypes, offering a path to identifying novel biomarkers of senescence in T cells. It also informs whether T cells from older individuals are more susceptible to senescence, contributing to a deeper understanding of age-associated immune decline.

ABSTRACT 91

The single-cell intrahepatic hepatitis B virus transcriptional landscape in people with chronic infection

Prakriti Sinha, Naomi Esrig, Ashwin Balagopal, and Chloe L. Thio

Chronic hepatitis B (CHB) can be treated but not easily cured. HBV persists in cells in two forms: cccDNA, which produces all viral transcripts, and HBV DNA integrated into host genome (iDNA) and both contribute to the production of hepatitis B surface antigen (HBsAg). In this study, we studied transcription from cccDNA and iDNA at single-cell resolution from livers of people with CHB with and without treatment.

We included liver tissues from 5 people with CHB: 3 on treatment and 2 not on treatment. Using laser capture microdissection, we isolated 150 to 300 single cell equivalents from each liver sample. The total HBV DNA, cccDNA, and HBV RNA transcripts that were used to distinguish cccDNA-derived and iDNA-derived transcription, were quantified using digital PCR platforms.

The serum HBV DNA was <2 log10IU/ml for the 3 people on treatment, and 6 - 8 log10IU/ml for the 2 persons not on treatment. The percentage of infected cells increased from 15.9% to 98.2% as serum HBV DNA levels increased (R2=0.664, p-value=0.0931). People not on treatment compared to those on treatment had higher total HBV DNA per cell (4-600 copies vs 4-12 copies, respectively, p=<0.0001) and higher RNA transcripts per cell (8-2212 copies vs 8-80 copies, respectively (p=<0.0001). Viral transcription in untreated people derived from both cccDNA (13-80% and iDNA (1-3%) whereas there was a greater proportion of cells transcribing from iDNA in people on treatment (5-83% of transcribing cells). While viral transcription is suppressed in people on treatment, iDNA-derived transcription continues. New treatments are required to suppress transcription from iDNA.

ABSTRACT 92

Impact of extreme heat on asthma exacerbations: identifying health disparities in susceptible populations

Emily Scott, Aparna Balasubramanian, Kirsten Koehler, Darryn Waugh, Benjamin Zaitchik, Bianca Corpuz, Jaime Madrigano, Scott Zeger, Meredith McCormack

Rationale: Asthma exacerbations represent a high burden of morbidity and can be triggered by environmental exposures including air pollution, aeroallergens, and extreme temperatures. This study sought to quantify the contribution of ambient temperatures to exacerbation risk and identify patients most susceptible to temperature-related effects.

Methods: Maryland residents from the Johns Hopkins Asthma Precision Medicine Center of Excellence with evidence of asthma exacerbation during June-August were included. Each patient's address at the time of exacerbation was linked to environmental exposure data and sociodemographic data including Area Deprivation Index (ADI). Time stratified case-crossover models were used to estimate the relationship between temperature and exacerbation risk, with effect modification by age, sex, and ADI.

Results: We identified 3,132 asthma exacerbations during summer months among patients living in Maryland. Among 18–39-year-olds, exacerbation risk increased by 20% (5-38%) per 10°F increase in maximum daily temperature. This significant association was not observed among children or older adults. The effect of heat on exacerbation risk among young adults was modified by ADI, with individuals living in high deprivation regions experiencing the greatest increase in risk.

Conclusion: Elevated temperatures are associated with increased asthma exacerbation risk among young adults, with the largest effect among individuals in socioeconomically deprived regions. The difference in susceptibility to heat could be driven by disparities in access to resources such as air conditioning, or occupations that necessitate time outdoors. These results highlight an important health disparity and the need for increased preventive care during summer months for patients vulnerable to heat-induced exacerbations.

ABSTRACT 93

Scalable Doxorubicin Nanoparticle Formulation with Tunable Release Profiles

Yuanmuhuang Long, Sachin V. Kammula, Yicheng Zhang, Hai-Quan Mao

The study presents the sequential flash nanocomplexation (FNC)–flash nanoprecipitation (FNP) process as a scalable method for producing polymeric nanoparticles (NPs) to efficiently control the release of doxorubicin (DOX). DOX-loaded NPs were prepared using poly(ethylene glycol)-b-poly(lactic acid-co-glycolic acid) (PEG-b-PLGA) dissolved in various water-miscible organic solvents, which significantly influenced release rate. This FNC–FNP process produced NPs with a sustained release duration of up to two weeks when dimethyl sulfoxide (DMSO) was used as the solvent. Additionally, the optimized process demonstrated excellent reproducibility and scalability, with minimal batch-to-batch variations. This NP assembly process is complemented by scalable purification with the tangential flow filtration (TFF) method, showing preserved size distribution and DOX release kinetics. This study underscores the technical advantages and translational potential of the FNC–FNP process for nanotherapeutic manufacturing.

ABSTRACT 94

Chronic neck or back pain is an independent risk factor for constant abdominal pain in patients with chronic pancreatitis

Zahra Yousefli, Zachary Kassir, Mahya Faghih, Christopher Fan, Niloofar Jalaly, Elham Afghani, Venkata S. Akshintala, Søren S. Olesen, Asbjørn M. Drewes, Vikesh K. Singh.

Background: Constant abdominal pain among patients with chronic pancreatitis (CP) is associated with poor treatment outcomes and a significantly lower quality of life. We aimed to identify demographic and clinical characteristics associated with constant pain in CP.

Methods: The demographic and clinical data of all patients with definite CP according to the M-ANNHEIM criteria between 2010-2023 were retrospectively reviewed. Abdominal pain presence and pattern at the index clinic visit classified patients into 3 categories: 1) primary painless/no pain within 1 year; 2) Intermittent pain; and 3) Constant pain. The first category (n=78) was excluded. Co-existing pain syndromes included disorders of gut-brain interactions, migraine, and musculoskeletal pain. High-potency opioids were defined according to the WHO analgesic ladder. Psychological disorders including anxiety, depression, and/or PTSD were obtained through a review of referring physician notes. Multivariable analyses were conducted to identify variables associated with constant pain.

Results: A total of 474 patients with a mean age of 50.7±15.2 years and 48.5% female were included. Of these, 266 (56.1%) had intermittent and 208 (43.9%) had constant pain. The risk factors for CP included alcohol± smoking, smoking alone, genetic/idiopathic, and others in 34.6%, 12.7%, 47.3%, and 5.5% of the patients, respectively. Age (OR=0.98[0.96-0.99], p=0.002), psychological disorders (OR=1.6[1.1-2.4],p=0.02), high-potency opioid use (OR=2.1[1.4-3.2], p=0.001), smoking alone (OR=2.3[1.2-4.5],p=0.01), and chronic neck or back pain (OR=3.7 [2.2-6.5], p=0.01) were independently associated with constant pain. However, a history of >3 surgeries, a history of abdominal surgery, and other co-existing pain syndromes were not associated with constant pain (p>0.05).

Conclusion: Chronic neck or back pain is an independent risk factor for constant pain in CP, unlike other co-existing pain syndromes. The mechanism of this finding deserves further study.

ABSTRACT 95

A comparison of single versus dual treatment with stabilizers and silencers in transthyretin amyloid cardiomyopathy

Vrinda Gupta, Muhammed A. Rahim, Yazan Alshawkani, Lisa Yanek, Michael J. Polydefkis, Joban Vaishnav

Introduction: Treatment for transthyretin amyloid cardiomyopathy (ATTR-CM) with TTR stabilization or gene silencing depends on the pathogenic variant and phenotype. There is limited data on efficacy of dual treatment with TTR stabilizer and silencer.

Methods: Patients with ATTR-CM on single treatment with stabilizer (Tafamidis, Diflunisal) or silencer (Patisiran, Vutisiran), or on dual treatment with both stabilizer and silencer, for >6 months, were included. Mortality data was collected through 5 years from diagnosis. Cox proportional hazard regression models were used to assess relationships with mortality.

Results: Of 183 patients, 144 (79%) were on single treatment and 38 (21%) were on dual treatment. Patients on dual treatment were more likely to be younger (70.1 [8.3] v 76.1 [9.0] years), have hereditary disease (79.0% v 43.9%), higher eGFR, lower NT-proBNP, and less likely on loop diuretic (39.5 v 69.9%) at baseline, all $p<0.05$. There was no difference in sex, race, or disease stage by groups at baseline. In univariate Cox analysis, dual treatment significantly reduced risk of death (HR 0.363, 95% CI 0.164-0.801, $p<0.05$); however, in multivariate model including age, dual treatment was no longer statistically significant (HR 0.468, 95% CI 0.21-1.07 $p=0.07$).

Conclusion: In a large ATTR-CM cohort, dual treatment with stabilizers and silencers was not associated with mortality reduction when adjusted for age. Our findings suggest that the high expense of dual treatment is unlikely to be cost-effective or of incremental clinical benefit. Future studies are needed to determine optimal treatment for the various phenotypes associated with ATTR-CM.

ABSTRACT 96

Tuning extracellular fluid viscosity to enhance transfection efficiency

Jingyao Ma, Yining Zhu, Jiayuan Kong, Di Yu, Wu Han Toh, Milun Jain, Qin Ni, Zhuoxu Ge, Jinghan Lin, Joseph Choy, Leonardo Cheng, Konstantinos Konstantopoulos, Maximilian F. Konig, Sean X. Sun, Hai-Quan Mao

Statement of Purpose: Gene therapy and cellular programming rely on effective cell transfection in vitro and in vivo. While numerous transfection techniques exist, the biophysical parameter of extracellular fluid viscosity has been largely overlooked. Here, we report the influence of culture media viscosity on the transfection efficiency of various gene delivery vehicles.

Methods: We investigated extracellular fluid viscosities ranging from 0.77 to 15 cP (at 37°C) across multiple cell types using plasmid DNA (pDNA) or mRNA-based lipid nanoparticles (LNPs), polyplex nanoparticles, and viral vectors. LNPs were synthesized based on Moderna's benchmark formulation. Pathway inhibition studies were performed using chemical inhibitors to identify changes in cellular entry mechanisms under different viscosity conditions.

Results and Discussion: Transfection efficiency of mRNA LNPs increased by 2- to 30-fold in higher-viscosity media across cancer cell lines, immune cells, and other commonly used cell types. The optimal viscosity range varied by cell type, typically between 1 and 4 cP. Lentiviral vector-mediated transduction of PBMCs also showed viscosity dependence. In human primary B cells, mRNA LNP transfection efficiency doubled, and mean fluorescence intensity increased by 80% at 2 cP compared to 0.77 cP. Pathway inhibition studies in B16F10 cells revealed a shift in LNP uptake mechanisms at higher viscosities, favoring clathrin-dependent endocytosis and macropinocytosis. These findings highlight viscosity as a critical factor for optimizing transfection efficiency and suggest new opportunities for improving gene delivery technologies.

ABSTRACT 97

Left-to-right ventricular volume ratio as a predictor of cardiovascular events: The Multi-ethnic Study of Atherosclerosis (MESA)

Malak Hoballah, Omar Chehab, Ashkan Abdollahi, Colin O. Wu, Bruna Scarpa, Wendy Post, Norrina Allen, David A. Bluemke, Bharath Ambale Venkatesh, Joao A. C. Lima

Background: Relative left ventricle (LV) to right ventricle (RV) volume imbalances may indicate pathological changes even when the individual chamber volumes fall within their respective 'normal' ranges. We aimed to define the prognostic value of volumetric imbalance between the LV and RV in the general population.

Methods: The study sample consisted of 4,073 asymptomatic participants from the Multi-Ethnic Study of Atherosclerosis who had a cardiac MRI at baseline. The left to right ventricular volume ratio (LRVR) was defined as LV volume/RV volume at end diastole. LRVR was categorized into balanced (0.8-1.3), low (<0.8), and high (>1.3). Multivariable cox regression models were used to study the association between LRVR and heart failure (HF), atrial fibrillation (AF), and death.

Results: The mean age of participants was 61.3±10 years, with 52% females, followed for up to 18 years. During follow up, 239 (5.9%) participants developed HF, 772 (19%) developed AF, and 906 (22.2%) died. High LRVR was associated with increased risks of HF (HR 2.6, $p<0.01$), AF (HR 1.6, $p<0.01$), and death (HR 1.6, $p<0.01$) compared to balanced LRVR. Low LRVR was not significantly associated with events. In a subgroup of participants with both absolute RV and LV volumes within normal ranges, high LRVR was still associated with increased risk of HF, AF, and death.

Conclusion: In healthy asymptomatic participants at baseline, LV volume exceeding RV volume by at least 30% is associated with increased risk of HF, AF, and death, independent of cardiovascular risk factors and absolute volume of either ventricle.

ABSTRACT 98

Engineered Tubular Microchannels for Smooth Muscle Cell Alignment Under Dynamic Cyclic Stretch

Tatsuya Matsubara, Sara Kaufman, Jihyun Hwang, Minjae Do, Jihoon Lee, Hidetoshi Takashima, Byunggik Kim, Mahin Gadkari, Lakshmi Santhanam, Deok-Ho Kim

Smooth muscle cells (SMCs) are affected by external factors such as curvature and mechanical stimuli, but their combined effects remain unclear. To investigate this interaction, we developed polydimethylsiloxane (PDMS)-based stretchable microtubular structures (diameters: 0.4 mm, 1.1 mm, and 2.0 mm) for studying SMC alignment. These structures, fabricated through high-precision 3D printing and molding processes, feature controlled wall thickness (e.g. 0.3 mm). The dimension was designed by finite element analysis. These microtubes simulate arterial expansion and contraction by applying pneumatic negative pressure, allowing precise control over strain levels (e.g., 15%), frequency (e.g., 1 Hz), and curvature. SMCs, specifically A7r5 cells, and hASMCs, were seeded onto ECM-coated inner surfaces of the microtubes. After applying dynamic deformation, cell orientation was quantitatively analyzed using confocal fluorescence microscopy and Imaris software. Under static conditions, SMCs aligned circumferentially, whereas longitudinal alignment occurred under specific strain levels. Additionally, the curvature of smaller microtubes amplified passive effects, requiring higher strain to induce alignment transitions. We successfully controlled the alignment angle by fine-tuning cyclic stretching parameters, highlighting the relationship between mechanical stimuli and curvature effects. This study provides a controlled in vitro environment to investigate how passive curvature effects interact with active mechanical stimuli to regulate SMC behavior. These findings contribute to understanding the mechanisms underlying the spiral alignment of SMCs in vivo and identify conditions that promote such configurations in arterial structures.

ABSTRACT 99

A quantitative systems pharmacology model for predicting responses to PD-1/PD-L1 checkpoint blockade in classical Hodgkin lymphoma

Yunhan Liao*, Yuanmuhuang Long*, Jacob L Martin*, Shreyanshu Ray*, Marc Donohue
*These authors contributed equally

Classical Hodgkin lymphoma (cHL) is a malignant lymphoproliferative disorder characterized by the presence of Hodgkin and Reed-Sternberg (HRS) cells in an inflammatory background. cHL constitutes approximately 15% of all lymphomas, with an annual incidence rate of around 2.6 cases per 100,000 individuals in the United States. The standard of care for cHL involves multi-agent chemotherapy regimens, which are frequently combined with radiotherapy. However, unmet clinical needs of relapsed/refractory disease and treatment-related morbidity remain. Recently, immune checkpoint therapies targeting programmed cell death protein 1 (PD-1) and programmed death-ligand 1 (PD-L1) have emerged as promising options for relapsed/refractory cHL. These therapies counteract the immune evasion mechanisms of HRS cells by inhibiting PD-1 and PD-L1, restoring the immune system's capacity to target malignant cells and reducing treatment-associated toxicity. Nonetheless, prognostication for cHL remains challenging due to its heterogeneous nature and difficulties in identifying predictive biomarkers to determine which patients will respond favorably to checkpoint inhibition. Traditional staging systems often fail to account for factors such as the tumor microenvironment (TME), genetic and epigenetic alterations, and host immune response. These highlight the necessity for more precise and predictive models. Here we offer a quantitative systems pharmacology (QSP) model for cHL that integrates immune-cancer cell interactions, multiple compartments, and patient-derived data. The proposed model aims to identify novel biomarkers, predict the therapeutic efficacy of anti-PD-1/PD-L1 in cHL patients, and address the disparity in relapsed/refractory disease. Our model may yield improved and personalized treatment regimens for cHL patients.

ABSTRACT 100

Towards Robust Automation of Surgical Systems via Digital Twin-based Scene Representations from Foundation Models

Hao Ding, Lalithkumar Seenivasan, Hongchao Shu, Grayson Byrd, Han Zhang, Pu Xiao, Juan Antonio Barragan, Russell H Taylor, Peter Kazanzides, Mathias Unberath

Large language model-based (LLM) agents are emerging as a powerful enabler of robust embodied intelligence due to their capability of planning complex action sequences. Sound planning ability is necessary for robust automation in many task domains, but especially in surgical automation. These agents rely on a highly detailed natural language representation of the scene. Thus, to leverage the emergent capabilities of LLM agents for surgical task planning, developing similarly powerful and robust perception algorithms is necessary to derive a detailed scene representation of the environment from visual input. Previous research has focused primarily on enabling LLM-based task planning while adopting simple yet severely limited perception solutions to meet the needs for bench-top experiments but lack the critical flexibility to scale to less constrained settings. In this work, we propose an alternate perception approach – a digital twin-based machine perception approach that capitalizes on the convincing performance and out-of-the-box generalization of recent vision foundation models. Integrating our digital twin-based scene representation and LLM agent for planning with the dVRK platform, we develop an embodied intelligence system and evaluate its robustness in performing peg transfer and gauze retrieval tasks. Our approach shows strong task performance and generalizability to varied environment settings. Despite convincing performance, this work is merely a first step towards the integration of digital twin-based scene representations. Future studies are necessary for the realization of a comprehensive digital twin framework to improve the interpretability and generalizability of embodied intelligence in surgery.

ABSTRACT 101

T1 Signal Intensity Ratio of the Pancreas to the Spleen and Paraspinal Muscle Predicts Fibrosis in Patients with Recurrent Acute and Chronic Pancreatitis

Aida A Metri; Mahya Faghih; Elizabeth Thompson; Rita Kalyani; Elham Afghani; Venkata Akshintala; Daniel Warren; Niraj M Desai; Zhaoli Sun; Christi Walsh; Martin A Makary; Rifat Mannan; Ralph Hruban; Jin He; Vikesh K Singh; Atif Zaheer

Introduction: There are no accurate noninvasive biomarkers for asses sing fibrosis in patients undergoing evaluation for chronic pancreatitis (CP). We aim to evaluate the association between the fibrosis score (FS) and the T1 signal intensity ratio (SIR) on MRI among patients undergoing total pancreatectomy with islet autotransplantation (TPIAT).

Methods: Patients who underwent TPIAT between 2011-2023 and had MRI imaging done within 6 months prior to surgery were classified into 3 groups: definite CP (n=23) and indeterminate CP (n=11) by M-ANNHEIM criteria; and recurrent acute pancreatitis (RAP) defined as ≥2 episodes of imaging documented acute pancreatitis (n=22). Excisional biopsies were obtained from the proximal and distal pancreas at the time of TPIAT. The FS categorizes fibrosis as focal/diffuse and perilobular/intralobular with scores of 1-6, with 6 being the most severe. Total FS was the average perilobular and intralobular FS of proximal and distal pancreas. We measured the T1 signal intensity of the pancreas and reference organs (spleen and paraspinal muscle), on pre-contrast fat saturated T1 gradient echo sequence, to obtain the respective T1 SIR. Multiple regression analysis was used to evaluate the association between T1 SIR and FS.

Results: A total of 56 patients with a mean age 37.8±13.6 years and 28 (50%) females were included. Genetic (48.2%) and idiopathic (23%) were the most common etiologies of pancreatitis. The mean duration of disease was 8.1±7.8 years and the mean FS was 6.29±3.5. Pancreas-to-spleen T1 SIR and pancreas-to-paraspinal T1 SIR, after adjusting for age, BMI, exocrine insufficiency, duration of disease, DM and clinical diagnosis, were shown to be independently associated with pancreatic fibrosis. DM, RAP, and CP were also shown to be independent predictors of pancreatic fibrosis.

Conclusion: The T1 SIR of the pancreas-to-spleen and pancreas-to-paraspinal muscle can predict pancreatic fibrosis. It could be a potential non-invasive biomarker to evaluate fibrosis in pancreatitis.

ABSTRACT 102

Autoantibodies To Transcription Factor A Mitochondria are associated with damage accrual, malignancy risk and mortality in SLE

Eduardo Gomez-Banuelos, Daniel Goldman, Merlin Paz, Michelle Petri, Felipe Andrade

Background: We recently identified a subclass of autoantibodies in SLE that target transcription factor A mitochondrial (TFAM), a critical protein in mitochondrial DNA transcription and packaging1. These autoantibodies are strongly associated to vascular events and antiphospholipid syndrome (APS) in SLE, independent of APS-associated antibodies or lupus anticoagulant. Given that vascular events play a significant role in the accumulation of damage and higher death rates in SLE, we investigated the potential role of anti-TFAM antibodies as predictors of damage accrual, and mortality in SLE.

Methods: We screened sera from 158 SLE patients in the "Study of biological Pathways, Disease Activity and Response markers in patients with Systemic Lupus Erythematosus" (SPARE) for anti-TFAM antibodies. SPARE is a 2-year prospective cohort of adult patients treated according to standard clinical practice. In addition, we measured normal anti-TFAM antibody levels in 98 healthy controls (HC). Damage accrual was measured using the Systemic Lupus International Collaborating clinics/American College of Rheumatology Damage (SLICC). Mortality and malignancy data were collected from the National Death Index and clinical charts, respectively.

Results: Thirty percent (48/158) of SLE patients were positive for anti-TFAM antibodies. Anti-TFAM positive patients had higher SLICC scores compared to anti-TFAM negative patients (3.9 vs 2.3) (Fig 1A). Malignancy was the most frequent subdomain linked with elevated SLICC in anti-TFAM positive patients (29%), followed by diabetes mellitus (21%), ruptured tendon (15%), pericarditis (8%), muscular atrophy (8%), skin ulcers (8%), and deep vein thrombosis (6%). Among other SLE-related autoantibodies (Fig 1B), only anti-TFAM antibodies were associated with a greater risk of malignancy (OR 3.5). Anti-TFAM antibodies were not linked to any specific type of cancer. Intriguingly, there was no association between malignancy and thrombotic events in anti-TFAM positive patients. Furthermore, 23% (11/47) of anti-TFAM SLE patients died during follow-up (OR 4.4, Fig 1C). The most common cause of death in anti-TFAM positive SLE were cardiovascular related in 36% (4/11).

Conclusions: Anti-TFAM antibodies identify a subset of patients with SLE at higher risk for unfavorable outcomes, including malignancy and death. The lack of association between malignancy and thrombotic events in anti-TFAM positive patients suggests the existence of at least two subsets of anti-TFAM antibodies of distinct significance (i.e., thrombosis-related vs. cancer-related). The higher mortality among anti-TFAM positive SLE patients, with cardiovascular causes being the leading factor, highlights the importance of developing targeted interventions to prevent adverse outcomes in patients with anti-TFAM antibodies.

ABSTRACT 103

Dorsal-Ventral and Rostral-Caudal Patterning of Human Brain Organoids using a Localized Passive Diffusion-based Morphogen Gradient Generator

Feiyu Yang, Narciso Pavon, Taysuya Matsubara, Rebecca Sebastian, Beatruz Martinez-Martin, ChangHui Pak, Yubing Sun, Deok-Ho Kim

Positional patterning during human brain development is orchestrated in a highly coordinated manner by a small number of inductive signals produced locally by surrounding tissues. While previous studies have used animal models to reveal general signaling pathways during early development, the signal perturbations underlying the proper development of the human brain remain unclear. Current technologies are limited in their ability to generate morphogen-induced spatially patterned organoids in terms of flexibility in fine-tuning the spatial-temporal dynamics and establishing small-scale gradients. Here, we report a Matrigel-free passive diffusion-based morphogen gradient generator (PdMG) reliably established a steep (<2mm) and flexible tunned exogenous uniaxial morphogen signaling gradient in the developing hESCs-derived brain organoids with precision. We established dorsal-ventral (D-V) forebrain, rostral-caudal (R-C) fore-midbrain, and R-C fore-mid/hindbrain/spinal cord (SC) transitional patterning by inducing Sonic Hedgehog (Shh)/ WNT-inhibitor, WNT activator, and retinoic acid (RA) molecule gradients during organoid development, respectively. We then mapped the spatial transcriptomic (ST) atlas and analyzed the cell lineage progressions of the patterned organoids using the 10x Visium ST assay. We confirmed dorsal, lateral/caudal ganglionic eminence (LGE/CGE), and medial ganglionic eminence (MGE) identities induced by the Shh/WNT-inhibitor gradient in day 25 D-V patterned forebrain organoid. Additionally, we observed active neurogenesis and synaptogenesis, along with the regional emergence of glutamatergic, and the migrations of GABAergic interneurons, as demonstrated by ST analysis of long-term cultured D-V patterned organoids. Furthermore, we confirmed the vital role of RA gradient in inducing HOX family genes for hindbrain/SC identities for R-C patterned organoids. Together, this study modeled the spatial-temporal morphogen dynamics for regulating the cell fate specifications and axis formations, as well as established the comprehensive ST atlas to decipher key developmental trajectories of patterned brain organoid models.

ABSTRACT 104

Enhancing Glaucoma Referral Decisions with Explainable AI

Catalina Gomez, Ruolin Wang, Katharina Breininger, Corinne Casey, Chris Bradley, Mitchell Pavlak, Alex Pham, Jithin Yohannan, Mathias Unberath

Optometrists and primary eye care providers are essential in triaging glaucoma referrals to specialty care, as delays can lead to permanent vision loss. Artificial Intelligence (AI) solutions specialized in glaucoma referrals could enhance first-line providers' referral decisions, a task made challenging by their generalist eye training. Such specialized versus generalist training creates a knowledge imbalance between the AI system and the provider that explainable AI can bridge by helping providers calibrate their reliance on AI. This study investigates how various AI explanations influence providers' interpretations and use of AI recommendations to distinguish between immediate and non-urgent specialist referrals. We built AI models for identifying high-risk patients requiring urgent referrals from routine eye care data. We incorporated intrinsic and post-hoc explanations supporting the model's predictions to assist referral decisions under knowledge imbalance. Through a user study with 87 optometrists, we assessed human-AI team performance, measuring referral accuracy and analyzing interactions with AI, including agreement rates and perceptions of the experience. Our findings revealed performance gains of the human-AI teams relative to the humans alone, yet a performance gap remained below that of the AI alone, even with explanations. Participants felt that AI support did not increase workload, confidence, and trust, but reduced task challenges. User experiences favored intrinsically explainable models compared to post-hoc methods for preference, perception, and reducing undesired outcomes, such as over-claiming urgency and algorithmic over-reliance. Key challenges remain around providers' considerations in determining when to rely on AI recommendations and integrating their general expertise with AI's specialized insights.

ABSTRACT 105

Microstructure Engineering to Optimize Corrosion Resistance and Biocompatibility in Mg-9Al Implants

Camryn Byrum, Veronica Ivanovskaya, Sreenivas Raguraman, Suhas Prameela, Timothy P. Weihs

Magnesium (Mg) alloyed with aluminum (Al) is a promising biodegradable material for medical implants due to excellent mechanical properties and tunable degradation rates. However, Al release during degradation poses biocompatibility challenges and potential systemic toxicity. This study examines how microstructural control, achieved through solution heat treatment (ST) at 450 °C and peak aging (PA) at 150 °C, influences the in-vitro corrosion behavior and Al release in Mg-9Al alloys. PA samples, characterized by Mg17Al12 particles, show roughly 2X higher aluminum ion release rates, as well as higher corrosion rates compared to ST samples, where precipitates are absent. SEM-EDS analysis highlights greater residual aluminum content on ST surfaces, corresponding to reduced ion release. XRD confirmed the microstructural differences between ST and PA conditions. These findings demonstrate that despite identical elemental compositions, the degradation rate and Al release rate can be effectively modulated by controlling the microstructure. Such in-vitro insights are crucial for advancing Mg-Al alloys as biocompatible, biodegradable implant materials.

ABSTRACT 106

The XBB.1.5 mRNA Booster Vaccine Does Not Significantly Increase XBB.1.5 Mono-Reactive T Cells

Joel Sop, Alicia Mercado, Alexis Figueroa, Tyler P. Beckey, Caroline C. Traut, Li Zhang, Kellie N. Smith, and Joel N. Blankson

Background: SARS-CoV-2 variants such as XBB.1.5 and BA.2.86 have emerged with mutations that allow them to evade neutralizing antibodies elicited by ancestral and bivalent mRNA vaccines. Despite the introduction of the XBB.1.5 monovalent booster to improve T cell immunity, it remains unclear whether this vaccine induces stronger XBB.1.5-specific T cell responses compared to the ancestral/BA.5 bivalent vaccines. We hypothesized that the XBB.1.5 booster would significantly increase the percentage of XBB.1.5 mono-reactive T cells.

Methods: We used the IFN-gamma ELISpot assay to determine the targeted epitopes and the functional expansion of specific T cells (FEST) assay to assess the percentage of CD4+ T cells that cross-recognized ancestral, BA.5, and XBB.1.5 spike proteins versus those that were mono-reactive. The FEST assay involves culturing antigen-specific T cells with spike peptides, followed by TCR sequencing to identify expanded clonotypes. 11 participants who received either the ancestral/BA.5 bivalent mRNA vaccine or the XBB.1.5 monovalent mRNA booster vaccine were included in the study.

Results: Our analysis revealed robust T cell responses to ancestral, BA.5, and XBB.1.5 spike proteins. However, the XBB.1.5 booster did not significantly increase the percentage of XBB.1.5 mono-reactive T cells. The percentage of spike-specific CD4+ T cell receptors that were XBB.1.5 mono-reactive did not increase significantly after the booster shot (7.6% pre-booster to 12.3% post-booster, p=0.4375. Instead, cross-reactive CD4+ T cells dominated the spike-specific T cell response. Furthermore, the percentage of T cell-targeted epitopes containing XBB.1.5 mutations did not significantly change after the booster (27.9% pre-booster to 23.75% post-booster, p= 0.6667).

Conclusions: Our findings suggest that the XBB.1.5 monovalent booster does not substantially enhance XBB.1.5-specific T cell responses, with cross-reactive T cells continuing to dominate the immune response. These results have important implications for future vaccine strategies targeting emerging variants.

ABSTRACT 107

Brachytherapy Seed Placement by Robotic Bronchoscopy with Cone-Beam CT Guidance for Peripheral Lung Cancer: A Human Cadaveric Feasibility Pilot

Ardian Latifi, Michael Roumeliotis, Sarah Quirk, Ulysses G. Gardner, Daniel Y. Song, Travis Ferguson, and Lonny Yarmus

Purpose: Current first-line treatment for early-stage lung cancer includes stereotactic body radiation therapy (SBRT), in which external beams of radiation target a tumor. This approach causes unavoidable healthy tissue irradiation that result in devastating side effects. An alternative mode of radiation, low dose-rate brachytherapy (LDR-BT), involves precise implantation of radioactive seeds within a tumor to reduce collateral irradiation but has never been used in lung cancer due to lack of available technology to reliably implant the radioactive seeds. This study evaluates the feasibility of utilizing a robotic bronchoscopy with cone beam computed tomography (RB-CBCT) platform to precisely place LDR-BT implants in a human cadaveric. Additionally, this study compares post-implant dosimetry with standard SBRT plans.

Methods: A prospective study of 8 human cadavers with implanted pseudotumors was performed. LDR-BT dosimetry plans were created a priori with a prescription dose of 100 Gy. The RB-CBCT platform was used to implant inert LDR-BT seeds. Accuracy of implant placement was measured, and post-implant dosimetry was modeled and compared to standard SBRT treatment plans.

Results: All pre-planned 41 LDR-BT seeds were successfully implanted across 8 pseudotumors. The average implant accuracy was 3.8 ± 1.1 mm. Post-implant dosimetry achieved an average V95% of 99.4 ± 3.3% and D90% of 128 ± 23Gy. When compared to SBRT plans, BT post-implant dose conformity (V25%/VPTV) was superior (8.0 vs 17.6, $p<0.05$).

Conclusions: RB-CBCT is a feasible technology for implantation of LDR-BT seeds in peripheral lung tumors and can achieve pre-planned dosimetry goals with better dose conformity compared to SBRT.

ABSTRACT 108

Disparities in post-discharge care provided to patients discharging 'before medically advised' following hospitalization for asthma exacerbation

J Henry Brems, Aparna Balasubramanian, Kevin Psoter, Mary Catherine Beach, Michelle Eakin, Emily Brigham, Tianshi David Wu, Nadia N Hansel, Robert A Wise, Meredith C McCormack

Introduction: Before medically advised (BMA) discharges – alternatively known as 'against medical advice'—are associated with poor outcomes among patients with asthma, but factors contributing to this risk are unknown. We evaluated patterns of post-discharge care (i.e. medication prescriptions and follow-up) after hospitalizations for asthma exacerbation among patients discharging BMA versus non-BMA.

Methods: We developed an electronic cohort of adults admitted within the Johns Hopkins Health System for asthma exacerbation. All admissions were classified as either a BMA or planned (i.e. non-BMA) discharge. We evaluated the proportion of discharges in which the patient received each of the following at discharge: an oral steroid prescription, inhaled corticosteroid prescription, or scheduled follow-up with a primary care physician or pulmonologist within 14-days. Differences in each component of care were compared using logistic regression models with clustered standard errors, adjusted for patient and hospital characteristics.

Results: This cohort included 5,507 admissions for asthma exacerbation, of which 205 (3.7%) resulted in a BMA discharge. Compared to non-BMA discharges, those discharged BMA were younger (39 vs 48 years, $p<0.001$) with a higher area deprivation index (67 vs 50, $p<0.001$). Compared to non-BMA discharges, those discharged BMA were less likely to receive an oral steroid prescription (54% vs 76%, $p<0.001$), inhaled corticosteroid prescription (32% vs 49%, $p<0.001$), or scheduled 14-day follow-up (19% vs 27%, $p=0.01$). All results were similar in adjusted models.

Conclusions: Patients discharging BMA following an asthma exacerbation are less likely to receive outpatient medications and follow-up. These treatment gaps present potential opportunities to improve care.

ABSTRACT 109

Reduced Hypusination of eIF5A impairs ribosomal translation resulting in Heart Failure with Preserved Ejection Fraction

Navid Koleini, Mariam Meddeb, Mohammad Keykhaei, James Saba, Farnaz Farshidfar, Seoyoung Kwon, Thea Angela Calahatian, Twisha Sharma, Shunyao Lei, Olivia Hanselman, Liang Zhao, Raghothama Chaerkady, Virginia Hahn, Kavita Sharma, Mark Ranek, Erika L Pearce, Racheal Green, David A Kass

Heart failure with preserved ejection fraction (HFpEF) accounts for more than half of HF cases while its etiology remains unknown. Multiomic interrogation of human HFpEF myocardium revealed a discrepancy between transcription and translation and the polyamine spermidine as the most upregulated metabolite. Spermidine is evolutionary essential in ribosomal translation through posttranslational modification, hypusine, of elongation factor 5A (eIF5AHyp). Surprisingly, we found depressed eIF5AHyp ,uniquely, in human HFpEF along with the hypusinating enzyme, deoxy-Hypusine synthase (DHPS). I generated an inducible cardiomyocyte specific DHPS knockout (ciDHPS-KO). Eight weeks post tamoxifen, DHPS and eIF5AHyp were reduced similar to the levels observed in human HFpEF myocardium. Echocardiographic assessment of the hearts revealed preserved ejection fraction, normal ventricular dimensions in systolic and diastolic, mild increase in wall thickness, and a significant elevation in E/E' suggesting increased filling pressure. ciDHPS-KO mice demonstrate reduced exercise tolerance.

Using ribosome sequencing, to identify transcripts with impaired translation, I found ubiquitin precursors and its deubiquitinases as possible eIF5AHyp sensitive targets. I showed that eIF5AHyp reduction declines free and total ubiquitin in cardiomyocytes while increasing accumulation of misfolded proteins. Total ubiquitination decreased in the ciDHPS-KD mice and human HFpEF.

In conclusion, we identified a unique translational impairment in the HFpEF myocardium resulting in impaired protein quality control and accumulation of misfolded proteins; in vivo studies showed development of a HFpEF phenotype in mice with cardiomyocyte restricted DHPS-KO. To our knowledge, HFpEF is the first disorder in which free ubiquitin deficiency, through impaired translation, has been identified as the underlying mechanism.

ABSTRACT 110

Aberrant N-glycosylation in carriers of ZIP8 391T with Crohn's disease: Opportunity for genotype-driven therapy

Vartika Tomar, Ruxian Lin, Natasha Zachara, Joanna Melia

A missense mutation in the manganese (Mn) transporter ZIP8 (rs13107325; A391T) increases the risk of Crohn's disease (CD), particularly in the ileum. ZIP8 A391T is the second most common coding variant associated with risk of CD. Manganese is a critical co-factor for metalloenzymes, like glycosyltransferases of the N-glycosylation cascade. We and others have shown that ZIP8 391T associates with a relative Mn insufficiency and decreased abundance of complex N-glycans in blood indicating impairment of the N-glycosylation cascade. Our central hypothesis is that aberrant N-glycosylation underlies CD pathogenesis in ZIP8 391T carriers and therapy targeting the N-glycosylation defect is necessary and safer than Mn supplementation alone. Here, we studied if there is differential N-glycosylation in the ileal epithelial compartment (IEC) in carriers of ZIP8 391T, if there is evidence of ileal epithelial dysfunction, if defects are recapitulated in Zip8 393T knock-in mice (equivalent to ZIP8 391T), and if glycan-specific therapy is effective.

For our study, we chose two lectins to delineate between complex (Phaseolus vulgaris leucoagglutinin; L-PHA) and truncated (succinylated wheat germ agglutinin; sWGA) N-glycans (Fig. 1A). Immunofluorescence staining demonstrated that in healthy individuals, the IEC is dominated by L-PHA staining (sWGA/L-PHA ratio of 0.25). In contrast, there is increased sWGA staining in patients with CD, especially with active disease; WGA/L-PHA intensity ratio increased from a mean of 0.69 to 1.65 ($p=0.000995$) (Fig. 1B). In a cohort of genotyped patients, we found greater sWGA staining at the apical/brush border of IECs in 391T carriers compared to non-carriers ($p=0.01$), consistent with a genotype-driven effect on IEC N-glycosylation (Fig. 1C). In further support, in Zip8 393T-KI mice, sWGA staining is markedly increased in IECs compared to L-PHA (Fig. 1D). The rate-limiting substrate of the N-glycosylation cascade is N-acetylglucosamine (GlcNAc); we hypothesized that GlcNAc supplementation would increase N-glycan branching, a treatment strategy informed by the treatment of patients with congenital disorders of glycosylation. Zip8 393T-KI mice were treated with GlcNAc (0.25 mg/ml) in drinking water for 7 days, restoring L-PHA staining in IECs (Fig. 1E). GlcNAc supplementation also corrected defects in bile acid homeostasis in Zip8 393T-KI mice, suggesting amelioration of IEC dysfunction (Fig. 1F-G).

In conclusion, we position aberrant N-glycosylation as an important driver of Crohn's disease in carriers of ZIP8 391T. Our study provides initial evidence that a glycan-targeted therapy may be an important adjunctive therapy in patients with Crohn's disease who carry ZIP8 391T.

ABSTRACT 111

ScaleMAI: Accelerating the Development of Trusted Datasets and AI Models

Wenxuan Li, Alan Yuille, Zongwei Zhou

Building trusted datasets is critical for transparent and responsible Medical AI (MAI) research, but creating even a small, high-quality dataset can take multidisciplinary teams years. Ironically, AI cannot benefit until the data is fully prepared, and during this lengthy process, it is often unclear how much data and what level of annotation quality are necessary–prolonging the endeavor and increasing costs. We challenge this separation between human-centric data creation and AI-centric development. Rather than treating them as sequential endeavors, we propose ScaleMAI, an AI-integrated data curation and annotation agent, allowing data quality and AI performance to improve in a self-reinforcing cycle and cutting development time from years to months. We adopt pancreatic cancer detection as an example. First, ScaleMAI progressively creates a dataset of 25,362 CT scans, including per-voxel annotations for benign/malignant tumors and 24 anatomical structures. Second, through progressive human-in-the-loop iterations, ScaleMAI provides Flagship AI Model that can approach the proficiency of expert annotators (30-year experience) in detecting pancreatic tumors. Flagship Model significantly outperforms models developed from smaller, fixed-quality datasets, with substantial gains in tumor detection (+14%), segmentation (+5%), and classification (72%) on three prestigious benchmarks. More importantly, we have extended ScaleMAI to pancreatic tumor staging and radiotherapy planning, showing the potential of creating larger medical datasets for a variety of applications.

ABSTRACT 112

Transformative Effect Of FMT on Restoration of Intestinal Micro Ecology in Patients with Recurrent Clostridioides Difficile Infection

Sandeep Verma, Elad Firnberg, Sudhir K Dutta

Introduction: Application of metagenomic analysis to fecal samples from patients with RCDI has demonstrated unique and reproducible shifts in bacterial microbiome from phyla firmicutes to pathogenic proteobacteria. However, simultaneous interactions in bacteria, fungi and viruses in human intestinal microbiome have not been studied in fecal samples from RCDI patients and healthy control subjects. To determine the trans-kingdom simultaneous alterations in the various components of intestinal microbiome, we studied patients with RCDI before and after FMT and also corresponding healthy donors.

Methods: Fecal samples were collected for 22 patients before and 1 month after FMT and their corresponding healthy donors. For fungal analysis, the DNA from fecal samples was isolated using the QIAGEN DNeasy PowerSoilPro kit and quantified by Qubit and Illumina Nextera XT libraries. The raw ITS2 amplicon metagenomic data was analyzed using UNITE database. For bacterial strains and bacteriophages, the Illumina HiSeq 4000 platform was used, and results uploaded to CosmosID for analysis.

Results: We identified a total of 1687 bacterial strains, 437 bacteriophages and 361 fungal species in 66 samples from RCDI patients and healthy donors. Marked alterations in intestinal bacteriome were noted, characterized with significant decrease in firmicutes ($p<0.001$) and increase in pathogenic proteobacteria ($p<0.001$). Interestingly, we also observed a statistically significant positive correlation between pathogenic bacteria and fungi; Escherichia coli and Candida_u_s ($r=0.68$, p, 0.0001), Clostridioides difficile P28 and Candida glabrata ($r=0.63$, p, 0.0001), Klebsiella oxytoca and Agaricales_u_s ($r=0.63$, p, 0.0001). Furthermore, significant correlations were seen between bacteria and bacteriophages which are associated with Clostridioides difficile toxin production. Some top statistically significant correlations were: C. diff with multiple bacteriophage strains; Clostridium phage; phi CD111 ($r=0.56$, $p<0.001$), phiCD506 ($r=0.56$, $p<0.001$), phiCD6356 ($r=0.56$, $p<0.001$), and phiCDHM19 ($r=0.56$, $p<0.001$. It is noteworthy that, in the healthy control subjects, the relative abundance of these pathogenic bacterial strains was markedly diminished, fungi were minimally detectable and these bacteriophages were undetectable.

Discussion: To date, this is the first demonstration of simultaneous trans-kingdom microbial interactions in the intestinal microbiota in healthy human subjects and patients with RCDI before and after FMT. These new observations revealed a closely interconnected picture of marked changes in the micro ecology of human intestinal microbiome which includes bacteria, fungi and viruses. Furthermore, these trans-kingdom microbial alterations were modulated by FMT, leading to restoration in microecology similar to what was observed in healthy human population.

ABSTRACT 113

Optimal sequential hypothesis testing with costly information acquisition

Renyuan Xu, Luhao Zhang, Haotian Zong

We study the sequential testing problem of two alternative hypotheses when observations are costly. Mathematically, we frame this as an optimal stopping problem in which the decision-maker aims to minimize classification errors plus a running cost proportional to the duration of information acquisition. By formulating a value function that captures both the expected decision risk and the running cost, we derive a set of variational inequalities that govern the evolution of the optimal strategy. Our analysis encompasses two different informational regimes: Gaussian and Poisson. We characterize the continuation regions within which further information collection is optimal and derive monotonicity properties with respect to different parameters, including the noise level, running cost, difference between the two hypotheses, and the relative importance of false positive and false negative errors. For Poisson signals, we utilize a diffusion approximation to study the asymptotic regime of frequent small jumps. Overall, our model advances understanding of how observation costs reshape classical sequential hypothesis testing. It also offers practical guidelines for designing adaptive and non-adaptive testing schemes in medicine, engineering, and related fields under real-world resource constraints.

ABSTRACT 114

Microfluidic blood-brain barrier chip for identifying repurposable drugs as glioblastoma chemotherapeutic agents

Zhipeng Dong, Satvik Kethireddy, Jeonghyun Yoo, Asmitha Sathya, Deok-Ho Kim, Eun Hyun Ahn

Glioblastoma multiforme (GBM) is the most aggressive brain tumor. Development of GBM therapeutics has been significantly limited by the selective permeability of the blood-brain barrier (BBB). Furthermore, preclinical models recapitulating GBM in the presence of a BBB and predicting clinical outcomes are yet to be established (1). We have developed a microfluidic model that simulates the 3D tumor microenvironment in conjunction with the BBB. The microfluidic chip features a polydimethylsiloxane (PDMS) block bonded to the glass slide, which forms three channels. In our 3D microfluidic model, a fibrin hydrogel is mixed with astrocytes, pericytes, and GBM-patient derived xenograft (PDX) spheroids, and is then injected into the middle channel of the chip. The side of this fibrin hydrogel-embedded tissue is coated with human brain microvascular endothelial cells. These three different types of cells can form a BBB over the interface between the brain channel and the blood side channel and maintain tight junctions and barrier integrity. We hypothesize that invasiveness of GBM spheroids in our 3D extracellular matrix (ECM) BBB environment will faithfully reflect GBM aggressiveness. Using this 3D GBM-BBB microfluidic model, we have evaluated the inhibitory abilities of FDA-approved or stage three clinical trial non-oncology drugs (2) on the growth and invasion of GBM spheroids. Our results indicate that these drugs significantly inhibit the growth and invasiveness of GBM spheroids in our 3D model. We present this 3D microfluidic BBB model as a brain tumor microenvironment-mimetic scalable platform for evaluating drugs and elucidating the mechanisms of chemotherapeutic drugs against GBM.

ABSTRACT 115

In vitro corrosion-fatigue testing methodology for magnesium alloys in biomedical applications

Tunde Ayodeji, Sreenivas Raguraman, Beril Ulugun, Timothy P. Weihs

Magnesium (Mg) alloys have recently emerged as promising materials for use in biomedical applications due to their biocompatibility and biodegradability. However, alongside these advantages exist factors limiting the use of Mg alloys, notably their high corrosion rate. Further, corrosion can be accelerated by cyclic loading, leading to unpredictable behavior and rapid degradation. Corrosion-fatigue (the combination of cyclic loading and a corrosive environment), has received little attention, though, unlike corrosion without load. This research seeks to expand the characterization of magnesium alloys through the development of a methodology for in vitro fatigue testing of bulk processed Mg alloys. Specifically, fatigue test grips will be designed, manufactured, and tested, followed by corrosion-fatigue testing in simulated body solutions at regulated temperature and pH. Ultimately, this will lead to the development of stronger, fatigue-resistant biomedical implants and address the current lack of a standard methodology for corrosion-fatigue testing.

ABSTRACT 116

An efficient automated diagnostic approach for cancer subtypes from H&E whole slide images using a context-aware attention deep learning model

Tawsifur Rahman, Alex S. Baras, Rama Chellappa

Deep learning has revolutionized medical image analysis, particularly in histopathology, where H&E-based Whole-Slide Images (WSIs) are crucial for diagnosing diseases like cancer. However, WSIs are highly complex, large, and diverse, making manual annotation both expensive and time-consuming. Multiple Instance Learning (MIL) has shown potential for analyzing Whole Slide Images (WSIs) in digital pathology. Still, it faces challenges related to redundant information learning and generalization due to limited supervision and the computational complexity of Gigapixel WSIs. Many MIL-based methods apply a small weight matrix to all WSI patches. This study focuses on developing computationally efficient models that improve MIL-based WSI classification by processing fewer patches while improving performance. We propose an attention-based approach using knowledge distillation, where a compute-intensive "instructor" model analyzes all WSI patches to train a resource-efficient "learner" model, which considers only a subset of patches. Comprehensive evaluations on four cancer subtype datasets—TCGA-BRCA, TCGA-NSCLC, TCGA-RCC, and PANDA—demonstrate that an "observe-everything" instructor can effectively train an "observe-minimally" learner network. Overall, our proposed learner network enhances performance by 4% compared to the state-of-the-art, while reducing inference time by 45% and FLOPs by approximately 88%.

ABSTRACT 117

Unraveling the Role of OGT/OGA-Mediated Modifications in Cardiac Dysfunction: A Focus on MAOB and ACADM as Therapeutic Targets

Jiali Harriet He

Introduction: Essential post-translational modifications, including O-GlcNAcylation, regulated by OGT (O-GlcNAc transferase) and OGA (O-GlcNAcase), are collectively important for cellular processes central to cardiac physiology. Dysregulation of O-GlcNAcylation has been associated with oxidative stress, mitochondrial dysfunction, and metabolic imbalance, contributing to cardiac diseases. Using OGT transgenic models with abnormal cardiac phenotypes, OGA models with normal phenotypes, and TxA models that rescue cardiac abnormalities, we investigated the transcriptomic landscape to identify potential genetic regulators.

Hypothesis: We hypothesize that MAOB and ACADM play critical roles in OGT/OGA-mediated cardiac dysfunction by regulating oxidative stress and metabolic homeostasis.

Method: We identified MAOB and ACADM, through proteomic analysis and transcriptomic analysis, as potential regulators for oxidative stress, and metabolic homeostasis. Differential expression and pathway enrichment analysis of WT, OGT, OGA transgenic models also supported these findings. Gene expression will be validated using qPCR and Western Blot. And bioinformatics analyses will follow, including transcriptomics, functional enrichment and single-cell RNA sequencing (e.g. Seurat).

Results: Preliminary analyses identified two key genes—Monoamine Oxidase B (MAOB) and Middle-Chain Acyl CoA Dehydrogenase (ACADM). MAOB is associated with oxidative stress and mitochondrial dysfunction, while ACADM's involvement in fatty acid metabolism highlights its relevance as a cardiac biomarker.

Conclusion and Future Direction: By integrating wet-lab validation with advanced Bioinformatics this research aims to confirm the critical role played by the selected gene in heart dysfunction caused by OGT/OGA. These findings can be used to guide future wet lab studies and translational trials, which will emphasize cost-effective ways of prioritizing therapeutic targets.

ABSTRACT 118

Polymer-based strategies for the induction of immunity and tolerance

Scott Wilson, Sandeep Kumar, Sabrain Chen, Mengheng Yang, Ian McKnight

While considerable progress has been made in the development of vaccines that muster antibody-mediated immunity, the clinical success of other ASIs, such as subunit vaccines that elicit T cell-mediated immunity and inverse vaccines capable of curing autoimmunity, have yet to match their pre-clinical promise. Here, we will introduce approaches that utilized synthetic polymeric glycosylations to target antigens and immunostimulatory adjuvants to specific subsets of antigen presenting cells for the induction of antigen-specific immunity or tolerance. In the context of immunity, we will present a polymeric glycol-adjuvant that when conjugated to a malaria-specific protein induces a more robust antibody- and T cell-mediated immune response than malaria-specific protein formulated with the adjuvant used in the most clinical advanced malaria vaccine. In addition, we will highlight the development of another class of synthetic glycopolymers that, by targeting autoantigens to the liver's immunosuppressive microenvironment, elicit durable autoantigen-specific immunological tolerance marked by auto-reactive T cell anergy and functional regulatory T cells. In concert, these antigen-glycopolymer conjugate platforms represent promising clinically viable treatments for a variety of complex infections and autoimmune disorders.

ABSTRACT 119

Evaluating collagen remodeling in dimethyl-prostaglandin E2 (dmPGE2)-induced short cervix model

Vivian H Su, Marina Better, Nicholas T Gigliotti, Mitra Taheri

Early cervical shortening is often a clinical predictor of spontaneous preterm birth (PTB). The loss of mechanical integrity in the cervix is associated with the remodeling of the collagen network. Collagen is a structural protein that makes up most of the cervical structure. To better understand the biological mechanisms that cause short cervix, we examine the chemical and structural effects of dimethyl-prostaglandin E2 (dmPGE2) on collagen in mice cervices across different length scales. We hypothesize that dmPGE2-induced short cervices exhibit lower stiffness compared to normal pregnant cervices due to an increased ratio of immature to mature collagen crosslinks. To determine the effect of collagen crosslinks on the global tissue properties, we developed a tensile stage to conduct load-to-break ring tests of normal and dmPGE2-induced cervices at the same gestational age and nonpregnant cervices. Preliminary results showed a nearly 20-fold decrease in both the normal and dmPGE2 cervices compared to nonpregnant ones, similar to previously reported instantaneous stiffness load-to-break studies of mouse cervices. The results also indicated a slightly lower stiffness of dmPGE2 cervices compared to normal pregnant ones. Microscopy techniques such as second harmonic generation (SHG) will be used to correlate the tensile strength of the cervix with the maturity of collagen fibril crosslinks.

ABSTRACT 120

Augmented LLMs for multimodal clinical data analysis

Felix Parker, Nimeesha Chan, Chi Zhang, William Bennett, James Fackler, Kimia Ghobadi

In intensive care units (ICUs), clinicians must process vast amounts of multimodal data for critical care decisions. This includes high-frequency signals from medical devices (ventilator waveforms, electrocardiograms, etc.), vital signs, electronic health records (EHR), clinical notes, and laboratory results. Clinicians must monitor and interpret an overwhelming volume of data daily, creating a substantial cognitive burden in the high-stakes ICU environment where rapid decision-making is crucial.

While Large Language Models (LLMs) have demonstrated remarkable capabilities in reasoning and knowledge integration, they traditionally struggle with numerical and time series data. However, their natural language interface and ability to integrate diverse information streams present an opportunity to revolutionize clinical decision support. We have created a framework that adapts LLMs to consolidate information across different temporal and data modalities, providing clinicians with real-time, actionable insights.

We apply this framework in three core areas: automated generation of patient state reports, question-answering about patient conditions, and prediction of adverse events such as cardiac arrest or need for mechanical ventilation. Our system processes multiple input streams (including time series data from medical devices, clinical notes, and EHR data) and generates outputs combining natural language insights with time series predictions.

This work aims to enhance ICU decision-making and patient outcomes by reducing cognitive burden on providers, enabling earlier intervention, and optimizing treatment through data integration and analysis. By providing clinicians with a tool that mirrors their holistic approach to patient care, we aim to support more timely and informed clinical decisions in critical care settings.

ABSTRACT 121

Pro-angiogenic Response to Hyaluronic Acid Hydrogel Matrix With a Tunable Degradation Profile

Kailei Ding, Jiayuan Kong, Hexiang Feng, and Hai-Quan Mao

Statement of Purpose: Hyaluronic acid (HA) hydrogel is known for its biocompatibility and biodegradability. We developed an HA hydrogel with tunable degradation kinetics by combining microparticles with different degradation rates. This gradual degradation was hypothesized to enhance immune cell recruitment, immunomodulation, pro-angiogenic properties, and soft tissue remodeling.

Methods: We crosslinked HA using 1,4-butanediol diglycidyl ether (BDDE) at pH 2.0 and pH 13.0 to create two microgels with different degradation rates. To obtain HA hydrogel with tunable degradation, the microgels were mixed in a 1:1 ratio. Degradation rates were monitored by shear storage modulus (G'), and subcutaneous injections were tested in Sprague-Dawley rats. CD38+ and CD163+ macrophages, pro-angiogenic, and adipogenesis responses were assessed via immunostaining.

Results: HA hydrogels crosslinked at pH 2.0 and 13.0 had similar G' (~250 Pa) but distinct degradation rates. The pH 2.0 hydrogel degraded in 7 days, while the pH 13 hydrogel retained 50% volume by day 56. The microgel mixture showed higher macrophage counts and better endothelial (RECA-1+) and pericyte (α-SMA+) infiltration from day 7–56 compared to the pH 13 microgel. It also induced more adipogenesis and displayed enhanced collagen deposition and neo-tissue formation (Masson trichrome staining) by day 56.

Conclusion: The engineered hydrolysable HA microgel mixture with a tunable degradation profile creates pores within the HA hydrogel gradually after implantation in vivo. The degraded HA microgel may serve as a biostimulatory cue facilitating infiltration and polarization of host macrophages to augment pro-angiogenic responses and potentially tissue remodeling.

ABSTRACT 122

Microrobotic Grippers for Upper Urinary Tract Biopsy

Wangqu Liu, Ridwan Alam, Si Young Choi, Yan Wan, Ruili Zhang, Ezra Baraban, Andres Matoso, Brian R. Matlaga, Jared S. Winoker and David H. Gracias

Microrobots offer significant potential for advancing medical and surgical interventions in small, complex anatomical regions, particularly for diseases requiring precision diagnostics and treatment. Accessing the upper urinary tract, including the ureter and the pelvicalyceal system, is crucial for diagnosing and treating diseases such as Upper Tract Urothelial Carcinoma (UTUC). Challenges in this domain include adequate tissue sampling, precise disease grading, and targeted or extended medication delivery using existing ureteroscopic tools. To address this, we developed biopsy microgrippers (μ-grippers) with a pre-activation size of 717 μm, deployable via urinary catheters. These μ-grippers autonomously activate at body temperature, self-folding into 200 μm microcages that capture tissue through differential stress energy in thin metal films. Magnetic retrieval enables sample collection for histopathological analysis, while external magnetic fields allow precise steering.

Our findings indicate that the μ-grippers can be delivered via clinically used urinary catheters with a successful delivery rate ranging from 80 to 88%. The μ-grippers exhibited multimodal locomotion, including moving, tumbling, and tissue tearing, on ex vivo urothelial tissues. Experiments on ex vivo pig ureters showed that the μ-grippers could successfully biopsy tissue, producing samples suitable for histopathological examination, including H&E and GATA3 immunostaining. The μ-grippers' compact size, scalability for high-throughput production, and multifunctionality make them ideal for statistical tissue sampling. Comparative simulations reveal their superior efficacy over traditional tools like forceps and baskets. We anticipate μ-grippers will enhance tissue sampling capabilities, enabling early detection of small, low-grade, and hard-to-reach lesions, thus advancing diagnostic and therapeutic options for urinary tract diseases.

ABSTRACT 123

Intelligent Control of Robotic X-ray Devices using a Language-promptable Digital Twin

Benjamin D. Killeen, Anushri Suresh, Catalina Gomez, Blanca Inigo, Christopher Bailey, and Mathias Unberath

Robotic C-arm X-ray devices are becoming more common in a range of surgical procedures. Natural language offers a convenient, flexible interface for controlling these devices, making advanced functionality and controls easily accessible. However, enabling language interfaces requires specialized artificial intelligence (AI) models that interpret X-ray images to create a semantic representation for language-based reasoning. The fixed outputs of such AI models fundamentally limits the functionality of language controls. Incorporating flexible and language-aligned AI models that can be prompted through language control facilitates more flexible interfaces for a much wider variety of tasks and procedures. Using a language-aligned foundation model for X-ray image segmentation, our system continually updates a patient digital twin with the desired anatomy. This allows for multiple autonomous capabilities, including visualization, patient-specific viewfinding, and automatic collimation from novel viewpoints, enabling complex language control commands like "Focus in on the lower lumbar vertebrae." In a cadaver study, multiple users were able to visualize, localize, and collimate around structures from across the torso region using only verbal commands to control a robotic X-ray system, with 84% end-to-end success. Overall, we show how intelligent robotic X-ray systems can incorporate physicians' expressed intent directly. Our results suggest that as these models become more capable, they can facilitate highly flexible, intelligent robotic C-arms.

ABSTRACT 124

Bioresorbable Shape-Morphing Microrobots for Safer Precision Medicine

Wangqu Liu, Derosh George, Yulun Wu, Arijit Ghosh, Ruili Zhang, Gayatri Pahapale, Zijian Zhong, David H. Gracias

Shape-morphing microrobots, capable of adapting to environmental changes and transforming their geometry or functionality, represent a breakthrough in biomedical intelligent systems. These microrobots autonomously perform tasks such as locomotion, drug delivery, and microsurgery with minimal invasiveness in unstructured in vivo environments. However, existing designs either rely on soft polymeric materials lacking the mechanical rigidity for surgical operations or on non-degradable metallic materials requiring surgical removal—posing significant safety concerns.

We introduce a novel class of bioresorbable, shape-morphing microrobots fabricated from metallic materials, such as iron, molybdenum, zinc, and magnesium oxide. Utilizing a liquid-free shadow mask method, we overcome photolithography limitations with water-soluble materials, employing stencil lithography to preserve microstructures on a dissolvable polymeric sacrificial layer. These microrobots leverage intrinsic stresses in metal bilayers for self-folding into 3D structures, such as microtubes and multi-fingered microgrippers. Precise control of their folding dynamics and degradation timelines is achieved through fabrication parameters, guided by finite element analysis.

These microrobots demonstrate predictable degradation rates, dissolving completely in physiological conditions ranging one day to 30 days, and their biocompatibility is validated in cell culture studies. Designed for medical applications, they can effectively perform tasks such as biopsies and drug delivery without requiring surgical retrieval. This bioresorbability enhances patient safety and broadens the scope of microrobotic technologies in minimally invasive medicine, offering a safer and more efficient approach to diagnosis and therapy.

ABSTRACT 125

DURABLE: Dual HRV and Blood Pressure Assessment for Neurological Evaluation

Prachi Agarwal, Mingfeng Cao, Yu Guo, Payam Gharibani, Romergryko Geocadin, Nitish Thakor

Neurological recovery post-cardiac arrest (CA) is challenging to predict due to the absence of rapid, reliable, and accessible bedside tools. While MRI and EEG provide detailed insights, their cost, time requirements, and logistical challenges make them impractical for emergency scenarios. DURABLE, a novel approach integrating heart rate variability (HRV) and blood pressure (BP) through Dual Poincaré methods, addresses this gap by offering a non-invasive biomarker for early prognosis and actionable triage.

The study utilized an asphyxial CA rat model, where adult Wistar rats were subjected to 7 minutes of CA followed by resuscitation. Continuous HRV and BP data were collected immediately post-resuscitation using a Tucker-Davis System3 acquisition setup. Sequential HRV intervals and corresponding BP values were plotted to create Dual Poincaré plots, visualizing the real-time interplay between autonomic and vascular regulation. Unlike traditional baroreflex sensitivity assessments, which measure long-term averages, this approach captures the complex, dynamic, beat-to-beat interactions critical for post-CA recovery. Density-Based Spatial Clustering of Applications with Noise identified distinct physiological patterns correlating with outcomes, assessed by the Neurological Deficit Score (NDS).

Rodents exhibiting dispersed clusters in the Dual Poincaré plots showed higher NDS scores and better recovery, while tight clusters were associated with poor outcomes and lower NDS scores. Logistic regression confirmed DURABLE's predictive capability, achieving 90% accuracy and 88% sensitivity in forecasting recovery outcomes.

By leveraging easily available HRV and BP signals, DURABLE provides a rapid, cost-effective, and scalable bedside tool. This approach bridges early diagnosis with advanced care, enabling timely interventions and better critical care outcomes.

ABSTRACT 126

Uncertainty-quantified Pulse Signal Recovery from Facial Video without Video Pre-training using Score-based Generative Priors

Vineet R. Shenoy, Yu Sun, Rama Chellappa

Imaging Photoplethysmography (iPPG), defined as the re-construction of the underlying blood volume pulse waveform using only the pixel readout from a camera, has emerged as an exciting research field with applications in non-contact health monitoring, perfusion assessment, affective computing, and more. While current algorithms have shown outstanding performance on benchmark datasets, nearly all state-of-the art algorithms train models on highly sensitive facial data and provide only point-estimates of recovered waveform, precluding an uncertainty analysis that is critical for clinical adoption. We address thesedeficiencies though a new paradigm named Plug-and-Play Monte Carlo for iPPG (PMC-iPPG), a regularized optimization method that uses score-based generative priors for high fidelity pulse signal denoising from video, all without facial video during training. Additionally, our score-based paradigm allows us to sample the highest-probability waveforms in solution space, leading to robust statistical analyses of uncertainty in waveform recovery. Experimental results on four datasets, including synthetic to real-world training and testing, show that PMC-iPPG provides superior reconstruction quality and uncertainty estimates of the recon struction, a critical tool for the eventual adoption of iPPG algorithms in clinical and consumer settings.

ABSTRACT 127

A mathematical model of penetration of zona pellucida

Prajakta Bedekar, Daniel Anderson, Zachary Goecker, Anthony Kearsley

Fertilization is the process by which new life forms and its study illuminates deeper understanding of organisms, improves animal husbandry, leads to discovery of new birth control methods, and insights into parent-offspring genetic transmissions. Mammalian fertilization consists of spermatozoa motion towards an oocyte, followed by penetration of zona pellucida, the outer layer of an oocyte. Experimental explorations reveal that glycan and enzyme kinetics are important for this process despite their roles not being well understood.

Mathematical models help bridge the gap between theory and experimentation. I will present, with numerical results, our reaction-diffusion model yielding in-silico insight into underlying competing physiological factors. I will demonstrate how our model displays desirable properties such as positivity and boundedness, while remaining general enough to accommodate a myriad of reaction mechanisms for the underlying chemicals. To illustrate this, I compare model predictions for second order reversible reaction against the frequently employed, Michelis Menten model. Furthermore, I will discuss the role advection (sperm motility) plays and competing definitions for the likelihood of fertilization.

This study demonstrates that more intricate reaction mechanisms paired with space-time diffusion-based models provide a valuable sandbox to examine competing biological hypothesis in-silico. Our approach yields insights used to define new experimental paradigms which will be investigated with biologists at the National Institute of Standards and Technology (NIST). This research provides the crucial link to a fuller understanding of fertilization, opening the door to future investigation.

ABSTRACT 128

Evaluation of Hemodynamic Data in Transthyretin Amyloid Cardiomyopathy Patients

Muhammed Rahim, Vrinda Gupta, Lisa Yanek, Yazan Alshawkani, Mark Ranek, Kavita Sharma, Joban Vaishnav

Transthyretin amyloid cardiomyopathy (ATTR-CM) is an infiltrative cardiomyopathy secondary to deposition of misfolded transthyretin. There are limited investigations on the prognostic significance of hemodynamic data in ATTR-CM patients. Our study sought to evaluate four hemodynamic profiles based on congestion and perfusion of ATTR-CM patients stratified by genotype and assess their association with mortality and heart failure hospitalization. We included 187 patients diagnosed with ATTR-CM at Johns Hopkins Hospital who underwent right heart catheterization. These patients were grouped by congestion/perfusion profile based on the median of the cohort: cold/warm (cardiac index </≥ 1.8 L/min/m2) and dry/wet (PCWP </≥ 18 mmHg). Comparisons were made using ANOVA, chi-square, Wilcoxon, or t-tests. Kaplan-Meier curves and Cox models assessed relationship to mortality. Sixty-four patients were warm/dry (34%), 30 warm/wet (16%), 41 cold/dry (22%), 52 cold/wet (28%). V122I was the most common genotype in the cold/wet group. The cold/wet group had the lowest 3-year survival (log-rank p=0.007) and was associated with mortality when adjusted for age, sex, race (HR 2.86, 95% CI 1.34-6.13, p=0.007). Right atrial pressure, mean pulmonary artery pressure, pulmonary capillary wedge pressure, and cardiac index were associated with mortality independent of the most severe biomarker-based prognostic stage (National Amyloidosis Center Stage 3 disease). Overall, patients in the cold/wet group had the worst survival. Hemodynamics were independently predictive of mortality on top of the most common prognostic scoring system. Though there has been an increase in non-invasive diagnosis of ATTR-CM, our study highlights the ongoing role of hemodynamic data in these patients.

ABSTRACT 129

Impact of Internet Use on Knowledge of Clinical Trials: An analysis using the Health Information National Trends Survey (HINTS) Dataset

Zaib Hussain, Erin D. Michos, Hailey N. Miller, Cheryl Himmelfarb, Payam Sheikhattari, Rifath Ara Alam Barsha, Timothy B. Plante

Background: Research shows substantial gaps in effective cardiovascular clinical trial (CT) engagement among diverse populations, particularly due to a general lack of knowledge about research. We seek to bridge these gaps by assessing the role internet plays in improving access to health information, knowledge, and participation in CTs.
Objective: We examine how internet use impacts CT knowledge.

Methods: HINTS 5, Cycle 4, is a cross-sectional, nationally representative survey of US adults. Participants self-reported use of the internet (yes/no) and knowledge of CTs (dichotomized as none or little vs. higher knowledge). Logistic regression was used to estimate relative odds of higher knowledge of CTs (outcome) by internet use (exposure) in models adjusting for demographic, health-related, and socioeconomic factors. The analysis was stratified by race/ethnicity, gender and different modalities of internet use to explore variations in knowledge acquisition.

Results: Among a weighted sample of 249,896,898 participants (mean [SD] age 47 [17.2] years, 50% women), 86% used the internet, and 10% reported higher CT knowledge. There were significantly greater odds of CT knowledge among adults using the internet in models adjusted for demographics and cardiovascular risk factors (OR 3.24, 95% CI 1.68 – 6.27). However, after additional adjustment for socioeconomic factors, this was no longer significant (OR 1.64, 95% CI, 0.82–3.25) Stratified analyses demonstrated that combined mobile phone and home-based internet use was positively associated with higher knowledge about CT (OR=4.77, 95% CI=1.26-18.07). There were no significant interactions between internet use and CT knowledge by race/ethnicity or gender.

Conclusions: Our results underscore the importance of employing online platforms to engage potential participants. Investing in internet-based recruitment strategies potentially could augment the efficacy of CT recruitment efforts. Furthermore, a wider net should be cast for CT recruitment to ensure non-users of the internet get equity in access to information.

ABSTRACT 130

Polyhedral Origami Shell MEAs for Brain Organoids

Derosh George, Chris Acha, Ziwei Ouyang, Itzy E. Morales Pantoja, JinXun Chen, Lena Smirnova, David H. Gracias

Recently, organoids have become important in vitro tools for tissue engineering and biomedical engineering. Brain Organoids (BOs), as stem cell-derived tissue models, are highly relevant for developmental biology and neuroscience. Due to their non-uniformity 3D shapes, conventional 2D MEAs fail to interrogate the entirety of the organoid. Here, we discuss the shape and size of customizable 3D MEAs in the form of polyhedra that function to both (a) contain and customize the shape of growing BOs and (b) interrogate the entirety of the BO surface. We discuss fabrication, characterization, and preliminary electrophysiological data using these systems. We anticipate that such polyhedral MEAs could be used not just for BOs but also for other electrogenic organoids (e.g., cardiac) as well as other organoid culture systems.

ABSTRACT 131

The immune map of lupus nephritis: a spatially-resolved kidney proteomic approach

Chen-Yu Lee, Matthew Caleb Marlin, Xiaoping Yang, Alessandra Ida Celia, Vasileios Morkotinis, Richard Furie, Jill Buyon, Chaim Putterman, Jennifer Barnas, Kenneth Kalunian, Peter Izmirly, Betty Diamond, Anne Davidson, Diane Kamen, Jeff Hodgin, the Accelerating Medicines Partnership RA/SLE, Judith James, Michelle Petri Joel Guthridge, Avi Rosenberg and Andrea Fava

Background/Purpose: Treatment response in lupus nephritis (LN) remains suboptimal. While single-cell transcriptomics catalogs LN cell states, spatial organization is less understood. This study maps immune cell spatial organization in LN.

Methods: We employed an 18-plex serial immunohistochemistry (sIHC) workflow with imaging and destaining cycles. HALO software facilitated AI-assisted tissue classification. Immune cells were identified using PCA and clustering algorithms. Cellular aggregates, defined as three or more cells within 50 µm, were categorized by size: small (<30 cells), medium (30–99 cells), and large (>100 cells). K-means clustering assessed aggregate subtypes, and clinical correlations were analyzed using Pearson's coefficient.

Results: From 29 LN biopsies, 1,913,845 cells (182,783 immune cells) and 12,371 aggregates were analyzed. Small aggregates comprise the majority (97%), but medium and large aggregates contain up to 33.7% of the immune cells. Proliferative and mixed LN showed increased glomerular aggregates, primarily CD68+ myeloid cells, which negatively correlated with UPCR. Tubulointerstitial (TI) aggregates, present across LN classes, negatively correlated with GFR. Over 10 aggregate subtypes emerged, with small aggregates containing 1–2 cell types and larger aggregates showing mixed cell types resembling germinal centers. Aggregate subtype-specific correlations with clinical and pathological features were observed.

Conclusion: This study highlights the spatial heterogeneity of glomerular and TI immune cell structures in LN, linking specific aggregate subtypes to clinical and pathological features. These findings provide insights into LN pathogenesis and potential immune cell interactions.

ABSTRACT 132

Extracellular Vesicle-incorporated Biostimulatory Matrix Prevents Radiation Dermatitis

Jiayuan Konga, Kedar Krishnan, Hexiang Feng, Kailei Dinga, Sashank K. Reddy, and Hai-Quan Mao

Radiation dermatitis (RD) is a prevalent and severe side effect of radiation therapy, affecting approximately 95% of cancer patients undergoing treatment. Despite the critical need for effective interventions, no FDA-approved therapies currently exist for the treatment or prevention of RD. In this study, we present a novel subcutaneously (s.c.) injected biostimulatory nanofiber-hydrogel composite (NHC) matrix, embedded with adipose-derived stem cell extracellular vesicles (ADSC-EVs). This composite enables a sustained therapeutic release of EVs over a period of approximately one month in vivo. In a murine radiation dermatitis model, a single s.c. injection of the NHC matrix resulted in the restoration of skin tissue architecture and function, inhibition of fibrosis progression, and induction of neo-follicle formation. Our results indicate that the prevention of RD is mediated by the combined effects of the NHC matrix, which establishes an anti-fibrotic microenvironment that modulates the activity of recruited macrophages and fibroblasts, together with the EVs, which elevates regenerative responses. This synergistic action promotes the repair of skin structures and the regeneration of vasculature and hair follicles.

ABSTRACT 133

Hepatocyte-specific knockout of BCOR changes coagulation factor expression and increases clotting.

William O. Osburn, Emily Paris, Pablo Toledano Sanz, Hari Easwaran, Marios Arvanitis, and Charles J Lowenstein

Venous thromboembolism (VTE) is a significant public health problem affecting 900,000 individuals and causing over 100,000 deaths per year. GWAS analyses identified numerous genetic loci associated with altered risk of VTE. We identified genes associated with VTE by filtering potential candidate genes by novelty, liver expression, and hepatocyte expression, since coagulation factors are primarily produced in hepatocytes. A genetic variant in BCL6 corepressor (BCOR), member of the non-canonical polycomb repressor complex 1.1 (ncPRC1.1), was associated with increased risk of VTE. Therefore, we hypothesized that BCOR protects against VTE by altering hepatocyte coagulation factor gene expression. To test this, we used siRNA to knock down BCOR expression in HepG2 cells, a human hepatocellular carcinoma cell line which significantly up-regulated Factor VII mRNA and intracellular protein levels. Also, expression of over 11,000 genes were altered following BCOR knockdown suggesting that BCOR plays a role in regulating the expression of numerous genes. Next, we searched for proteins that might interact with BCOR, by using proximity labeling techniques. This analysis identified members of ncPRC1.1 and ADA2A-containing complex (ATAC) complexes as being in proximity to BCOR and knockdown of specific ATAC and ncPRC1.1 members increased Factor VII levels. Finally, hepatocyte-specific BCOR knockout (BCOR cKO) mice had normal liver histology but increased Factor VII plasma levels. Importantly, BCOR cKO mice had significantly decreased PT, but not aPTT, time and decreased tail vein bleeding time, indicating a clotting phenotype. Taken together, these results suggest that BCOR decreases hepatic coagulation Factor VII gene expression to protect against VTE.

ABSTRACT 134

Programming antitumor gamma delta T cells via a phosphoantigen nanoparticle delivery vehicle

Sandeep Kumar, Arthur Li, Lauren Robinson, Megha Lingamsetty, Stephany Tzeng, Scott Wilson

Vγ9Vδ2 T cells are a powerfully cytotoxic subset of gamma delta T cells which can eradicate cancerous tumors. Adoptive cell therapies utilizing these cells are being explored clinically but require expensive and cumbersome on-site cell isolation and ex vivo activation. Activating Vγ9Vδ2 T cells in situ would overcome these issues, but delivery challenges of activation agents have stymied clinical development. Vγ9Vδ2 T cell activation and tumor cell killing are mediated by internalization of small molecule phosphoantigens (pAgs) by tumor or antigen presenting cells. We present a self-assembling nanoparticle (NP) composed of a hydrophilic, tumor-targeting block and a hydrophobic polymer block containing pAg prodrug monomers (pAgMAs). We hypothesize that these high-dose pAg nanoparticles will program Vγ9Vδ2 T cells in situ to an interferon gamma (IFNγ)-expressing phenotype, resulting in tumor cell cytotoxicity and recruitment of other anti-tumor immune cells.
pAg-NPs displayed preferential uptake at 37°C as compared to 4°C and significant cytotoxic effect against multiple cancer cell lines (MeWo, PC3, OVCAR3) in the presence of Vγ9Vδ2 T cells. Tumor cell/Vγ9Vδ2 T cell co-cultures treated with pAg-NPs produced 100-fold more IFNγ than untreated co-cultures. In vitro demonstration of active uptake and cytotoxicity due to Vγ9Vδ2 T cell activation indicates promise for this therapy in vivo. We anticipate that pAg-NPs will localize to the tumor microenvironment and continually release their large payloads of pAgs into tumor cells, minimizing off-target effects and activating Vγ9Vδ2 T cell tumor eradication. We are currently translating this therapy into a mouse tumor model.

ABSTRACT 135

Just Trial Once: Ongoing Causal Validation of Updates to Machine Learning Models

Jacob M Chen, Michael Oberst

The use of machine learning (ML) models as clinician support tools is increasing in popularity. Evaluating the causal impact of deploying such models on clinical outcomes can be done with a randomized control trial (RCT), such as a cluster-randomized trial. However, ML models are inevitably updated over time, and we often lack evidence for the impact of these updates on the same clinical outcomes. While this impact could be repeatedly validated with ongoing RCTs, in practice, such experiments are expensive, time-consuming, and difficult to run. In this work, we present an alternative solution: using only data from a prior RCT that tested other models, we give conditions under which the causal effect of an updated ML model can be precisely estimated or bounded. Our assumptions incorporate two realistic constraints: ML predictions are often deterministic, and their impact depends on clinician trust in the model. Based on our analysis, we give recommendations for cluster randomized trial designs that maximize their ability to assess future versions of an ML model. Our hope is that following our proposed trial design will save practitioners time and resources while allowing for quicker deployments of updates to ML models.

ABSTRACT 136

Slide-free tissue histology using back-illumination interference tomography and virtual H&E staining

Anthony A. Song, Mayank Golhar, Marisa Morakis, Mostafa Abdulrahim, Seth Jayawardane, Gregory N. McKay, Risheng Xu, Alexander Baras, Nicholas J. Durr

Histological staining of tissue biopsies using hematoxylin and eosin (H&E) is the gold standard for disease diagnosis, but the process can be time-consuming, delaying results for days or weeks. Rapid tissue assessment with H&E-like contrast could improve procedures such as surgical margin assessment and cancer screening. To address this, we propose a rapid multimodal imaging system combining back-illumination interference tomography (BIT) and microscopy with ultraviolet surface excitation (MUSE) for generating virtual H&E (vHE) images from bulk tissue. Using BIT, we capture H&E-like contrast data, which is converted to vHE using a CycleGAN deep learning model. MUSE images, acquired with Hoechst and Rhodamine staining, provide pixel-wise registered ground truth comparisons using a physics-based staining model.

The BIT contrast mechanism is achieved using a partially coherent light source and an infinity-corrected objective lens, producing transmission-like illumination. MUSE imaging employs obliquely oriented UV excitation fibers for nuclear and cytoplasmic staining. Both modalities are integrated into a single optical system and imaged onto CMOS sensors. We obtained pixel-wise registered BIT and MUSE images of mouse brain tissue and trained a CycleGAN model to virtually stain BIT images, achieving excellent style transfer compared to standard brightfield H&E staining. MUSE-vHE images were used as ground truth to validate histological feature preservation. While BIT-vHE demonstrated strong agreement with MUSE-vHE, some failure cases in nuclear transformation were observed. This system demonstrates the potential for rapid, label-free vHE imaging for improved clinical workflows.

ABSTRACT 137

Role of O-GlcNAcylation and ERK1/2 phosphorylation in cardiac ischemia-reperfusion injury

Aidan Dunphy, Kyriakos Papanicolaou, Brian Foster

Ischemic heart damage is a common consequence of coronary artery disease due to impaired oxygen supply. O-GlcNAcylation, a form of glycosylation mediated by O-GlcNAc Transferase (OGT) and O-GlcNAcase (OGA), dynamically adapts to cellular stress by cycling on and off proteins. Previous work suggested that ERK1/2 undergo O-GlcNAcylation in cardiomyocytes, with OGT inhibition suppressing ERK1/2 phosphorylation. As BRAF activates Mek1/2, which in turn activates ERK1/2 via the MAPK pathway, we hypothesized that expressing BRAF V600E in cardiomyocytes could rescue ERK1/2 phosphorylation and provide ischemic protection despite O-GlcNAcylation inhibition. To test this, murine hearts underwent ex vivo ischemia-reperfusion (IR) injury. Four genotypes were evaluated: control, induced cardiomyocyte knockout of OGT (ickoOGT), BRAF V600E, and double transgenic (ickoOGT/BRAF V600E; DTG). Infarct size was assessed via TTC staining, and protein levels were quantified. Results showed increased ischemic damage in ickoOGT mice compared to controls. Interestingly, BRAF V600E mice exhibited greater injury than ickoOGT and DTG mice, with slight attenuation in DTG. Western analysis confirmed suppressed ERK1/2 phosphorylation in ickoOGT mice, but no restoration in DTG mice. Additionally, ischemic damage inversely correlated with reperfusion flow, indicating vascular adaptations may contribute to cardiac protection under IR stress. This study underscores the intricate interplay between O-GlcNAcylation and ERK1/2 phosphorylation and highlights the need for further investigation into the signaling mechanisms underlying cardiac ischemia-reperfusion injury.

ABSTRACT 138

Engineering Brainstem Organoids: A Novel Platform for Modeling Neurological Diseases

Anannya Kshirsagar, Sai Kulkarni, Kai Cheng, Oce Bohra, Annie Kathuria

Neurological disorders affecting the brainstem, a critical region of the central nervous system, present significant challenges in both research and treatment due to limited access to human tissue models. While recent advances in organoid technology have enabled the generation of various brain regions, modeling the complex cellular architecture and neural circuits of the brainstem has remained challenging. Here we present a specialized protocol for generating brainstem organoids that recapitulate key features of the mid/hindbrain region. Through targeted manipulation of developmental signaling pathways, we successfully generated three-dimensional tissue models containing characteristic brainstem neural populations and nuclei. Immunohistochemical analysis confirmed the presence of region-specific neuronal subtypes, while single-cell RNA sequencing revealed the molecular heterogeneity of the cellular populations. Electrophysiological recordings demonstrated functional neural activity, validating these organoids as a physiologically relevant model system. This brainstem organoid platform represents a significant advancement in our ability to study this crucial brain region in vitro. The system enables detailed investigation of brainstem development, disease mechanisms, and potential therapeutic approaches for disorders affecting vital functions controlled by brainstem circuits. These organoids provide an unprecedented opportunity to model human brainstem development and dysfunction in a controlled experimental setting.

ABSTRACT 139

Magnetically Actuated Bioactuator for Promoting Skeletal Muscle Tissue Maturation through Frequency-Dependent Hybrid Stimulation

Hyoryong Lee, Byunggik Kim, and Deok-Ho Kim

Skeletal muscle tissue (SMT) engineering holds immense potential for disease modeling and drug screening by offering physiologically relevant in vitro platforms. However, existing models often fail to replicate native muscle functionality, limiting their application in studying muscular disorders and evaluating therapeutics. This study addresses these challenges by developing a novel bioactuator that integrates hybrid mechanical and electrical stimulation to enhance SMT maturation and functionality.

The proposed bioactuator integrates mechanical and electrical stimulation components, featuring two parallel-aligned posts having the standard 96-well plate format. For mechanical stimulation of SMT, a permanent magnet is embedded in one of the two posts, enabling SMT stretching at low magnetic field frequencies to promote cellular alignment. For electrical stimulation, magnetoelectric nanoparticles are coated on the tips of both posts within a hydrogel, generating electricity at high magnetic field frequencies to enhance functional maturation. This innovative design replicates the native muscle microenvironment and improves the predictive validity of SMT models. Additionally, the bioactuator, configured in a 96-well plate format, supports 3D high-throughput experimentation.

In this study, the proposed bioactuator demonstrated that hybrid stimulation could be achieved by varying the magnetic field frequency, resulting in enhanced cellular alignment and functional properties of SMT. This represents a significant step toward developing robust, scalable SMT models for disease modeling, and drug screening. By streamlining the delivery of multiple stimuli and enabling high-throughput workflows, the proposed system aligns closely with goals to accelerate discoveries in biomedical research and pharmacology.

ABSTRACT 140

Understanding the role of AGTR1-mediated signaling in modulation of pericyte function during emphysema development

Liz Gonye, Sarah Gidner, Alla Malanina, Enid Neptune

Emphysema is one of the main causes of chronic obstructive pulmonary disease (COPD), the 6th leading cause of death in the US. Despite this extremely high health burden, treatments for emphysema are extremely limited and not curative. Multiple human and mouse model studies identify a protective effect of angiotensin receptor blocker (ARB) treatment on COPD morbidity and mortality. Emphysema is in part characterized by gross vascular dysfunction, but the mechanisms leading to microvascular breakdown are understudied and provide a new opportunity for treatment. In the microvasculature, endothelial cells (ECs) exist in close opposition to pericytes (PCs), a mural cell type specialized for EC support and regulation. In the lung, PCs comprise a majority of angiotensin II receptor 1 (AGTR1)-expressing cells. Thus, the efficacy of ARB treatment to prevent emphysema is likely mediated through ARB action at PC AGTR1 receptors. This work studies the role of PCs in maintaining vascular homeostasis via examining the effect of AGTR1 signaling on disrupting EC-PC homeostasis and destabilizing lung microvasculature. We use multiple experimental paradigms for both in vitro and in vivo emphysema models. These approaches examine elements of EC-PC interaction, observe alterations in EC/PC cell health, monitor PC motility/migration, and detect changes in overall lung structure and function. This work is the first to identify PCs as a crucial component of vascular dysfunction in emphysema and further elucidate the role of lung AGTR1 signaling in mediating emphysema development. These findings will solidify PC stabilization and regulation as a new preventative/restorative treatment for emphysema.

ABSTRACT 141

Evaluating the role of Alpha-Cell Dysfunction in the Longitudinal Progression to Type 2 Diabetes

Vijaya Subramanian, Arthur Sherman

Alpha-cell dysfunction is known to occur in type 2 diabetes (T2D) and to increase fasting glucose as well as exacerbate post-prandial glucose excursions. The role of alpha-cell dysfunction in the longitudinal development of T2D has not yet been modeled mathematically. Alpha-cell dysfunction occurs in tandem with the development of insulin resistance and beta-cell dysfunction. Several unanswered questions include the influence of alpha-cell dysfunction on beta-cell compensatory insulin secretion and subsequent failure in the progression from normal glycemia to T2D diabetes. We developed an extended physiological model of glucose homeostasis, where the fast dynamics of glucose, insulin, and glucagon is coupled to the slow dynamics of glucose-dependent beta-cell functional mass. We used the model to study the longitudinal progression to T2D in the presence of alpha-dysfunction in addition to the development of insulin resistance. The model was validated by matching the beta-cell functional mass obtained from the simulations of the longitudinal model to that obtained from fitting a model of oral glucose tolerance tests to a cross-sectional Caucasian cohort that spanned the gamut from normal to T2D. We conclude that, in addition to insulin resistance, mild alpha-cell dysfunction in the early stages of hyperglycemia, is required for robust beta-cell functional mass compensation through increased fasting glucose. When alpha-cell dysfunction is severe, however, glucose reaches levels that cause glucotoxicity, exacerbating beta-cell functional mass loss and precipitating the onset of T2D. In addition, we were able to simulate different pathways of progression to disease as observed in different ethnic groups.

ABSTRACT 142

Spatial transcriptomics uncovers IL-6 inflammatory signature, progressive osteopontin expression, and mitochondrial dysfunction in dermatomyositis-associated calcinosis cutis

Cassie Parks, York Wang, Lisa Christopher-Stine, Shira Ziegler, Joel Sunshine, Christopher Mecoli

To understand the pathophysiology of calcinosis cutis in dermatomyositis (DM), we performed Visium spatial transcriptomic analysis on 4 calcinosis samples from adult DM patients meeting 2017 ACR/EULAR criteria and 3 healthy adult controls. All samples contained "active" calcinosis with new or evolving lesions and associated signs of inflammation.

This analysis identified a distinct inflammatory signature with elevated IL-6 expression and upregulation of macrophage markers (CD68, MSR1) and chemokine CCL3. We observed increased immunoglobulin synthesis through elevated IgG, IgA, and J chain expression. Extracellular matrix dysregulation was evidenced by decreased keratin expression, elevated MMPs 1/9/13, and elevated cartilage-specific collagens. Osteopontin, which is involved in pathological calcification, was robustly elevated in lesional samples.

UMAP analysis revealed distinct transcriptomic clusters, with linear progression through UMAP space corresponding to increasing calcification burden. We identified three phases: the early, pre-calcific phase showed barrier dysfunction, increased immunoglobulin transcription, elevated IL-6 target gene FOS, and loss of stemness maintenance genes. The middle, propagative remodeling phase featured enhanced MMP9 expression, increased lysosomal enzyme transcription, and dysregulated extracellular matrix deposition. The late-stage calcification phase showed increased expression of mitochondrial genes and an oxidative stress response marked by ferritin upregulation. Notably, osteopontin expression showed a consistent increase at each step until the final transition to acellular cold calcification.

This study provides the first detailed spatial molecular map of calcinosis in dermatomyositis, suggesting a complex pathogenic cascade involving antibody synthesis, macrophage recruitment, IL-6/FOS signaling, robust osteopontin expression, and mitochondrial dysfunction culminating in tissue calcification.

ABSTRACT 143

IPMK and Metabolic Remodeling in Cardiomyocytes: Implications for Heart Failure

Ji-Hyun Lee, Ik-Rak Jung, Sunghee Jin, Rexford S. Ahima, and Sangwon F. Kim

Heart failure (HF) is a major global health challenge that significantly impacts quality of life and life expectancy. Obesity, a critical risk factor for HF, drives metabolic remodeling in cardiomyocytes, including reduced fatty acid oxidation, increased glycolysis, and diminished metabolic flexibility, which collectively exacerbate cardiac dysfunction and stress. Recent data revealed disrupted mitochondrial and lipid metabolic pathways and structural abnormalities in obese heart failure with preserved ejection fraction (HFpEF) patients. Our analysis further identified reduced expression of inositol polyphosphate multikinase (IPMK) in HF hearts. Since IPMK is a novel nutrient sensor at the cellular level, we hypothesized that disruption of cardiomyocyte IPMK may lead to metabolic dysregulation, driving cardiac dysfunction. To test this, we developed a cardiomyocyte-specific IPMK knockout mouse model (HKO) using the Myh6-Cre system. Using echocardiography, Western blotting, and transcriptomic analysis, we examined the progression of metabolic deficits and structural remodeling. At 5 weeks, echocardiography and RNA-seq analyses revealed no cardiac dysfunction or developmental abnormalities, while metabolic pathways such as aerobic respiration, oxidative phosphorylation, and purine ribonucleotide metabolic process were disrupted in HKO compared to wild-type mice (WT). By 15 weeks, metabolic insufficiency led to widespread fibrosis and the onset of HF. Western blot analyses confirmed reduced expression of critical metabolic regulators. These findings suggest early metabolic dysregulation as a driver of pathological cardiac remodeling, offering insights into potential therapeutic targets for HF. In conclusion, our study highlights the critical role of metabolic regulation in maintaining cardiac health, demonstrating the critical importance of investigating metabolic pathways to gain deeper insights into the fundamental mechanisms that drive HF progression and pathology.

ABSTRACT 144

A Novel Connection between OGA and YAP in the Murine HFpEF model

Seungyeon Julie Lee, Priya Umapathi

Metabolic risk factors are associated with cardio-metabolic heart failure with preserved ejection fraction (HFpEF) and increased levels of O-beta-N-Acetylglucosamine modified proteins in the heart (OGN). OGN is determined by O-GlcNAc levels and net activity of two enzymes, OGT (adds OGN) and OGA(removes OGN). Our prior work showed decreasing cardiac OGN by increasing OGA protected against cardiac hypertrophy in a murine TAC model. The data suggested increased OGA modulates the activity of the Yes-Associated Protein (YAP) and transcriptional co-activator, TEAD1, influencing hypertrophy and cardiac remodeling—features of HFpEF. We hypothesize that increased OGA reduces YAP activation in HFpEF.

Male WT mice or OGA TG mice were fed high-fat diet+L-NAME (WT-HFD, OGA -HFD) or normal chow diet (NCD) for 15 weeks to induce HFpEF. Body weight, blood pressure, glucose levels, exercise capacity, diastolic function, heart/lung weights, and cardiac proteins/ RNA were assessed at the end of the study. OGN, OGA, OGT, YAP levels were quantified.

OGA-HFD and WT-HFD mice had similar increases in body weight and reduced exercise capacity compared to mice on NCD. WT-HFD hearts had increased OGN levels and transcriptionally active YAP (low phospho-YAP/YAP) in comparison to WT-NCD. OGA-HFD hearts had lower OGN levels and less transcriptionally active YAP (high phospho-YAP/YAP) compared to WT-HFD hearts.

Our preliminary data support the hypothesis that OGA/OGN modulate activity of YAP/TEAD1 in a murine HFD+L-NAME model of HFpEF. Current experiments are testing the consequences of excess OGA activity on diastolic function, hypertrophy and aim to define the mechanistic basis of interaction between OGN/OGA and YAP.

ABSTRACT 145

Recent Advances in Multimaterial Extrusion Additive Manufacturing

Jochen Mueller

The convergence of human creativity, bioinspiration, and advanced computational tools holds the potential to yield the most captivating—and efficient—designs for new engineering materials, structures, and systems. Yet, realizing these designs in the physical realm presents an ongoing challenge. Amidst this pursuit, Additive Manufacturing (AM), or 3D Printing, has emerged as a compelling alternative to conventional methodologies. However, it has yet to fully meet its lofty expectations, often faltering when confronted with the intricate demands of materials options, structural complexity, throughput speed, and repeatability. Consequently, these limitations have hampered advancements in various related research domains.

In this talk, I will present how we can design and physically realize objects with exceptional properties for applications in architected materials, soft robotics, and beyond. This includes overcoming mutual exclusivities, integrating multifunctionality, and surpassing properties found in natural materials. First, we will explore how specific design requirements can lead to new AM technologies, realizing designs that cannot be manufactured through other means. Second, we will explore how these specialized AM processes can inspire unexpected designs outside the initial scope. Lastly, I will show examples of new fabrication techniques that address the general limitations of AM, expanding the available design space for soft matter fabrication.

ABSTRACT 146

Claims-Based Identification of Alzheimer Disease and Related Dementias using the National Health and Aging Trends Study (NHATS)

Seungyeon Julie Lee, Priya Umapathi

Accurate claims-based identification of dementia is critical for research, population health management, and risk adjustment. Prior studies evaluating the accuracy of Medicare claims in identifying dementia have found wide variation across claims-based definitions and sources of adjudication. Research employing the National Health and Aging Trends Study (NHATS), which collects information through annual interviews of a nationally representative sample of Medicare beneficiaries, as a reference standard to evaluate claims-based algorithms is lacking.

We performed sequential cross-sectional analyses of NHATS-Medicare linked data from 2015-2019. Using the validated NHATS dementia classification algorithm, we identified whether respondents had incident probable or no dementia in each survey wave from 2015-2019. We then applied Bynum-Standard, a validated claims-based algorithm, to identify incident dementia in linked fee-for-service Medicare claims data in the 18 months before and after each annual NHATS survey date. Using the NHATS measure as a reference standard, we calculated performance characteristics of the claims-based algorithm.

Among 12,357 individuals interviewed in NHATS between 2015-2019, probable dementia prevalence was 10.5%. Compared to those without dementia, individuals with probable dementia were more likely to be older, non-Hispanic black, Hispanic, and greater than high school educated. The Bynum-Standard algorithm had low sensitivity (56%), high specificity (97%), and positive predictive value (PPV) of 64% for probable dementia in NHATS.

Using NHATS probable dementia as a reference standard, the Bynum-Standard algorithm performed similarly to alternative reference standards. Sensitivity and PPV of the algorithm to identify dementia was low. Further development and validation of claims-based algorithms to identify dementia is needed.

ABSTRACT 147

Rapid Compaction of Granular Materials

Sohanjit Ghosh, Ryan Hurley

Granular materials like sand are integral to nature and industry but exhibit complex behaviors that defy conventional mathematical modeling. My research investigates the behavior of sand under extreme loads, such as during impacts, by analyzing interactions between individual grains and the collapse of voids under compression. This study provides insights into the hybrid nature of sand, which behaves neither like a pure solid nor a pure fluid. The research has broad implications, influencing fields such as projectile penetration for defense, powder compaction for manufacturing, and asteroid impact cratering for planetary defense.

To study the opaque internal structure of sand, I developed novel experimental methods using X-ray imaging to observe granular compaction during shock loading. These experiments, conducted at the Dynamic Compression Sector of the Advanced Photon Source, Argonne National Laboratory, were coupled with advanced numerical modeling. Funded by the Air Force Office of Scientific Research, this work focuses on the initiation of reactions in energetic powders and explosives. The findings reveal that compaction is highly heterogeneous, with localized high-pressure and high-temperature regions forming due to the intricate shapes and arrangements of grains.

This research has enabled the first-ever measurement of 3D kinematics and kinetics of granular materials during rapid compaction, offering groundbreaking insights into how local grain deformation influences macroscopic behavior. It sets a benchmark for developing models for pore collapse and dynamic responses of granular materials. Furthermore, the work has implications for modeling asteroid impacts, providing critical insights for future planetary defense missions, such as NASA's DART initiative.

ABSTRACT 148

A polymeric opioid conjugate vaccine against fentanyl abuse

Sandeep Kumar, Scott Wilson

The over-prescription and misuse of opioids have led to a sharp increase in addiction rates and overdose deaths, with fentanyl making the crisis even worse. Current clinical interventions, such as naloxone (Narcan), offer temporary relief but are limited by their short half-life (30-90 minutes) and the need for repeated administration, particularly for fentanyl overdose. This creates a critical need for more effective, long-term solutions against fentanyl related overdose. My postdoctoral research addresses this gap by developing an innovative polymeric opioid vaccine platform. Our vaccine works by generating fentanyl-specific antibodies that neutralize the fentanyl in the bloodstream, preventing it from reaching the brain and reducing overdose risk. Unlike short-acting interventions, this approach provides sustained protection against fentanyl exposure, offering a potential long-term solution for addiction treatment and overdose prevention. By incorporating immunomodulatory scaffolds into the polymer design, this platform enhances immune responses and can be adapted for use in other critical areas of biomedical research, such as antimicrobial resistance and viral infections, making it a versatile tool in combating a range of public health threats.

The central hypothesis is that a polymer-based vaccine platform decorated with fentanyl and incorporating TLR7/8 agonists will elicit robust and durable fentanyl-specific immune responses through the multimeric presentation of fentanyl to B cells, via enhance B cell receptor crosslinking (a crucial step in B cell activation and robust antibody response). Additionally, a self-immolative reduction-sensitive linker will facilitating release unmodified carrier proteins, for better T follicular helper cell help to B cells and overcoming the limitations of traditional conjugate vaccines, which suffer from irreversible hapten modifications on carrier proteins. Our vaccine design aims to improve the immunogenicity of existing hapten-based vaccines and address the challenge of opioid addiction and overdose prevention.

To test our vaccination approach, we synthesized water-soluble fentanyl-decorated block copolymers using RAFT polymerization, incorporating both TLR7/8 agonists and fentanyl monomers. The polymers were azide-terminated and conjugated to carrier proteins through strain-promoted azide-alkyne cycloaddition. The efficacy of the resulting vaccine formulations was evaluated in C57BL/6 mice after subcutaneous vaccination and measuring fentanyl-specific antibody levels in the serum and avidity using ELISA over predetermined time points. Additionally, antinociception was assessed using a hot plate assay following fentanyl challenge.

Findings: Our polymeric vaccine, CRM-p(TLR-b-Fent), induces a significantly stronger and more durable anti-fentanyl antibody response compared to existing state of art monomeric vaccine (fentanyl conjugated directly to carrier proteins) strategies. The presence of TLR7/8 agonists and the multivalent display of fentanyl on the polymer significantly enhance B cell activation, resulting in a 1000-fold increase in anti-fentanyl IgG antibody titers over 40 weeks. Additionally, the antibodies generated by the CRM-p(TLR-b-Fent) vaccine bind fentanyl with greater avidity, ensuring a highly specific immune response. our polymeric vaccine outperforms most clinically available adjuvants, including Poly (I:C), CpG, and Alum, in inducing superior anti-fentanyl IgG responses. Upon challenging mice with fentanyl, the polymeric vaccine provided better protection against fentanyl-induced anti-nociception compared to monomeric vaccines.